Integration of Offshore Wind Farms Through High Voltage Direct Current Networks

Luke Livermore
School of Engineering
Cardiff University

A thesis submitted for the degree of
Doctor of Philosophy
January 09, 2013

Contents

Abstract

Name of University: Cardiff University

Candidate's Name: Luke Livermore

Degree Title: Doctor of Philosophy

Thesis Title: Integration of Offshore Wind Farms through Multi Terminal High Voltage Direct Current Networks

Date: January 2013

The integration of offshore wind farms through Multi Terminal DC (MTDC) networks into the GB network was investigated. The ability of Voltage Source Converter (VSC) High Voltage Direct Current (HVDC) to damp Subsynchronous Resonance (SSR) and ride through onshore AC faults was studied.

Due to increased levels of wind generation in Scotland, substantial onshore and offshore reinforcements to the GB transmission network are proposed. Possible inland reinforcements include the use of series compensation through fixed capacitors. This potentially can lead to SSR. Offshore reinforcements are proposed by two HVDC links. In addition to its primary functions of bulk power transmission, a HVDC link can be used to provide damping against SSR, and this function has been modelled. Simulation studies have been carried out in PSCAD. In addition, a real-time hardware-in-the-loop HVDC test rig has been used to implement and validate the proposed damping scheme on an experimental platform.

When faults occur within AC onshore networks, offshore MTDC networks are vulnerable to DC overvoltages, potentially damaging the DC plant and cables. Power reduction and power dissipation control systems were investigated to ride through onshore AC faults. These methods do not require dedicated fast communication systems. Simulations and laboratory experiments are carried out to evaluate the control systems, with the results from the two platforms compared.

Declaration

This work has not previously been accepted in substance for any degree and is not concurrently submitted in candidature for any degree.

Signed ..... (candidate) Date .....

This thesis is being submitted in partial fulfilment of the requirements for the degree of PhD.

Signed ..... (candidate) Date .....

This thesis is the result of my own independent work/investigation, except where otherwise stated. Other sources are acknowledged by explicit references.

Signed ..... (candidate) Date .....

I hereby give consent for my thesis, if accepted, to be available for photocopying and for interlibrary loan, and for the title and summary to be made available to outside organisations.

Signed ..... (candidate) Date .....

I hereby give consent for my thesis, if accepted, to be available for photocopying and for interlibrary loans after expiry of a bar on access previously approved by the Graduate Development Committee.

Signed ..... (candidate) Date .....

Dedication

To my mother,
For inspiring my curious mind

Acknowledgements

This thesis would not have been possible without the guidance and the help of several individuals, who in one way or another contributed and extended their valuable assistance.

My utmost gratitude to my supervisors, Dr. Jun Liang and Prof. Nick Jenkins for their unselfish and unfailing support throughout the PhD study. Special thanks also to Dr. Janaka Ekanayake and Dr. Carlos Ugalde-Loo for their steadfast patience, direction and encouragement on research projects.

I also would like to thank the members of the Power Electronics group at CIREGS, who provided me with a great deal of additional insight during many hours of weekly meetings and discussions. In particular, to Qing Mu, Tianjun Jing and Alasdair Burchill for their assistance in developing the experimental test rigs, so crucial to this research.

I am indebted to many colleagues and friends at the Institute of Energy for sharing their views on my work, whilst sharing coffee and cakes.

Last but not the least, I would like to thanks my loving family for all their support, patience and encouragement.

Nomenclature

Abbreviations and Acronyms

AC	Alternating Current
AI	Analogue Input
AO	Analogue Output
CSC	Current Source Converter
DC	Direct Current
ENSG	Electricity Networks Strategy Group
FACTS	Flexible AC Transmission System
FBM	First Benchmark Model
FC	Fixed Capacitor
FRC	Fully Rated Converter
FRT	Fault Ride Through
GHG	Greenhouse Gases
GPC	Giga Processor Card
GTWIF	Giga Transceiver Workstation Interface Card
HVDC	High Voltage Direct Current
IEA	International Energy Agency
IGBT	Insulated Gate Bipolar Transistor
IGE	Induction Generator Effect
LRSP	Load Reference Set Point
MMC	Multi Modular Converter
MTDC	Multi-Terminal High Voltage Direct Current
OECD	Organisation for Economic Co-operation and Development
PSS	Power Systems Simulator
PWM	Pulse Width Modulation
RTDS	Real Time Digital Simulator
SSCI	Sub Synchronous Control Interactions
SSR	Sub Synchronous Resonance
SUB	Sub Synchronous Mode
TCSC	Thyristor Controlled Series Capacitor
TEC	Transmission Entry Capacity
TI	Torsional Interaction
TM	Torsional Mode
VSC	Voltage Source Converter

Symbols

α	Control signal for AC voltage reduction
β	Control signal for wind farm frequency increase
γ	Control signal for wind turbine frequency increase
δ	Duty cycle of the DC chopper circuit
δ_v	Voltage angle between V_1 and V_2
ΔV_{DC}	Voltage margin between DC voltages
f_{wf}	Wind farm frequency
f_{wf_rated}	Rated wind farm frequency
i_{abc}	Three phase current
i_{a_damp}	Phase a damping current
i_{b_damp}	Phase b damping current
i_{abc_damp}	Three phase damping current
I_A	Current at terminal A
I_B	Current at terminal B
I_C	Current at terminal C
i_d	Current in the d-axis
i_{d_ref}	Reference current in the d-axis
i_q	Current in the q-axis
i_{q_ref}	Reference current in the q-axis
k_f	Co-efficient of frequency deviation
OP_A	Operating point of terminal A
OP_B	Operating point of terminal B
OP_C	Operating point of terminal C
P	Active power
P_{ref}	Reference active power
P_{wf}	Wind farm power
P_{wf0}	Wind farm power initial power
$P_{chopper}$	Power dissipated in the DC chopper
Q	Reactive power
Q_{ref}	Reference reactive power
$R_{chopper}$	DC chopper resistance
V_1	Voltage at the sending end of a transmission line
V_2	Voltage at the receiving end of a transmission line

V_{abc}	Three phase voltage
V_{amp_a}	Phase a voltage from the amplifier converter
V_{amp_b}	Phase b voltage from the amplifier converter
V_{amp_c}	Phase c voltage from the amplifier converter
V_{ac_wf}	Wind farm AC voltage
$V_{ac\_wf\_rated}$	Rated value of wind farm AC voltage
V_{d}	Voltage in the d-axis
V_{d_ref}	Reference voltage in the d-axis
V_{d_ssr}	SSR damping voltage in the d-axis
V_{dc}	DC voltage
V_{dc_ref}	Reference DC voltage
V_{dc_start}	Threshold DC voltage for controller activation
V_{dc_max}	Maximum DC voltage
V_{q}	Voltage in the q-axis
V_{q_ref}	Reference voltage in the q-axis
V_{q_ssr}	SSR damping voltage in the q-axis
X	Reactance
X_{21}	Reactance of transformer at bus 2
X_{22}	Reactance of transmission line to bus 2
X_{11}	Reactance of transformer at bus 1
X_{12}	Reactance of transmission line to bus 1
X_{3}	Reactance of transmission line to bus 3
X_{C}	Reactance of series capacitor
X_{LINE}	Reactance of general transmission line

List of Figures

List of Tables

Chapter 1 -

Introduction

1.1 BACKGROUND

Over the coming decades it is expected that the energy requirements of the global population will increase, this is shown in Figure 1.1. OECD (Organisation for Economic Co-operation and Development) countries such as the UK and USA, show a slight rise in energy consumption. Non-OECD countries undergoing major development and growth such as Brazil, Russia, India and China show a large rise in energy consumption [1]. This increased energy demand comes at a time when the world's fossil fuel resources are becoming depleted and concern grows about the effect human beings are having on the Earth. The International Energy Agency (IEA) predicts that the share of global energy derived from fossil fuels will fall from 81% in 2010 to 75% in 2035 [2].

The nations of the European Union have committed themselves to reduce their emissions of Greenhouse Gases (GHG), by the year 2020 and onwards [3]. The Committee for Climate Change suggests energy targets of 15% renewable generation

by 2020 to meet the GHG reduction targets [4]. The Electricity Market Reform (EMR) white paper sets out the UK's strategy for achieving a low-carbon economy [5–7].

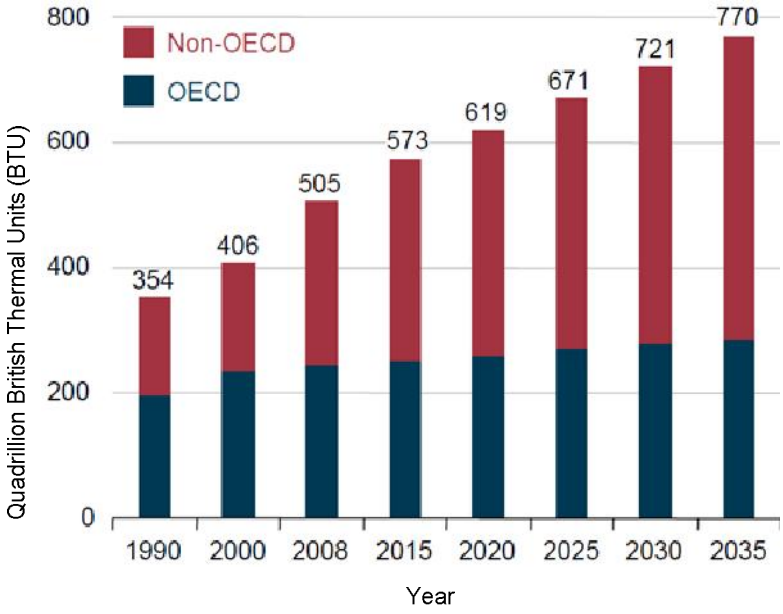

Figure 1.1: World Energy consumption 1990-2035 [Quadrillion British Thermal Units (1 Quadrillion BTU = 1.05×10^{18} joules)] [1]

In the UK, renewable generation is increasing quickly. At the end of 2011, UK electricity capacity from renewable generation sources totalled 12.2GW, an increase of 2.9GW from the end of 2010 [8].

1.2 OFFSHORE WIND FARMS

To meet demanding energy targets, national governments are turning to mature renewable technologies such as wind to fulfil a large part of the generation targets [9–12].

The UK's most plentiful resource of renewable energy is wind power and is therefore expected to form a major part of future generation [13]. During 2011, onshore wind capacity increased by 596MW and offshore wind capacity increased by 497MW. Several large offshore wind farms are being developed such as Ormonde, Greater Gabbard, Walney and Sheringham Shoal [8].

Offshore wind farms planned for UK's territorial waters are administered by The Crown Estate and a cumulative capacity of 16GW is planned for 2020 [14]. This is illustrated in Figure 1.2 which shows the Transmission Entry Capacity (TEC) of offshore wind farms up to the year 2020.

The distribution of planned offshore wind farms is shown in Figure 1.3 [13]. The wind farms of higher capacity are further from the shoreline and will therefore require long distance submarine transmission.

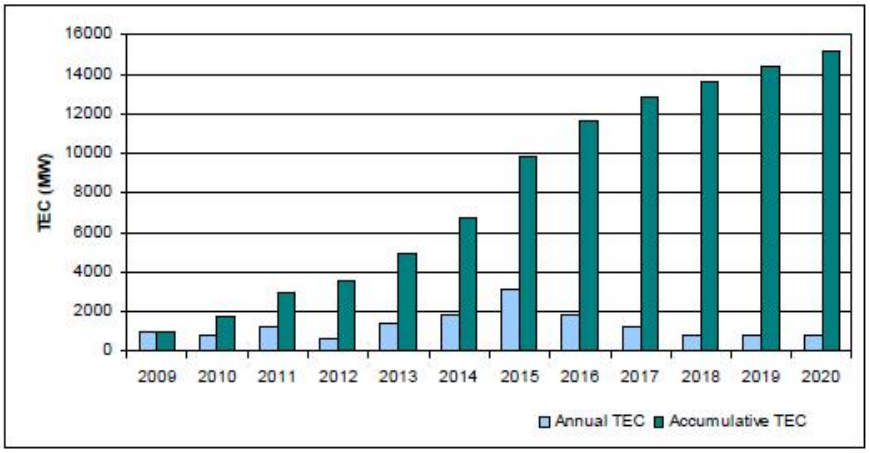

Figure 1.2: Transmission Entry Capacity (TEC) for offshore generation projects [14]

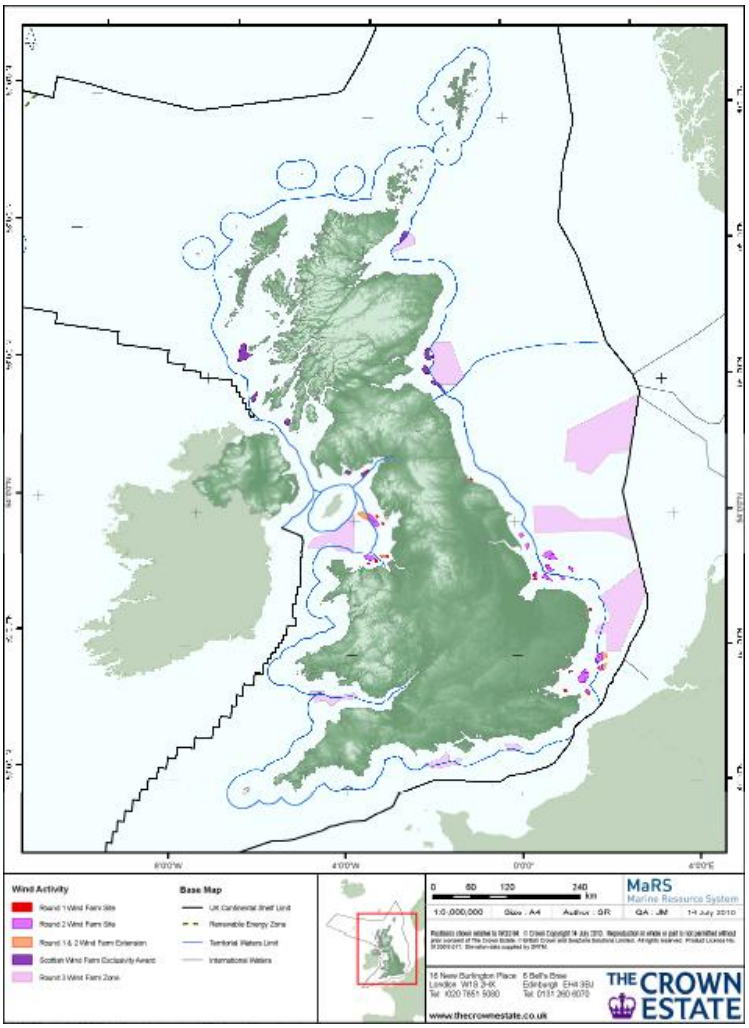

Figure 1.3: Offshore wind development map [13]

1.3 HVDC TRANSMISSION

All submarine transmission will need to use cables. However, AC cables suffer from a loss of active power capacity due to cable charging currents. This reactive current is the result of cable capacitance, increasing with cable length [15]. Therefore, it will not be possible to use AC cables to transport power from distant offshore wind farms

These wind farms will therefore need to be connected through HVDC links, which does not suffer from such reactive power limitations. It is possible for power to be transmitted great distances by DC cable. However, transmission at DC requires AC/DC conversion at either end of the cable, which incurs power losses and expense. The 'break even distance', that is the distance where DC becomes more economically

attractive than AC, for cables is typically 40-70km [16]. An example of a wind farm where HVDC would be essential is Dogger Bank which is located 125-290km offshore [17].

1.4 THE GB TRANSMISSION SYSTEM IN 2020

The shift from centralised onshore generation to offshore generation requires the UK transmission system to be reinforced and expanded. As renewable generation needs to be sited where the fuel source is most plentiful, the efficient transmission of electricity becomes more important.

The Electricity Networks Strategy Group (ENSG) has produced a report into the reinforcements required to facilitate the connection of planned generation to the GB transmission network by 2020 [18]. As the majority of the load is in the south of England and many generation sites are planned in Scotland, particular pressure on the England-Scotland boundary is expected. The existing transmission network at this boundary consists of two 400kV double circuits, on the east and west coast of the country. Due to planning restrictions, it is unlikely permission would be given for an additional overhead line.

Figure 1.4 shows the proposed improvement in transfer capacity of the Scotland-England transmission boundary in the years up to 2020.

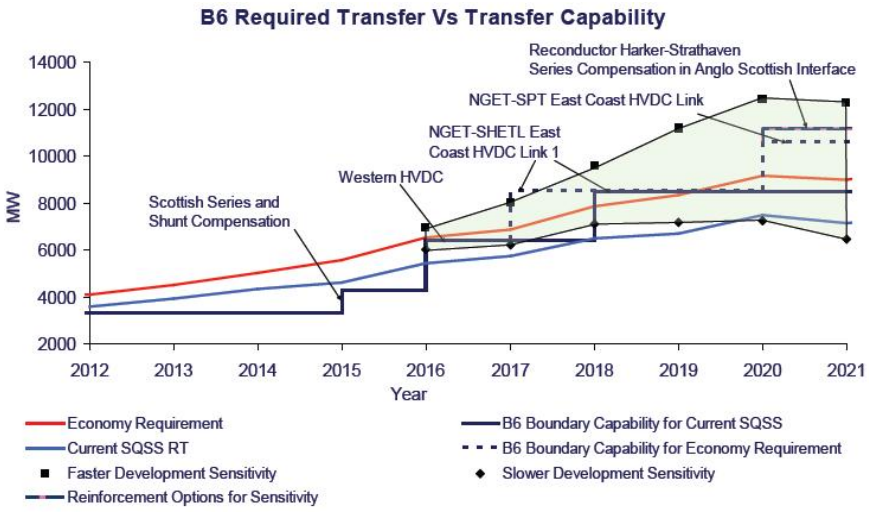

Figure 1.4: Transfer capability across the England-Scotland border [18]

To ease congestion at this boundary a number of solutions are proposed in the ENSG report:

- 2.1GW Eastern HVDC Link from Peterhead in Scotland to Hawthorne Pit in England.
- 2.1GW Western HVDC Link from Hunterston in Scotland to Deeside in England
- Series and shunt compensation within the AC systems
- Re-conductoring existing AC overhead lines.

The presence of series compensation in the GB system will not only alter line characteristics and their transient behaviour, but could also cause Subsynchronous Resonance (SSR) [19].

1.5 MORAY FIRTH MULTI-TERMINAL HVDC SYSTEM

A project in the north of Scotland represents the first opportunity for a multi-terminal HVDC network. The Caithness-Moray-Shetland (CMS) project [18], [20], [21] is considered as an 'offshore HVDC hub' connecting the island of Shetland with two onshore terminals either side of the Moray Firth.

The solution in Figure 1.5 shows the most economic and flexible way of connecting the wind farms from the generation rich island of Shetland with mainland Scotland. The proposed solution is a Multi-Terminal HVDC (MTDC) network consisting of three onshore terminals and an offshore hub terminal.

However, at this time MTDC networks present many technical challenges. In particular, the control and protection of such networks is immature. MTDC is the subject of research and development in academia and industry alike.

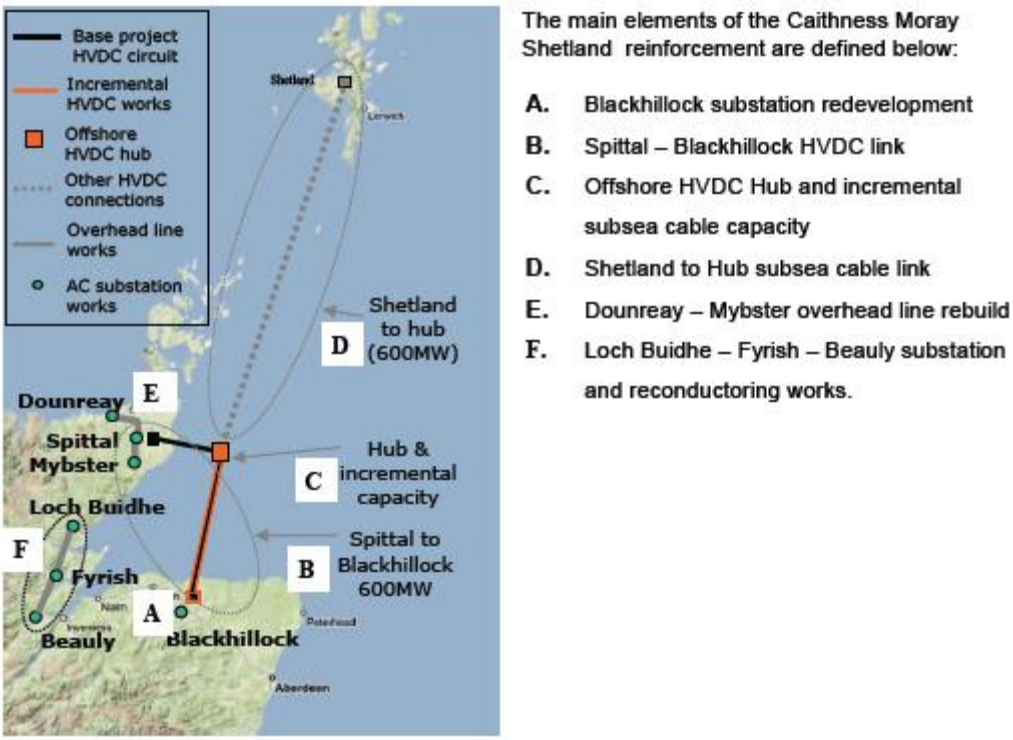

Figure 1.5: Caithness - Moray - Shetland potential reinforcements [18]

1.6 RESEARCH OBJECTIVES

The objective of this thesis was an investigation into the feasibility and capability of Voltage Source Converter (VSC) HVDC for the integration of offshore wind farms. Particular contributions in this area are:

- To design a control system for the damping of subsynchronous resonance in the 2020 GB transmission system. This was achieved through the addition of an auxiliary control loop within the control system of a VSC.
- To design and build a laboratory based experiment to demonstrate the auxiliary subsynchronous resonance damper. The AC system was simulated on a real time simulator connected to an experimental VSC rig.

- To design several fault ride through control systems for multi terminal HVDC networks, using power reduction and power dissipation techniques.
- To design and build a laboratory experiment to demonstrate the fault ride through control systems. A multi terminal VSC test rig was interfaced to a power systems simulator to model an onshore AC fault.

1.7 THESIS STRUCTURE

The thesis consists of 6 chapters.

Chapter 1 outlines the relevant policy drivers for offshore wind farms and HVDC in the UK.

Chapter 2 contains a literature review of previous research into the use of HVDC in power systems. The chapter begins with the history of HVDC and the architecture and operation of HVDC converter technology. The relative advantages and disadvantages of the different types of converter for multi-terminal HVDC networks are discussed. Previous work related to fault ride through of wind turbines and point-to-point HVDC links is described. The phenomenon of SSR is described and the negative implications of subsynchronous resonance are discussed. Relating SSR to the GB network reinforcements, the potential sources of SSR are described. Previous work on an IEEE benchmark model for SSR studies is referenced.

Chapter 3 describes a controller for damping SSR using a VSC. An existing AC network model for the GB transmission system is described, with modifications to suit the 2020 transmission system. The AC network model is simulated with a series compensated transmission line, the results show that SSR occurs. A planned offshore HVDC link between Scotland and England was considered for damping SSR. Using a VSC-HVDC link an auxiliary controller is designed to damp external SSR power oscillations in the onshore transmission system. The controllers are designed to provide the primary functionality of a HVDC link such as active and reactive power regulation. The controller design was tested with PSCAD simulation software.

Chapter 4 describes an experiment designed to demonstrate the operation of the SSR damper devised in Chapter 3. The experiment uses a Real Time Digital Simulator (RTDS) to model the AC system, whilst a real time VSC-HVDC test rig models the DC system. The results from the experiment are compared with the simulation results from Chapter 3.

Chapter 5 describes several control systems for the Fault Ride Through (FRT) capability of MTDC networks during AC onshore grid faults. Power reduction and power dissipation methods are compared with a combined power reduction and dissipation method as an optimum commercial and technical solution. The controller designs are tested with PSCAD simulation software and on a laboratory based experiment. The experiment uses a VSC-HVDC test rig to model the multi-terminal DC network, the onshore fault is provided by a Power Systems Simulator (PSS). A comparison is drawn between the simulation and experimental results.

Chapter 6 outlines the conclusions from the work described in the thesis. Future work for the development of an adaptive SSR damper is discussed.

Chapter 2 -

Literature Review

2.1 HISTORY OF HVDC

The history of HVDC stems from the War of Currents in the late 19th century. With the electrification of towns and cities in its infancy, the decision over whether to use AC or DC was an important one [22], [23]. Ultimately AC won the war, primarily due to the invention of the transformer, making AC transmission the standard since this time.

However, DC transmission always maintained a role within niche projects, such as the 20MW interconnection between the island of Gotland and mainland Sweden in the early 1950's [24], [25]. The submarine transmission distance of 96km would have been too far for conventional AC cable transmission due to reactive power limitations.

HVDC evolved through many types of converters between the 1950's and the present day [26] as shown in Figure 2.1. Early HVDC projects used mercury arc valves, an evacuated chamber containing a cathode formed of mercury and an anode of carbon [27]. Upon heating an arc is formed, conducting electrons from the cathode to the anode, forming a rectifier. In the 1970's semi-conductor thyristors were developed. These devices conduct when a gate pulse received, continuing until the voltage is

reversed [28]. For HVDC applications, thyristors are often placed in series and parallel to achieve the current and voltage ratings that are required. In the modern day, project designers have a choice between thyristor based converters and Insulated-Gate Bipolar Transistors (IGBT's). The IGBT is semiconductor device, with full control over switching the device on and off [29]. This brings advantages in the form of advanced control of the HVDC valve, allowing the converter station to become more flexible.

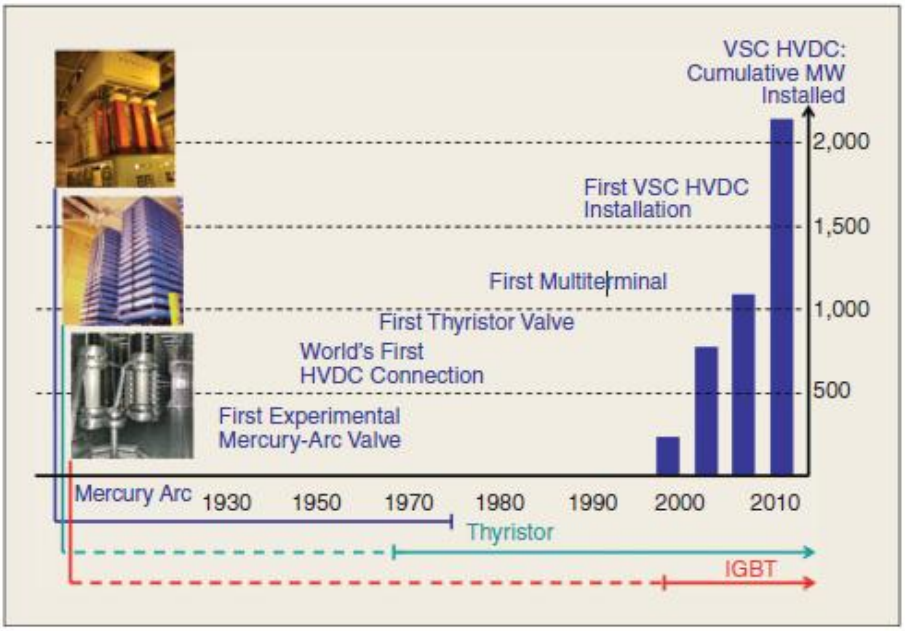

Figure 2.1: History of HVDC Systems [25]

HVDC schemes are often classified by the converter devices and their operation [30]. In Current Source Converters (CSC), the DC current is kept constant with a small ripple using a large inductor, thus forming a current source on the DC side. Typically a CSC uses thyristor valves and requires a strong synchronous voltage source in order to commutate from one valve to another. In Voltage Source Converters (VSC), the DC voltage is kept constant and the converter typically uses IGBT's this means that they are able to self commutate between valves.

HVDC schemes can be used to fulfil many power system needs such as: back-to-back converters connecting asynchronous or weak AC systems, long distance overhead

transmission, underground and submarine cable transmission and the increasing connection of renewable generation [16].

2.2 CURRENT SOURCE CONVERTER

Conventional HVDC transmission uses line commutated, current source converters based on thyristor valves. HVDC conversion is achieved through the use of a 6-pulse Graetz bridge, where the 3-phase supply commutates six times within a period [16]. Although the bidirectional transfer of active power is possible, the converter can only absorb reactive power. The commutation is performed by the voltage source and the leakage reactance of the converter transformer generally dominates the commutation circuit, in addition the firing angle of the thyristor dictates the level of reactive power consumption. Therefore, the fundamental component of the current lags the voltage.

LCC based systems are highly reliable and are used extensively, either for long distance connections or back-to-back converters connecting asynchronous AC systems.

2.2.1 ARCHITECTURE AND OPERATION

The basic architecture of a CSC is a six-pulse converter bridge consisting of thyristor valves shown in Figure 2.2.

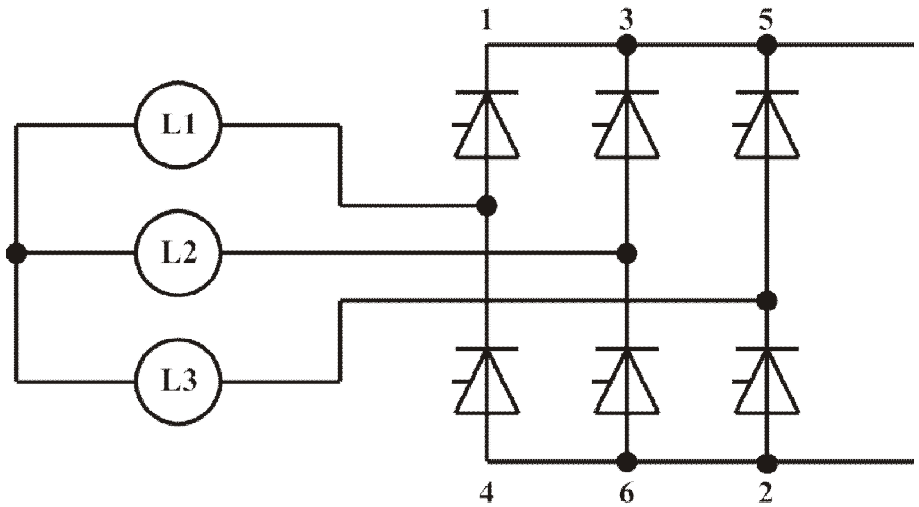

Figure 2.2: Six-pulse converter bridge consisting of thyristor valves

For current to flow through the valve the voltage across the valve should be positive and a firing pulse must be given to the thyristor. The current flow will end once the voltage across the valve becomes negative. The instant when the valve starts to conduct current or 'turn-on' can be controlled by delaying the firing pulse. This method permits the average value of the outgoing voltage of the converter to be changed. The instant when current conduction ends or 'turn-off' cannot be controlled as the reversal of current is external to the converter [31].

2.2.2 CONTROL OF TWO-TERMINAL CSC'S

A schematic for an HVDC point-to-point bipole link comprising of CSC converters is shown in Figure 2.3.

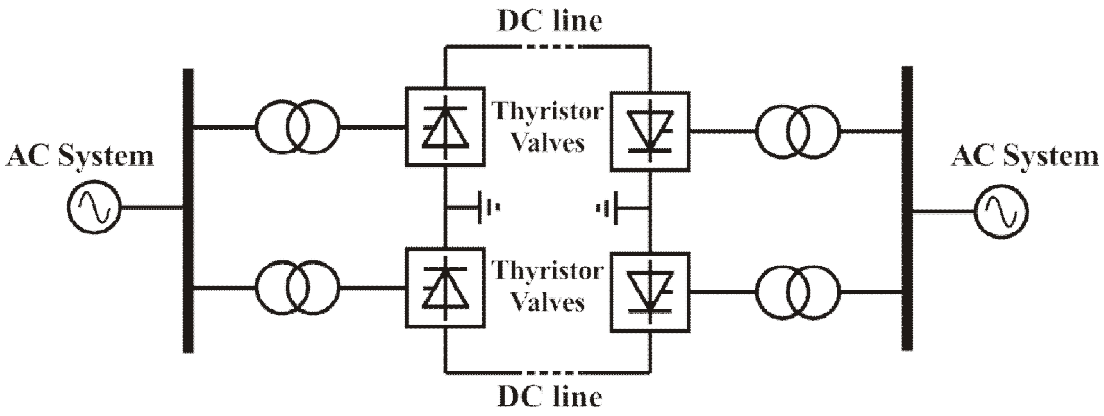

Figure 2.3: Schematic of a point-to-point CSC in bipole configuration

In a point-to-point scheme, the DC current is controlled by generating a larger voltage at the rectifier with respect to the inverter, thus creating a voltage drop across the transmission line resistance.

Hence DC voltage and DC current are fully controllable. Usually the inverter controls DC voltage, leaving the rectifier free to control DC current by varying its voltage. This is because in a fault condition, the fault current is limited at the rectifier, protecting the DC plant and cables.

The main parameters used to control DC voltage are the AC voltage, usually through a transformer on-load tap changer, and the firing angle of the thyristors. The response of changing firing angle is much faster, as this can be achieved on a cycle by cycle basis. A

tap change is a mechanical process and therefore is slower. In reality, it is often beneficial to use a combination of firing angle control and AC voltage control to meet the control objectives [15].

To ensure smooth operation, the control system operates a hierarchy of layers designated as station control, pole and valve control [29]:

1. *Station Control*: This high level control gives power orders and also manages auxiliary functions such as harmonic filter switching and shunt capacitors, which may need to be switched in or out due to changing conditions.

2. *Pole Control*: This layer derives the firing order of the pole converters following signal to change a power or DC voltage order.

3. *Valve Control:* This valve controller specifies the firing instants of the valves within a bridge and is also responsible for defining the firing angle limits.

Two-terminal CSC projects continue to increase in capacity, in 2010 a ±800kV DC system in Guangzhou, China was commissioned [32]. This link connects the large generation areas in western China with the large load areas of eastern China.

2.3 VOLTAGE SOURCE CONVERTER

Using VSC's allows a more flexible HVDC transmission solution based on using self commutating, fully controllable valves such as the IGBT. The technology is a development of low power motor control converters, which are now applicable to HVDC due to the increase in their valve ratings.

Advantages of VSC-HVDC over CSC-HVDC include the absence of commutation failure, they are fully functional with weak or passive AC grids, full control over active and reactive power, the terminal footprint is smaller and terminals can operate as STATCOM's when not connected to the DC line [33].

2.3.1 ARCHITECTURE AND OPERATION

The architecture of VSC converters have been constantly developing in recent times. Topologies fall generally into two categories; Two/Three Level Pulse Width Modulation (PWM) Converters and Multi-Level converters [34].

2.3.2 TWO/THREE LEVEL PWM CONVERTERS

Early VSC projects used two-level voltage converters, which use PWM to switch between voltage levels as shown in Figure 2.4. The sinus shaped waveform is formed through smoothing reactors.

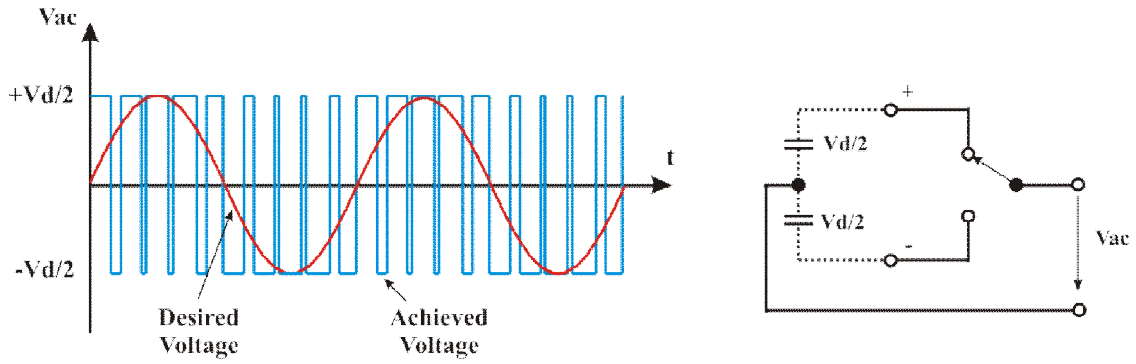

Figure 2.4: Two-level PWM waveform (left) and topology (right)

Uniform voltage distribution is ensured through switching all series connected devices simultaneously. The large voltage steps cause high component stresses, harmonics and high frequency noise.

A commercial topology is ABB's HVDC Light© solution [35]. This topology has been used in projects such as Troll A project in Norway, a HVDC point-to-point link connects the offshore natural gas platform with Norway's onshore grid [36].

The waveforms can be improved through a third level shown in Figure 2.5, although AC filters are still required. These are the product of topologies such as the diode-clamped neutral point converter and the flying capacitor converter described in [37].

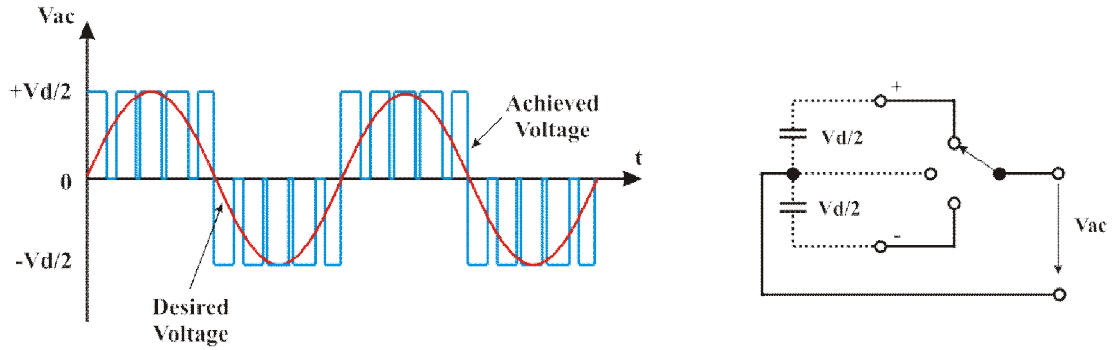

Figure 2.5: Three-level PWM waveform (left) and topology (right)

2.3.3 MULTILEVEL CONVERTERS

Recently commercial and academic research has been focussed on multi-level topologies, which use smaller voltage steps to build a sinus waveform.

A typical example of a commercial multilevel topology is Siemens Modular Multilevel Converter (MMC), HVDC Plus© [38]. In this topology the MMC consists of six converter arms, with each arm containing power modules in series. Each power module can be controlled individually to either charge the capacitor within the module or leave the capacitor unchanged. This builds the voltage in small voltage steps as power modules are switched in and out. The development of a sinus waveform can be seen in Figure 2.6. The MMC topology has been used successfully in the Trans Bay Cable project in San Francisco, USA [39].

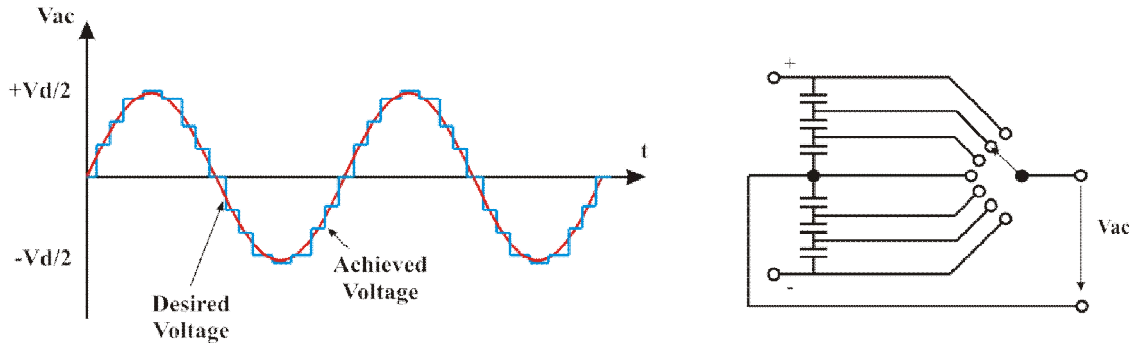

Figure 2.6: Multi-level MMC waveform (left) and topology (right)

Alstom Grid's HVDC MaxSine© topology [40] works in a similar way. The voltage waveform is created through the use of multi-level converter cells, however the

current is directed to the appropriate DC or AC network through series IGBT director switches [41].

The benefits of such approaches compared to PWM topologies are: lower component stresses, lower generation of harmonics, lower switching losses and omission of snubber circuits [42], [43].

2.3.4 CONTROL OF TWO TERMINAL VSC'S

A schematic for a HVDC point-to-point link comprising of VSC converters can be seen in Figure 2.7.

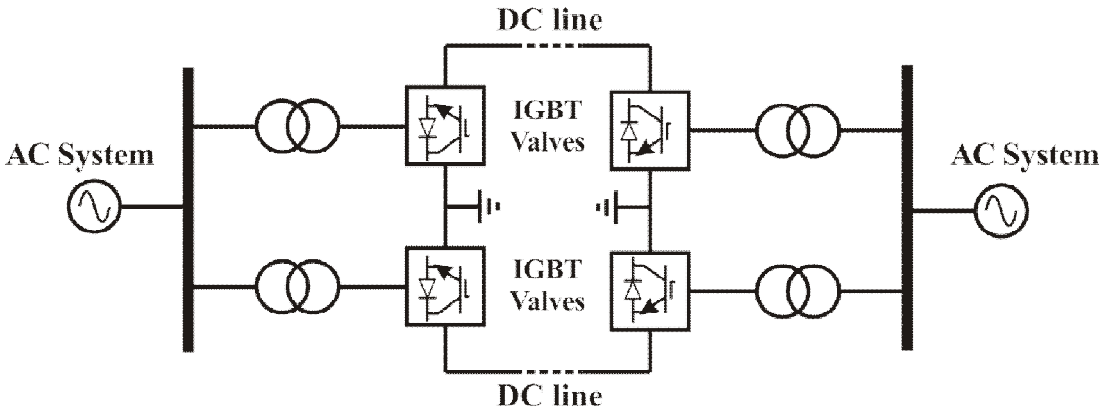

Figure 2.7: Schematic of a point-to-point VSC in bipole configuration

VSC imposes no restriction of current direction, so the direction of power flow can be changed without the need to reverse voltage polarity. However, there is a requirement for the voltage polarity remain the same [44].

In two terminal schemes, it is common for one converter to operate in DC voltage regulation mode (slack bus) and one converter to operate in power regulation mode. Unlike CSC there is no restrictions on which terminal provides voltage or power control. The system can, therefore, be designed to suit the AC systems (the power controlling converter at the weaker AC system side).

VSC converters can control power injected into DC lines through voltage magnitude and voltage angle control with AC systems. The voltage magnitude and angle of the AC system are set by the configuration of the onshore AC system, whereas the voltage

magnitude and phase of the converter can be fully controlled [45]. Controlling the converter relative to the AC system allows a controlled voltage drop across the total reactance (valve reactance plus the leakage reactance of the converter transformer) to determine the reactive current through the converter [29].

Real power is controlled by a change in phase angle:

$$P = \frac{v_1 v_2}{x} sin\delta_v \quad (1)$$

Whereas, reactive power is controlled by a change in voltage magnitude:

$$Q = \frac{v_1 v_2}{x} cos\delta_v - \frac{v_2^2}{x} \quad (2)$$

Alternatively the system can operate in dq control mode, where three phase voltages and currents are transformed to a direct-quadrature reference frame [46]. In this control scheme, secondary controls are used to set whether the converter is operated as a DC voltage regulation bus and the other in real power regulation bus. This provides current reference orders; the measured currents are controlled to match these orders by the primary current controllers.

For a point-to-point scheme where one terminal is a wind farm, a typical control scheme would be to operate the wind farm side as the power regulation terminal (to establish the wind farm AC voltage) and the onshore grid connection as the DC voltage regulation bus [47]. Figures 2.8 and 2.9 show typical control systems for power regulation and DC voltage regulation assuming multilevel VSC converter are used.

For point-to-point schemes between two onshore AC grid terminals, a typical control system would be to operate one terminal as constant power regulation and with the other operating in DC voltage regulation mode [48].

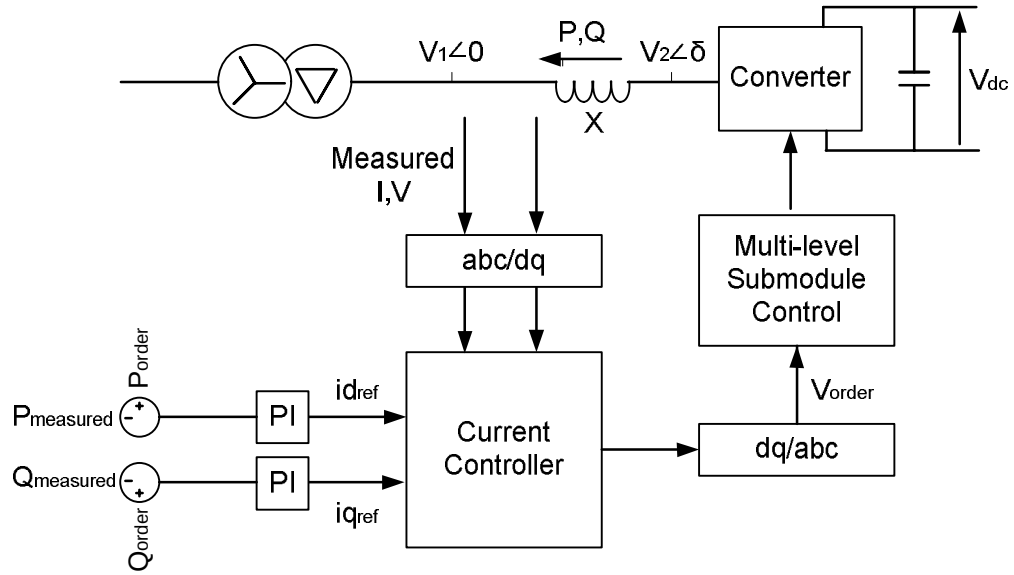

Figure 2.8: dq control scheme for a power regulation terminal

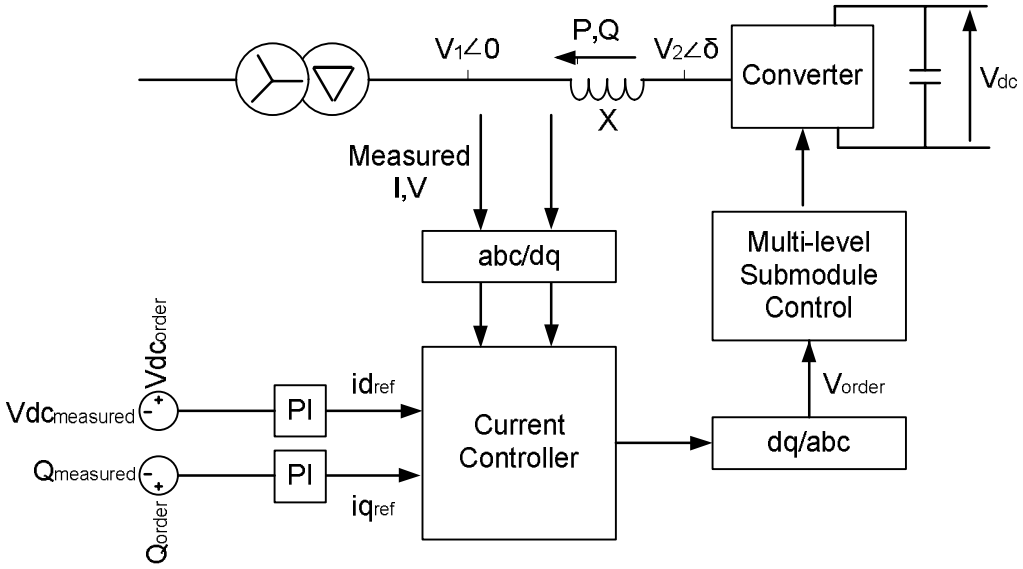

Figure 2.9: dq control scheme for a DC voltage regulation terminal

2.3.5 HIGH LEVEL/AUXILARY CONTROL FOR CSC'S AND VSC'S

In addition to controlling the HVDC link in 'steady-state' conditions, coordinated system control functions are often included for such capabilities as frequency control, power modulation control and power demand override.

Taking the example of power modulation control, the power being transferred through a HVDC link can be automatically modulated typically in the range 0.1 to 2Hz. This is to provide damping to low frequency power oscillations within either, or both, interconnected AC systems as determined by studies during the design phase of the HVDC scheme as shown in Figure 2.10 [15].

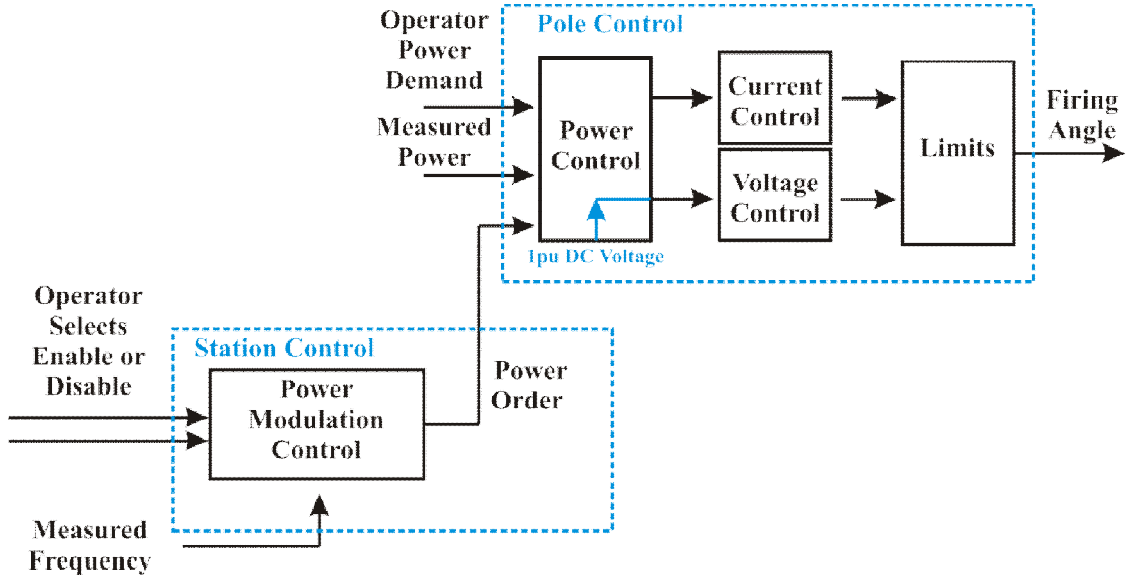

Figure 2.10: Typical power modulation controller [15]

2.4 MULTI-TERMINAL NETWORKS

Two terminal HVDC projects are well established and provide transmission links between areas of generation and demand. However, for the technology to evolve, multi-terminal HVDC (MTDC) grids are needed to improve redundancy, flexibility and cost effectiveness. With prototype DC breakers described [49] and power ratings of VSC converters improving, technical barriers to MTDC grids are being removed.

The prime candidate for an MTDC grid could be the North Sea [50–52]. European governments have supported this through the North Sea Countries Offshore Grid Initiative (NSCOGI) [53], [54]. The large number of wind farms in this area, combined with the benefits of interconnection between nations makes this an attractive proposition.

2.4.1 LIMITATIONS OF CSC'S IN A MULTI-TERMINAL ENVIRONMENT

Following the success of two-terminal CSC-HVDC schemes, the next logical step was to extended towards Multi-Terminal HVDC (MTDC) networks. Multi-terminal projects such as the SACOI (Sardinia-Corsica-Italy) and the Quebec-New England (Q-NE) project were developed in the early 1990's. The Q-NE project was originally intended to consist of five terminals, however due to reliability issues, only three terminals remain connected [55].

Table 2.1 below details the behaviour of MTDC networks consisting of CSC and VSC technology from the CIGRE report on the feasibility of MTDC grids [56].

Table 2.1: CSC and VSC comparison for MTDC networks [56]

	CSC	VSC
Power Reversal	Mechanical switches for voltage reversal as the current cannot change sign.	Change of current direction within the converter. There is no need for mechanical switches.
AC Disturbance	Commutation failure: short circuit of the HVDC grid for some time.	No more influence than some loss of active power.
AC Connection	Limited to medium and high short circuit capacity networks.	Connection to electrically weak AC-network or even black AC-network. Fault ride through capability.
AC Voltage Support	Always consumes ~50% reactive power.	Support of reactive power.
DC Side Short Circuit	DC grid breaker needed in overlay HVDC grid.	DC grid breaker needed in overlay HVDC grid.

With the likelihood being that MTDC network will require the flexibility to include wind farms and other weak AC networks, along with the difficulties of power reversal, VSC technology offers a better option for MTDC networks.

The main technical challenges associated with achieving MTDC grids regard the control and protection of such networks. Although some VSC-MTDC projects are in the planning stage, no project has yet to be completed.

2.4.2 STEADY STATE CONTROL OF VSC-MTDC

A simple form of MTDC network control is the voltage margin method described in [57] and shown in Figure 2.11. This control system assigns one converter the role of slack bus. As this converter reaches its voltage limit, it switches to constant power control. Instead another converter becomes the slack bus. The control scheme could work well for small MTDC networks with converters of similar ratings. However for large MTDC networks with converters of different capacities, constant changes to the converters operating conditions would make the system volatile.

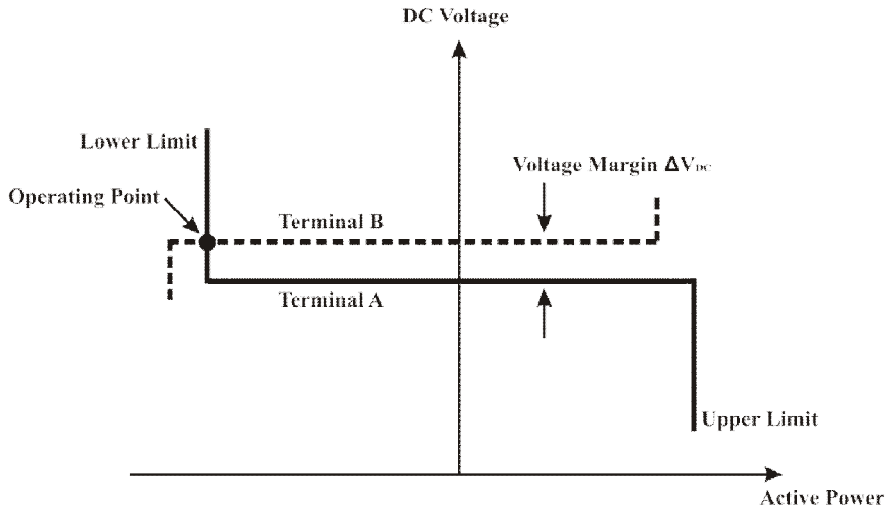

Figure 2.11: Operating point for a two terminal system using the voltage margin method [57]

Alternatively, a single slack bus converter could be replaced by sharing the voltage regulation across several converters, described as voltage droop control [58], [59]. This is an adaption of the operation of AC networks and therefore well understood by the power systems community, the operating points of a three terminal system are shown in Figure 2.12. Here the two wind farm terminals have an overlapping DC voltage droop characteristic, which allows the DC voltage to increase or decrease in a smoother fashion in the DC network.

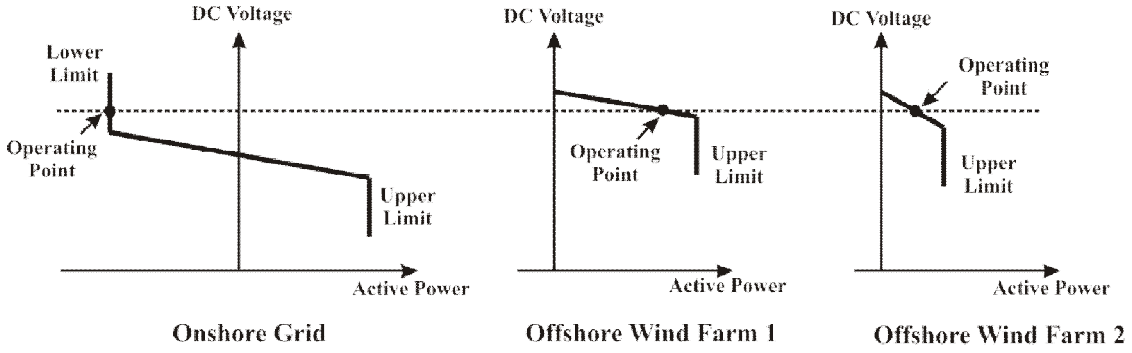

Figure 2.12: Operating point for a three terminal system using droop control [59]

Autonomous converter control of a MTDC grid is presented in [60] by Alstom Grid. Here AC network control practices are applied to a MTDC networks. Each converter is given a target DC voltage called a Load Reference Set Point (LRSP) and aims to match the reference as shown in Figure 2.13. The three coloured lines represent three separate terminals. This is similar to the target AC frequency reference sent to power plants for primary frequency response.

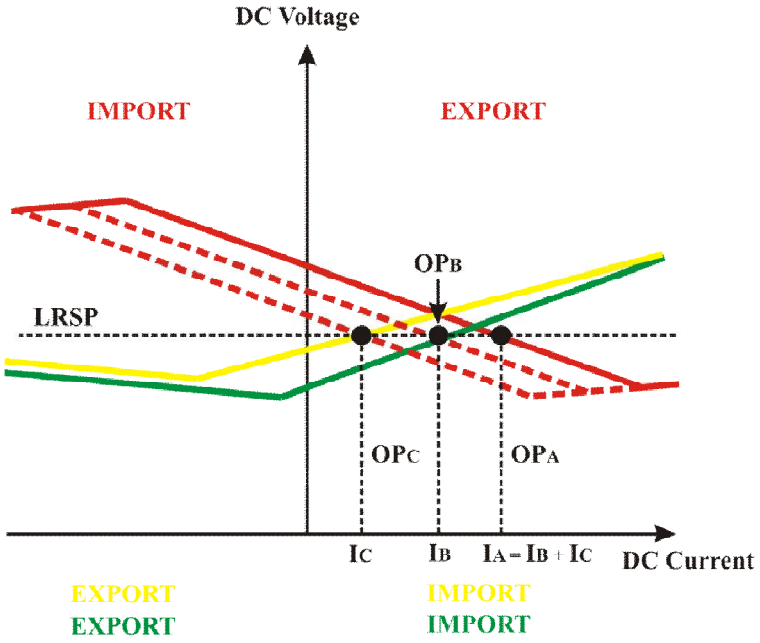

Figure 2.13: Operating points for a three terminal system using autonomous control [60]

The merits of combining voltage margin and droop are explored in [61] with undead-band voltage droop control. Here the MTDC network operates at a reduced droop close to the operating point and with a steeper droop close to voltage limits. This helps

to keep active power balance within large MTDC networks. The operating point for a single converter using undead-band control is shown in Figure 2.14.

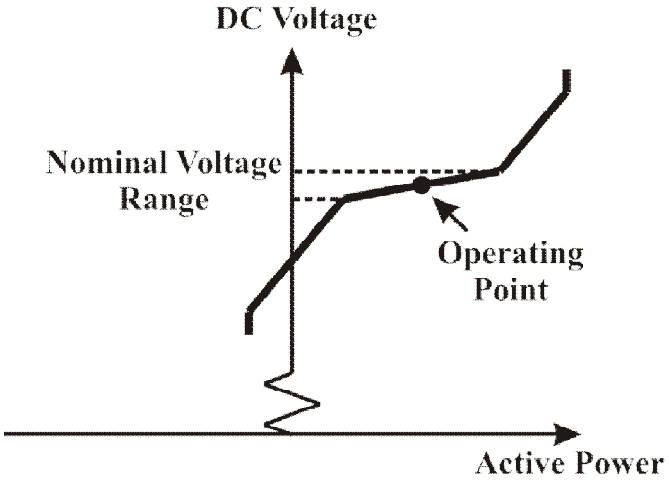

Figure 2.14: Operating point for a converter using undead-band droop control

2.4.3 PROTECTION REQUIREMENTS OF MTDC NETWORKS

AC circuit breakers have been understood and used in AC networks since transmission systems have been operational. Upon opening of the circuit breaker, arcs between the circuit breaker contacts are extinguished at current zeros. However in DC systems, DC current has no zeros so arcs remain, damaging the contacts. However with high power DC circuit breakers in the prototype stage [49], this problem should be overcome.

The protection of a MTDC network is described in [62], which uses DC circuit breakers and fast DC switches. In [63] the topologies of MTDC networks are investigated to find the optimum arrangement, minimising DC circuit breakers.

2.5 FAULT RIDE THROUGH FOR MTDC NETWORKS

Fault ride through capability is a key consideration for the operation of offshore MTDC networks, particularly when satisfying the grid codes specified by onshore transmission operators [64]. Most European Grid Codes specify that during short-term reductions in terminal voltage, generators should remain connected to the grid. This is often illustrated through voltage-time limit curves [65], National Grid Ltd defines FRT connection limits for the Supergrid through the curve in Figure 2.15.

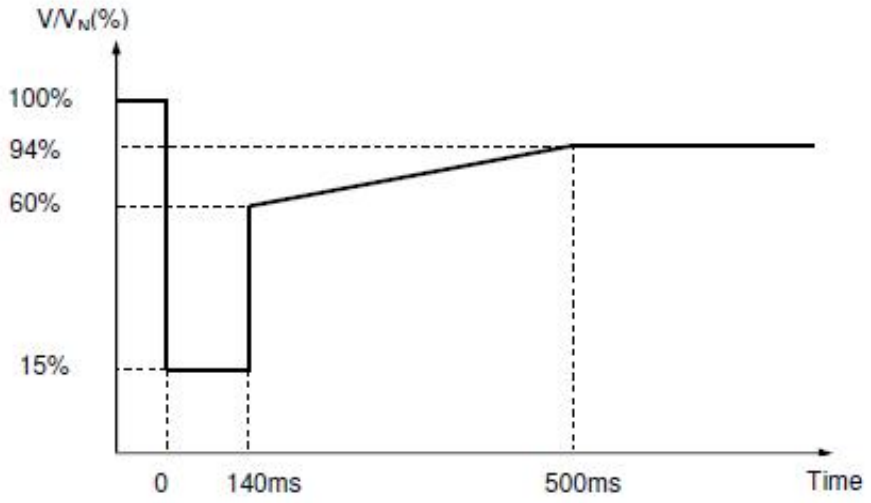

Figure 2.15: National grid FRT requirement for the Supergrid [65]

If there is a drop in AC voltage near an onshore converter, power cannot be completely transferred to the AC grid through this converter. This will cause an imbalance in the power imported and exported from the DC network which will in turn cause an under/over-voltage of the DC grid. A multi-terminal HVDC network has an advantage over a point-to-point HVDC link because some power can still be transferred between the DC and AC grids through other AC grid-connected converters.

Fast fault ride through approaches are required to reduce DC overvoltages, where DC currents are limited by constraints within the converters. DC overvoltages can be responsible for damage to cables and equipment. A number of methods to prevent DC overvoltages have been proposed in the literature [47] [48], which can be broadly grouped as:

- Fast communication systems to de-load wind turbines
- Local control using DC chopper circuits in the DC network
- Reduction of power from wind generators without communications

2.5.1 FAST COMMUNICATIONS SYSTEMS TO DE-LOAD WIND TURBINES

Fast communication systems can be used to reduce the power from the wind turbines when faults occur within AC onshore networks. In [68] a DC voltage droop controller for de-loading Fully Rated Converters (FRC's) was implemented.

The disadvantage of this approach is the reliability and inherent delays in communications, which means that the power reduction may not be quick enough to protect equipment from DC overvoltage damage.

2.5.2 POWER DISSIPATION USING A DC CHOPPER CIRCUIT IN THE DC NETWORK

A robust solution for power dissipation is the introduction of a DC chopper circuit into the DC network. In the event of an onshore AC fault the excess energy within the DC network can be dissipated as heat through this DC chopper circuit. Any wind farms connected to the DC network are unaffected by this approach.

In [69] a DC resistor with a simple controller was implemented for fault ride through. The use of a DC resistor with chopper circuit means additional cost and space is required. A severe AC fault may cause the DC chopper resistor to overheat and plant to be damaged on the DC network.

2.5.3 REDUCTION OF POWER FROM WIND GENERATORS WITHOUT COMMUNICATIONS

As a DC rise is detected, the wind farm converters of the VSC-MTDC takes appropriate action to reduce the voltage amplitude of the wind farm AC network so as to reduce the active power imported into the DC network. This in turn reduces the DC voltage to its nominal value as energy balance is restored. Any AC voltage drop in the offshore network would need to be suitable for any machine type that could be connected to the wind farm. The stable operation of the wind turbine relies on a low voltage ride through capability by the turbine [70], [71].

An alternative to reducing the voltage in an offshore AC wind farm network is to increase the frequency of the offshore AC wind farm network. When a variation of the wind farm frequency is sensed by the wind turbine converter through a Phase Locked Loop (PLL), a reduction in active power from the wind turbine occurs. As the frequency change is usually relatively slow, frequency response loops would need to be enhanced to detect frequency change within a few milliseconds.

Voltage reduction and frequency increase power reduction methods both operate without the requirement for fast communication systems. The control signals for wind turbine generators to reduce power output are contained within the wind farm AC voltage (or frequency).

Other work in this area has included a combined method, which uses both frequency increase and voltage reduction controllers. In [58] a decrease in wind farm AC voltage was performed in a multiterminal network as part of the DC voltage droop control scheme. In [72] a two stage controller was implemented, where a small increase in DC voltage is detected, the AC frequency controller is activated to reduce power from the wind turbines through pitch regulation. Under more extreme conditions, where a larger DC overvoltage is detected, a voltage reduction controller is activated.

2.6 SUBSYNCHRONOUS RESONANCE

Given the reinforcements and developments in power systems in the UK, there is a re-emergence of interest in Subsynchronous Resonance (SSR). The IEEE defines SSR as [73]

"...*Subsynchronous resonance* encompasses the oscillatory attributes of electrical and mechanical variables associated with turbine-generators when coupled to a series capacitor compensated transmission system where the oscillatory energy interchange is lightly damped, undamped, or even negatively damped and growing."

From this general description, SSR can be further divided into distinct interactions which generate subsynchronous effects [74]:

Induction Generator Effect (IGE) is a self excitation phenomenon which can occur in steady state conditions. The slip of the machine is negative as the rotor speed is higher than the magnetic field speed. It therefore behaves as an induction generator for induced subsynchronous currents on the machine rotor and exhibits a negative resistance. If the net resistance in the entire armature circuit is negative, self excitation occurs.

Torsional Interaction (TI) occurs when one of the natural torsional modes of the turbine-generator shaft is close to the induced subsynchronous torque in the generator and is more serious than IGE. The result of this interaction is increasing torque shaft oscillations, TI was traced to shaft failures at the Mohave generating station in the USA [75].

Transient Torques results from system disturbances in the network which excites oscillatory torques on the turbine-generator shaft. Following transient conditions, large torques can occur due to SSR interactions. Although these interactions may be damped and the torque decays eventually, repeated occurrences lead to shaft fatigue.

Subsynchronous Control Interactions (SSCI) results from control interaction between voltage sourced converters of Type 3 wind turbines with series compensated transmission lines. This has occurred where system faults have left wind turbines radially connected to series compensated transmission lines [76].

2.6.1 SOURCES OF SSR IN THE 2020 GB TRANSMISSION SYSTEM

The ENSG [18] has detailed the reinforcements planned in the GB transmission system by 2020. These plans include the use of series compensation in the onshore AC network and HVDC links, a potential source of SSR.

Series Compensation

Series compensation is the addition of capacitors in series to a transmission line to reduce the overall reactance of the transmission line. Power transfer across a line can be expressed [77]:

$$P = \frac{V_1 * V_2}{X_{LINE} - X_C} * sin(\delta) \quad (3)$$

where:

P = Active power transfer

V_1, V_2 = Voltages at either end of the transmission line

X_{LINE} = Line reactance

X_C = Reactance of the capacitor

In addition to increasing active power transmission over the circuit, series compensation also increases the angular and voltage stability of the line [78], [79]. This is due to the reduction in the overall reactance of the line which effectively reduces the angular difference (δ) between the line ends. These features have lead to the application of series compensation on long transmission corridors [80].

The GB network is unlike previous series compensated networks as it is tightly meshed. Additional load in England and generation capacity in Scotland have demanded the substantial reinforcement to the Anglo-Scottish AC transmission line. The current constraint on the circuit is 3.3GW due to stability limitations, this is below its thermal limit of 4.5GW [19]. The latest ENSG report [18] proposes multiple potential sites for series compensation across the England-Scotland boundary.

The nature of this series compensation could be either a Fixed Capacitor (FC) or Thyristor Controlled Series Capacitor (TCSC) [81][82]. The most common, simplest and cost-effective method of series compensation is through FC's, although SSR should be considered in this case. TCSC's are a more expensive and complex technical solution, however SSR would be avoided or even damped [83]. By controlling the firing angle of thyristors the effective reactance of the TCSC can be modified, together with the electrical resonant frequency of the compensated line [84].

HVDC Converters

Another source of SSR can be CSC's themselves. Rectifier current controllers can inject large currents into the AC network between 20Hz and 25Hz. Alstom Grid [15] design HVDC control schemes which ensure positive damping for all interactions that their converter controllers generate. EPRI provide a guide for measuring and damping SSR in HVDC systems in [85].

A common method for damping power oscillations (such as SSR) is through active and reactive power modulation [86], [87].

In [88] it is shown that the current controllers in VSC rectifiers do not interact with AC systems in the same way and therefore do not contribute to SSR themselves.

2.6.2 EIGENVALUE ANALYSIS

A common approach for examining the vulnerability of a system to SSR is to perform an eigenvalue analysis. Eigenvalue analysis uses linear, state space equations to evaluate system conditions and find resonant modes. Mathematical models of elements in a power systems network for eigenvalue analysis can be found in literature [74], [89], [90].

2.6.3 IEEE FIRST BENCHMARK MODEL FOR SSR STUDIES

Following concerns regarding the negative impact that SSR could have in power systems, the IEEE Working Group on SSR introduced the IEEE First Benchmark Model (FBM) for SSR Studies [91]. The FBM is a simple power network consisting of an infinite

bus connected to a synchronous generator through a series compensated transmission line as shown in Figure 2.16.

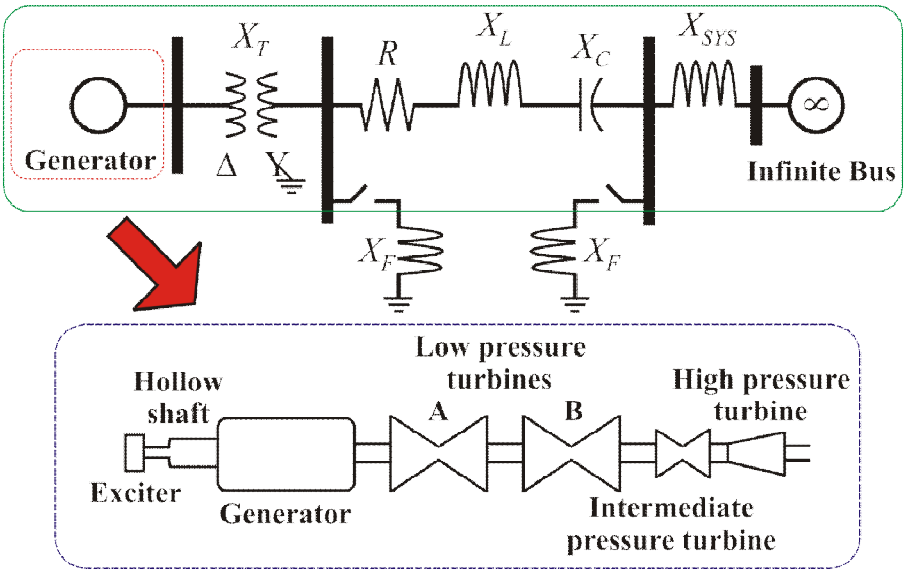

Figure 2.16: The IEEE First Benchmark Model

The FBM is based on a section of the USA's transmission system, the Navajo generation and transmission project [92]. The model consists of an 892.4MVA generator connected via a 500kV transmission line to an infinite bus, operating at 60Hz. To examine the interaction with the turbine-generator shaft, a multi-mass mechanical system consisting of four turbine sections, the generator and an exciter is modelled. Later a Second Benchmark Model, consisting of an additional generator and parallel transmission lines was presented [93].

A complete eigenvalue analysis and state space model of the IEEE FBM is carried out in [94] and the results are expressed in Table 2.2 and Figure 2.17. The IEEE FBM is characterised by four unstable torsional modes (TM1-4), associated with the shaft of the generator, which may become excited at different compensation values. Figure 2.17 plots the ranges of series compensation levels at which interaction and instability may occur. Where the real part of the eigenvalue is negative, the system is stable. Areas where the real parts of the eigenvalue are positive are considered unstable and the system is susceptible to SSR. The unstable areas occur at series compensation levels where the subsynchronous mode (SUB) frequency is in the vicinity of a torsional

mode frequency and is therefore considered a torsional interaction. A torsional interaction is likely to occur between the subsynchronous mode (SUB) and the relevant torsional mode (TM1-4) in this vicinity.

Table 2.2 shows the results of the eigenvalue analysis for a series compensation level of 60%. This example shows that at 60% compensation, the subsynchronous mode (SUB) crosses torsional mode 3 (TM3), here the real part of the eigenvalue is positive.

An eigenvalue analysis has also been carried out on the IEEE 14-bus five machine system in [95]. In this meshed AC system, SSR is also present for certain series compensation levels on certain AC transmission lines. The risk of SSR to generating stations should be assessed on a case by case basis when series compensation is considered.

Table 2.2: Eigenvalues of the IEEE FBM (60% Compensation)

Eigenvalue	Real part [s^{-1}]	Imag. part [*rad/s*]	Frequency [Hz]	Mode of oscillation
1,2	–1.173	±298.174	47.4559	TM5
3,4	–0.2249	±202.7425	32.2675	TM4
5,6	**+0.2984**	**±159.7359**	**25.4228**	**TM3**
7,8	–0.0463	±127.0871	20.2265	TM2
9,10	–0.0895	±99.4971	15.8355	TM1
11,12	–0.4338	±9.7113	1.5456	TM0
13	–40.3219			
14	–24.7941			
15	–2.9386			
16	–0.2135			
17,18	–4.9354	±598.5525	95.2626	SUPER
19,20	**–4.4069**	**±155.9041**	**24.8129**	**SUB**

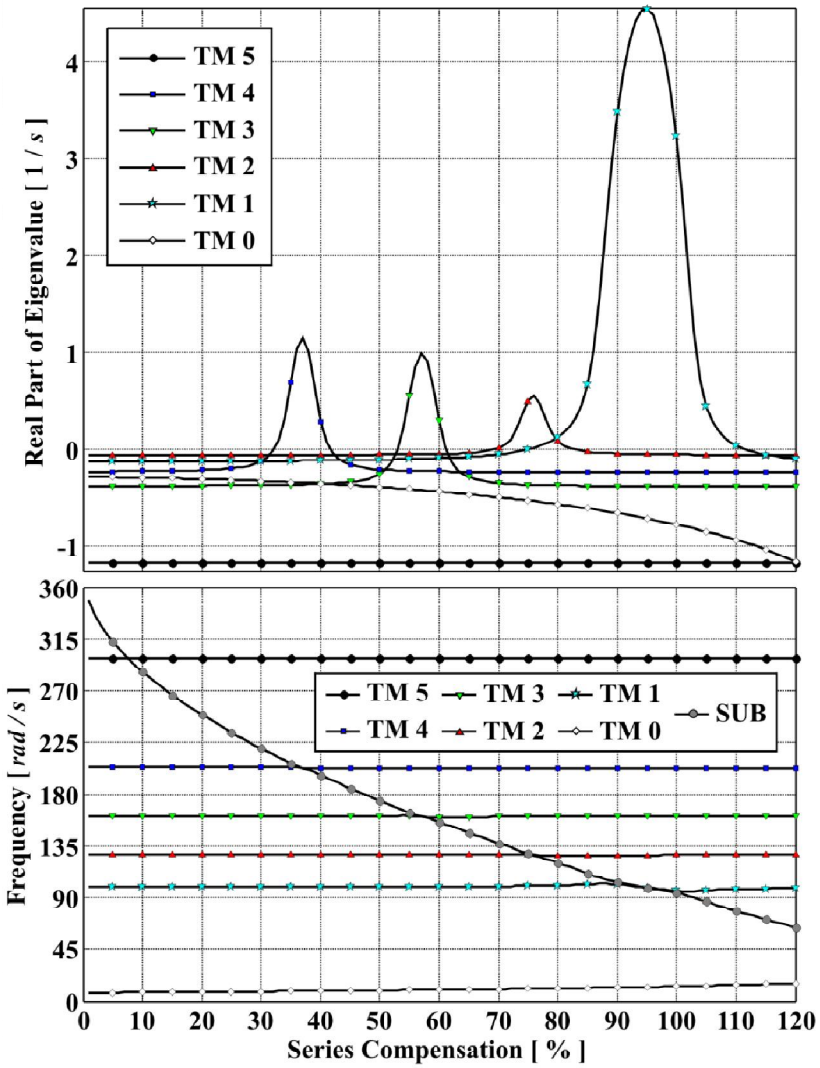

Figure 2.17: Stability of the torsional modes in terms of series compensation level and relationship with the subsynchronous mode frequency [94]

Chapter 3 -

Damping of Subsynchronous Resonance using a VSC-HVDC Link

The results in this chapter were the product of collaborations with Dr. Carlos Ugalde-Loo, Cardiff University.

3.1 INTRODUCTION

Series compensation and HVDC links are proposed to reinforce the GB transmission network. The inland reinforcements include the use of series compensation through fixed capacitors. This potentially can lead to Subsynchronous Resonance (SSR). The offshore reinforcements are proposed in the form of two HVDC links and it is possible that one of these links will use VSC technology.

In this chapter, control systems for a point-to-point VSC-HVDC link were implemented. In addition to its primary function of bulk power transmission, a HVDC link can be used to provide damping of SSR, and this auxiliary function has been designed and simulated. Simulations have been carried out in PSCAD/EMTDC with the results plotted in MATLAB.

3.2 POTENTIAL FOR SSR IN THE 2020 GB NETWORK

The potential for the generation of SSR within thermal generators is recognised by National Grid Ltd as a threat. It is widely known that series compensated AC

transmission lines can cause SSR interactions with thermal generators. VSC-HVDC links have been shown not to contribute to SSR, and the flexibility of this converter type means that SSR in the onshore network could be damped. LCC-HVDC links can be a source of SSR, although the control systems are usually designed to avoid this [74], [85].

3.2.1 THE THREE MACHINE NETWORK

A three-machine model, presented in [96–99], was used to represent the mainland GB system. The weighting of the size and type of generation in the GB network is modelled in this simple representation.

The three machine network was originally designed to resemble the operating conditions of the mainland GB system. The model acted as a base for testing wind generator machine types and FACTS devices.

3.2.2 IMPROVEMENTS IN THE THREE MACHINE NETWORK

The system shown in Figure 3.1 consists of three synchronous generators splitting the GB mainland system into three major generation areas: England and Wales, Southern Scotland and Northern Scotland. The rating of the England and Wales generator is 21,000 MVA. The Southern Scotland generator is rated at 2,800MVA and the Northern Scotland generator is rated at 2,400 MVA.

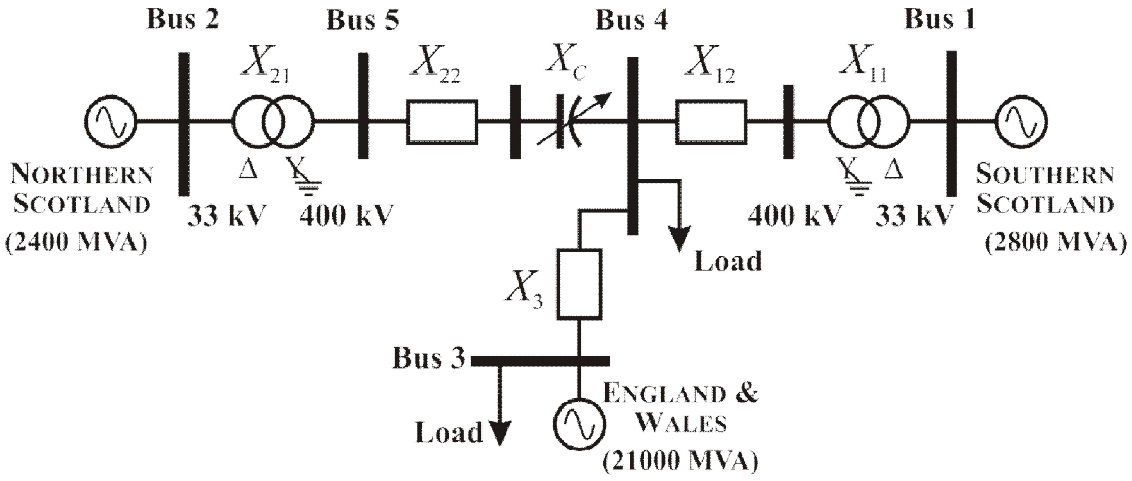

Figure 3.1: Three machine network with onshore reinforcement through fixed capacitors

To assess SSR in this model, a number of adjustments have been made to simulate the planned series compensation within the AC transmission lines. A series capacitor was included between buses 4 and 5 to represent the planned fixed capacitors between England and Scotland, required to increase transient stability. This will bring the transient stability limit up to the thermal capacity of the AC transmission line. The implementation of this series compensation changes the parameters of the electrical system and therefore its natural frequency.

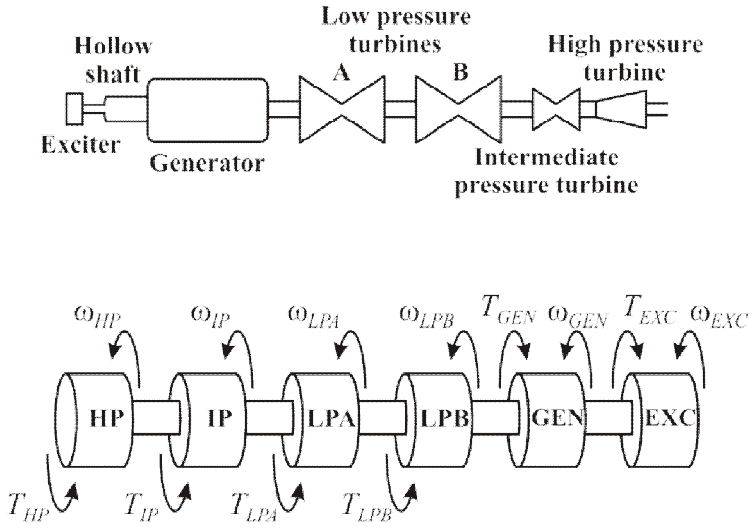

Figure 3.2: Shaft model of the Northern Scotland generator as a six mass system

The Northern Scotland generator shaft is an aggregation of all the thermal turbine generators in the Northern Scotland generation area. This aggregated generation was modelled as a multi-mass system consisting of four turbine sections, plus the generator and exciter, as shown by Figure 3.2. The parameters of the shaft are the same as the ones used in the IEEE First Benchmark Model and can be found in [91] and Appendix A. The system frequency for the three machine network is 50Hz.

The generic network model used reactances and resistances for the transmission lines and transformers, which can be found in [100] and Appendix A. Several approaches can be used to assess the risk of SSR in an AC system. An eigenvalue analysis can be performed, a time domain simulation can be carried out or a unit interaction factor

study can be carried out. In this study, an eigenvalue analysis and a time domain study are conducted.

3.3 RESULTS FOR THE 2020 GB NETWORK

To assess the vulnerability of the 2020 GB network to SSR, a time domain simulation of the model in PSCAD/EMTDC in Figure 3.1 was tested. The eigenvalue analysis in [100] was conducted on the same model, so a comparison was drawn between the PSCAD simulation and the eigenvalue analysis.

3.3.1 EIGENVALUE ANALYSIS

The 2020 GB network is characterised by five torsional modes (TM1-TM5), associated with the shaft of the Northern Scotland generator, which may become excited at different compensation values. Figure 3.3 plots the ranges of series compensation levels at which interaction and instability may occur. Where the real part of the eigenvalue is negative, the system is stable. Areas where the real parts of the eigenvalue are positive are considered unstable as the system is susceptible to SSR. The unstable areas occur at series compensation levels where the subsynchronous mode (SUB) is close to a torsional mode. A torsional interaction is likely to occur between the subsynchronous mode (SUB) and the relevant torsional mode (TM1-5) in these areas.

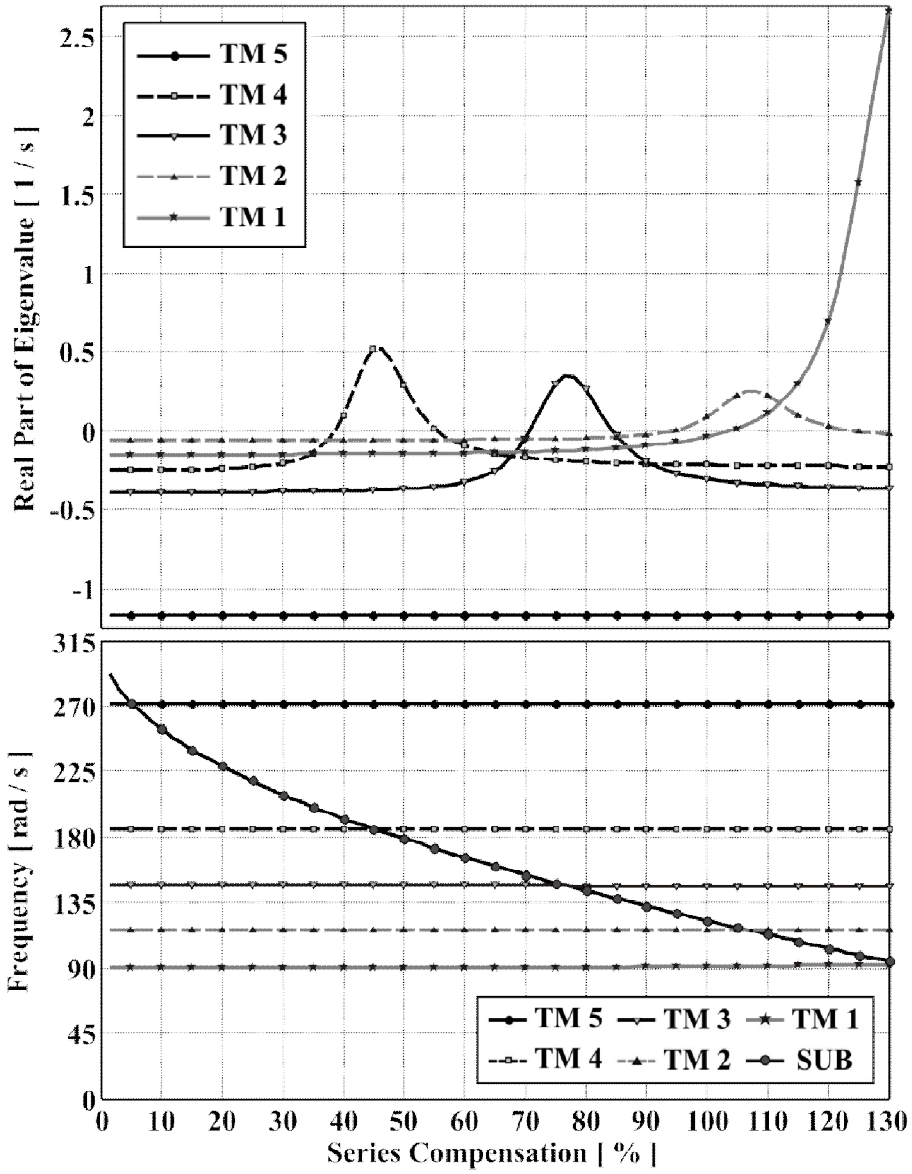

Figure 3.3: Stability of the torsional modes in terms of series compensation level and relationship with the subsynchronous mode frequency [100]

For example, Figure 3.3 shows that at 45% compensation, the subsynchronous mode (SUB) is close to torsional mode 4 (TM4), here the real part of the eigenvalue is positive.

Table 3.1 provides a direct comparison between two series compensation levels. At a series compensation level of 30%, all the real part of the eigenvalues are negative. At 40% compensation the real part of the eigenvalue is positive for torsional mode 4 (TM4). This indicates that a torsional interaction is likely to develop at the 40% series compensation level between the subsynchronous mode (SUB) and torsional mode 4

(TM4). As the level of series compensation is increased the chance of an interaction increases, it is likely that one of the torsional modes will become unstable.

Table 3.1: Relevant eigenvalues of the three-machine system [100]

	30% compensation		**40% compensation**	
Mode of oscillation	**Real part [s^{-1}]**	**Imag. part [*rad/s*]**	**Real part [s^{-1}]**	**Imag. part [*rad/s*]**
TM5	–1.173	±272.1935	–1.173	±272.1935
TM4	–0.2078	±185.4883	**+0.0976**	**±185.7151**
TM3	–0.3839	±146.6666	–0.3792	±146.6967
TM2	–0.0587	±115.9705	–0.0584	±115.9755
TM1	–0.1492	±90.5749	–0.1475	±90.6216
SUPER	–8.5183	±418.5203	–8.6653	±434.764
SUB	–7.4436	±209.2895	–7.6743	**±192.7548**

3.3.2 TIME DOMAIN SIMULATION IN PSCAD

A time domain simulation of the network in Figure 3.1 was implemented on PSCAD/EMTDC. In the simulation, a change in series compensation, from 30% to 40%, occurs at 2 seconds. From the results of the eigenvalue analysis, it would be expected that SSR would develop following the change in series compensation.

Figure 3.4(*a*) shows the frequency at Bus 5 of the AC transmission network, whereas Figure 3.4(*b*) illustrates the electromagnetic torque at the Northern Scotland generator. The increasing frequency and torque amplitude after the step change shows that this system becomes unstable due to SSR.

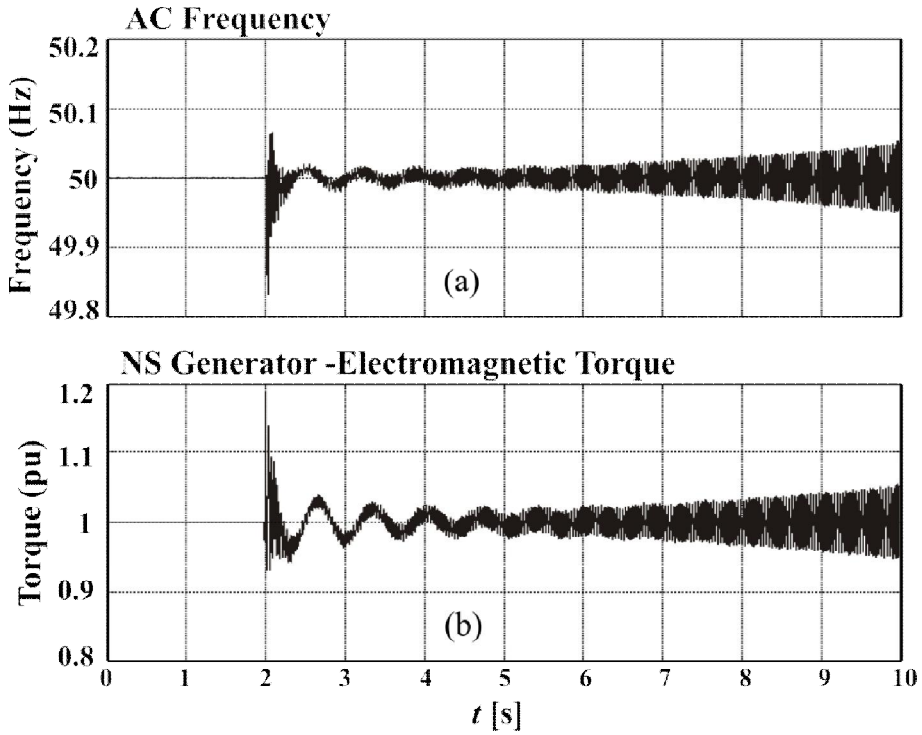

Figure 3.4: Simulation results from the '2020' GB transmission network.
(a) Frequency of phase a current of the Northern Scotland generator;
(b) Northern Scotland electromagnetic torque.

Figure 3.5 shows the torque interactions between individual shafts on the multi-mass turbine. The increasing torque amplitude after a step change from 30% compensation to 40% compensation shows that this system exhibits typical behaviour expected from SSR.

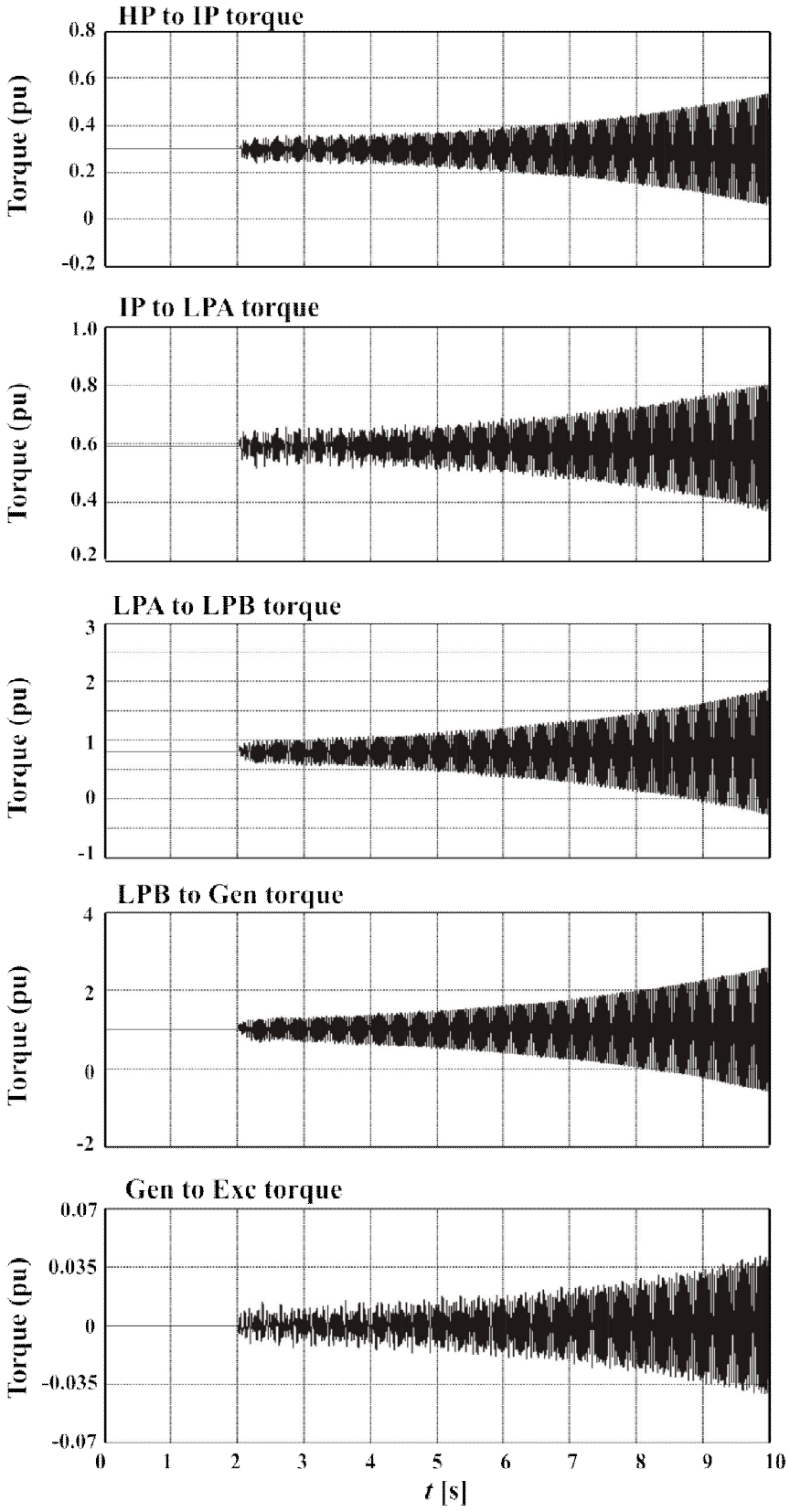

Figure 3.5: Simulation results from the '2020' GB transmission network. Torque interactions in the multi-mass shaft of the Northern Scotland generator

These results indicate that the three machine network with 40% compensation was susceptible to SSR. A potential solution could be to limit the series compensation level to 30%, although this would under-exploit the advantages of series compensation. Alternatively, Thyristor Controlled Series Capacitors (TCSC) rather than fixed capacitors could be used. However, this would be expensive and requires the use of previously un-commissioned devices into the GB network.

3.4 2020 TRANSMISSION NETWORK WITH VSC-HVDC LINK

A potentially cheap and efficient solution to avoiding SSR would be to use the proposed VSC-HVDC link for external SSR damping. This approach is examined in this chapter.

The primary design objective of a VSC-HVDC link between Bus 5 and Bus 4 is to ensure that active power control is achieved, along with local reactive power support for the grid. Controllers were designed at either terminal to control active and reactive power. Additionally, a CSC-HVDC link is planned between Bus 1 and Bus 4 is planned, however this is not included due to a limitation in the RTDS capacity in the experiment set-up (chapter 4).

In order to accomplish damping of SSR within the onshore grid, an auxiliary control system was designed. This control loop operates slower than the primary active and reactive power controllers. Other control schemes are used in this manner for frequency control, power modulation control and power demand override [15].

Using the VSC-HVDC link to damp externally generated SSR would offer an alternative solution to employing another device solely for this purpose. For the modelling of this transmission system, a VSC-HVDC link was connected between buses 4 and 5 of the three-machine network, shown by Figure 3.6.

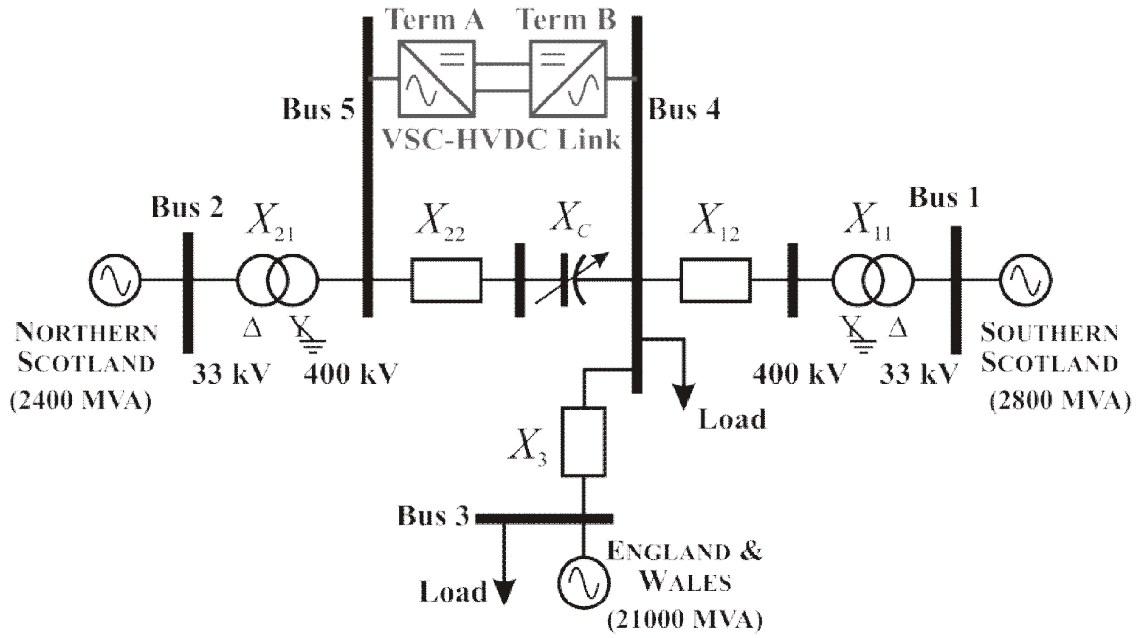

Figure 3.6: Three machine network with onshore and offshore reinforcements through series capacitors and a VSC-HVDC link

3.4.1 PRIMARY CONTROL SYSTEM

The primary system was designed to control the magnitude and direction of active power flow. Also, local reactive power was controlled at either end of the VSC-HVDC link. Therefore the parameters which were controlled were active power, reactive power at both terminals and the DC link voltage.

Figures 3.7 and 3.8 illustrate the control systems when the converter is operating in primary control mode. The controllers were designed using the *d-q* reference frame. PI controller, PI1, is used to regulate the active power to a set point (in terminal A, shown in Figure 3.7) or the DC voltage (in terminal B, shown in Figure 3.8); to achieve this it generates a reference current i_{qref}. PI controller PI2 performs this function at either end for the reactive power control and generates reference current i_{dref}. PI controllers PI3 and PI4 regulate the *dq* currents, setting the appropriate converter control signals. To avoid large variations from the outer loop controllers (P, Vdc and Q controllers), the existing system voltages (v_d and v_q) were added to the outer controller's output through feed-forward loops.

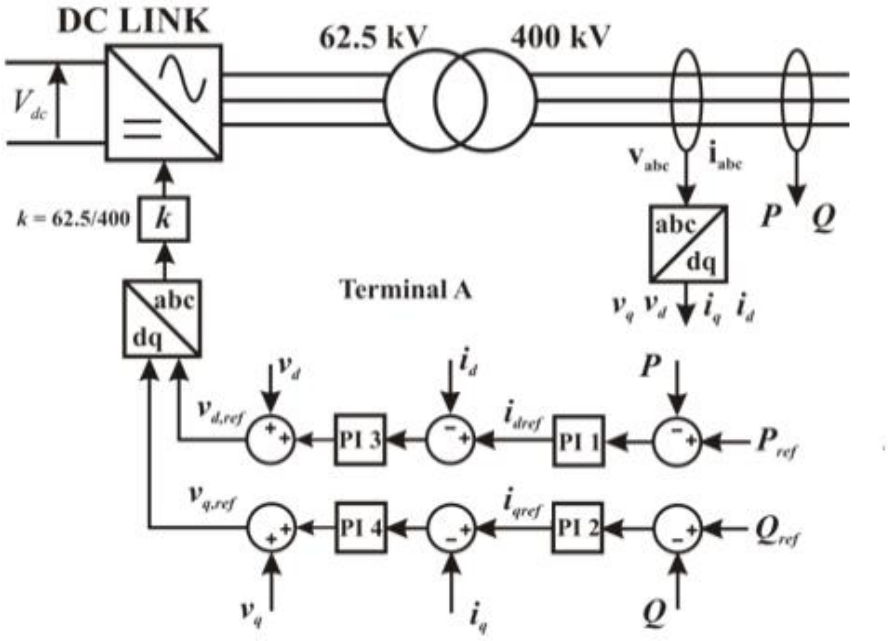

Figure 3.7: Primary control system for terminal A

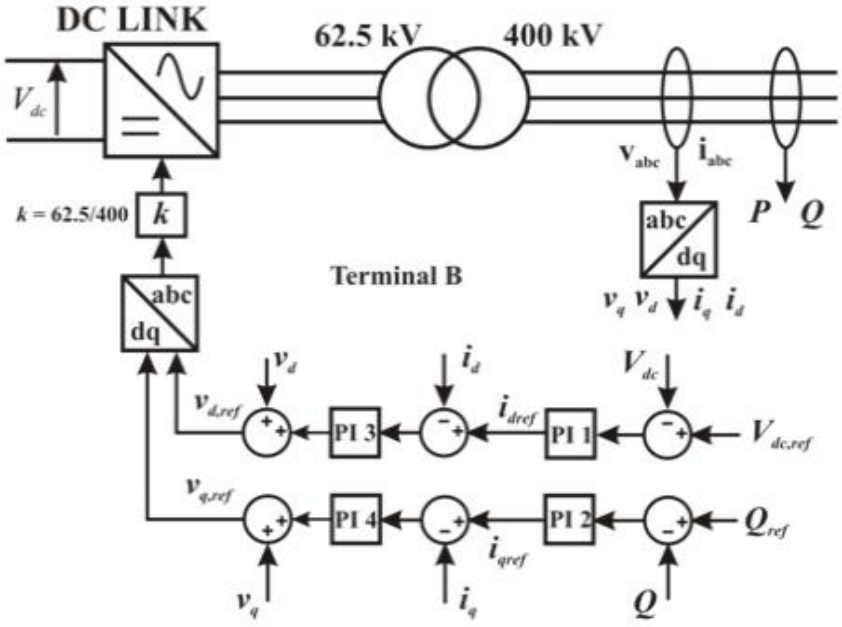

Figure 3.8: Primary control system for terminal B

In order to test this control scheme, the control schemes shown in Figures 3.7 and 3.8 were simulated in PSCAD. Simulations were carried out to ensure the system was stable and reaches desired reference values after a step change.

Terminal A: Power Control Mode at Bus 5

At terminal A, the converter was responsible for controlling active and reactive power. Power flow in the positive direction denotes a flow of power from Bus 5 to Bus . Absorption and generation of reactive power is required to support the local AC system.

The performance of the active and reactive power controllers were demonstrated in Figure 3.9, with step changes in ordered power. Initially, an active power set point of 250MW has been ordered, which is stepped down to 150MW at 2s, shown in Figure 3.9(a). A reactive power set point of 60MVAR (absorption) is ordered and stepped to 30MVAR, shown in Figure 3.9(b).

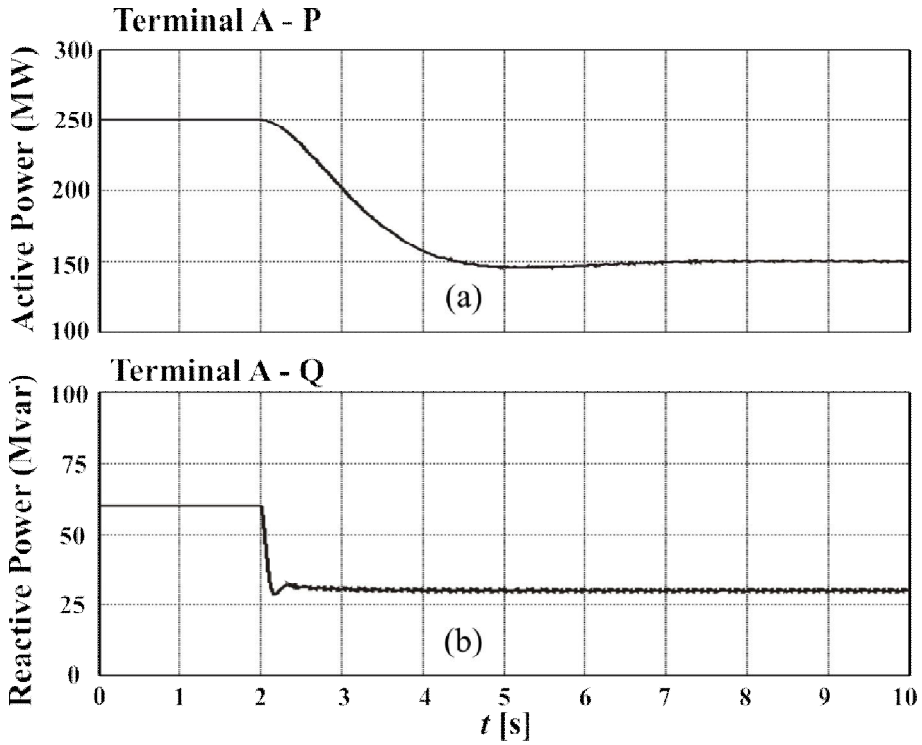

Figure 3.9: Terminal A of the VSC-HVDC link.
(a) Step change in active power from 250MW to 150MW.
(b) Step change in reactive power from 60MVar to 30MVar (absorbing)

Terminal B: DC Voltage Control at Bus 4

At terminal B, the converter is responsible for controlling DC voltage and reactive power. DC voltage is usually controlled to the maximum voltage limit of DC plant and cables. This means that DC current can be as low as possible, minimising power losses in the transmission line.

The performance of the DC voltage and reactive power controllers were demonstrated in Figure 3.10, for testing the simulation step changes in ordered DC voltage and reactive power were performed.

Initially, a DC voltage set point of ±300kV was ordered, stepped down to ±200kV at 2s, shown in Figure 3.10(a). A reactive power set point of 10MVAR (generation) was ordered and stepped to 20MVAR, shown in Figure 3.10(b).

From the step changes implemented at both terminals, in Figures 3.9 and 3.10, it can be seen that the primary controller exhibits good performance.

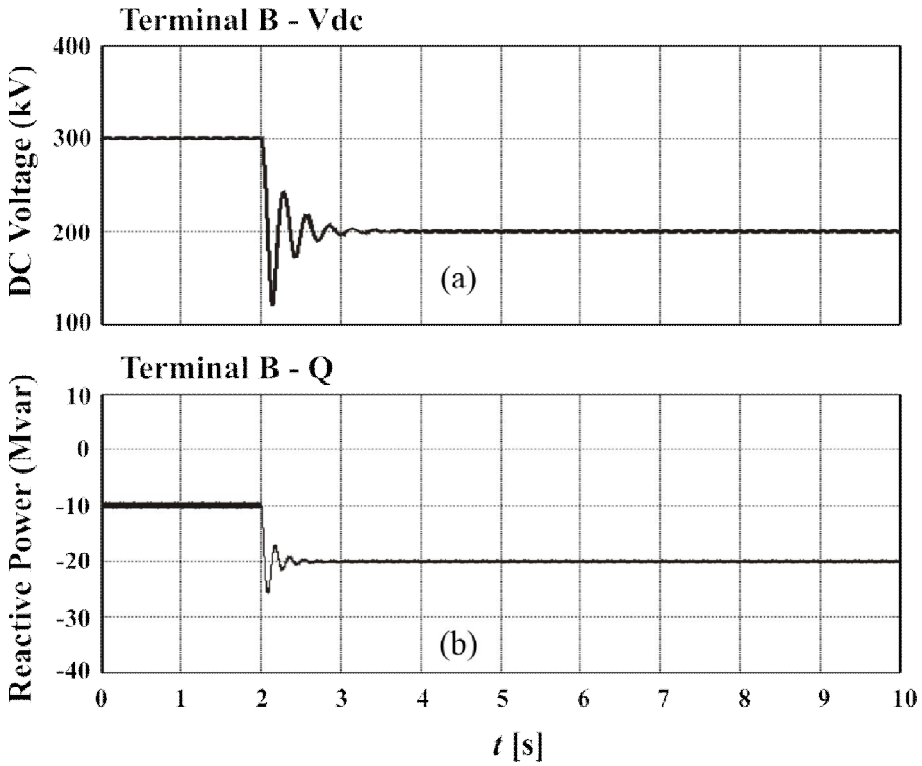

Figure 3.10: Terminal B of the VSC-HVDC link.
(a) step change in DC Voltage from 250kV to 150kV.
(b) step change in reactive power from 10MVar to 20MVar (generating)

3.4.2 HYBRID CONTROL SYSTEM

In order to damp SSR, an auxiliary controller was designed and incorporated into the controller at terminal A. This is shown as a hybrid controller in Figure 3.11 which consists of both the primary controller and the auxiliary controller.

Under this control scheme the VSC included a SSR damping controller which injects an anti-phase signal into the AC system at a target subsynchronous frequency. For this case, the auxiliary damping controller is designed for a target resonant frequency of 20Hz as this corresponds to the frequency of the subsynchronous mode (SUB). As shown by Figure 3.11, the controller works by isolating the target frequency component through a band pass filter, eliminating the voltage driving frequency (50Hz).

However, the filtering of the signal adds a phase and amplitude shift to the target signal. The lead-lag compensator corrects for this phase and amplitude displacement of the SSR signal. The parameters of the lead-lag compensator were chosen based on the phase and amplitude displacement and manually tuned for fine adjustments; these are shown in Table 3.2, full control parameters can be found in Appendix B. The anti-phase SSR damping signal is created by multiplying the SSR signal by -1, creating a complementary damping signal. The damping signal is injected back into the AC system bus where measurement took place, it is important to ensure the current is limited to within the converters limits. The auxiliary controller operates at a lower bandwidth than the inner primary loops.

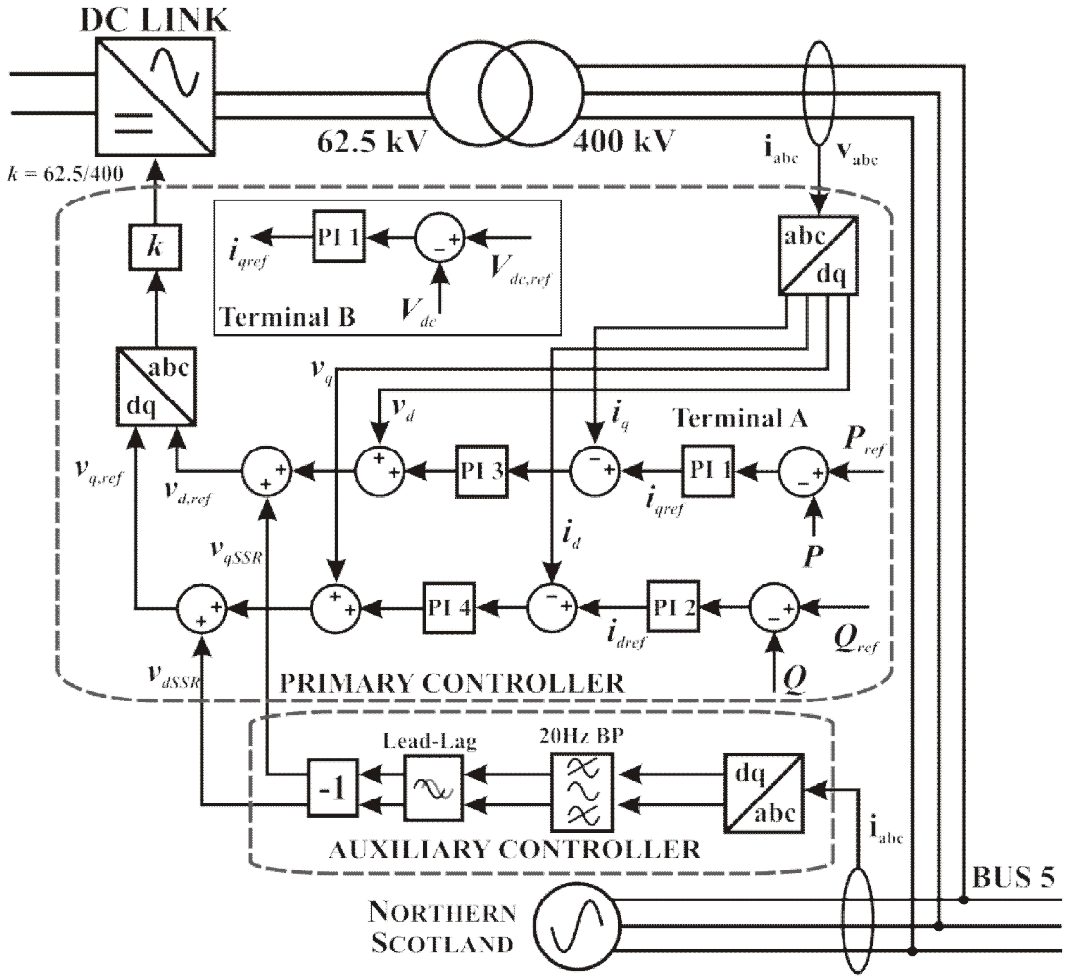

Figure 3.11: Hybrid control system, containing primary and auxiliary controllers, for the two terminal VSC-HVDC link

The controller does not need to be switched as it is tuned to only damp signals around 20Hz. In networks where SSR is not present, the oscillation around 20Hz will not be present and therefore no damping signal will be produced. As SSR increases following the step change the controller automatically damps the oscillation.

Table 3.2: Relevant control parameters for the hybrid control system

	Control Parameters	
Control Block	**Gain**	**Time Constant**
PI1	0.0001	0.05
PI2	0.01	0.5
PI3	2.5	0.01
PI4	–0.5	0.001
LEAD-LAG	5	0.004 (LEAD) 0.009 (LAG)

3.5 SIMULATION RESULTS

In order to test the effectiveness of the SSR damping controller within the hybrid controller, a simulation was carried out where the series compensation level was changed from 30% to 40%. The series compensated network with VSC-HVDC link, as shown in Figure 3.6, was implemented on PSCAD/EMTDC, using the hybrid controller.

Figure 3.12(a) shows the frequency of the AC transmission network, Figure 3.12(b) illustrates the electromagnetic torque at the Northern Scotland generator. Following the disturbance at 2s, SSR is successfully damped and the system remains stable.

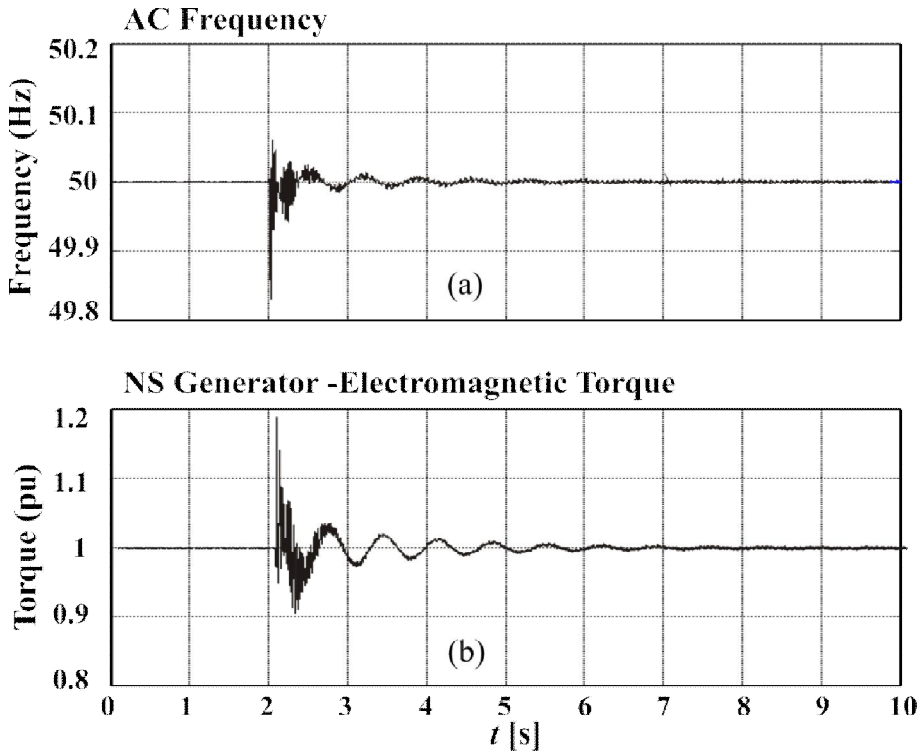

Figure 3.12: Hybrid controller in the VSC-HVDC link.
(a) Frequency of phase a current from the Northern Scotland generator;
(b) Electromagnetic torque at the Northern Scotland generator.

Figure 3.13 shows the torque interactions between individual shafts on the multi-mass turbine. Following the disturbance at 2s, the controller injects an anti-phase current into bus 5, damping the SSR. The torque interactions return to their stable operating points and reduces the turbine shaft damage associated with SSR

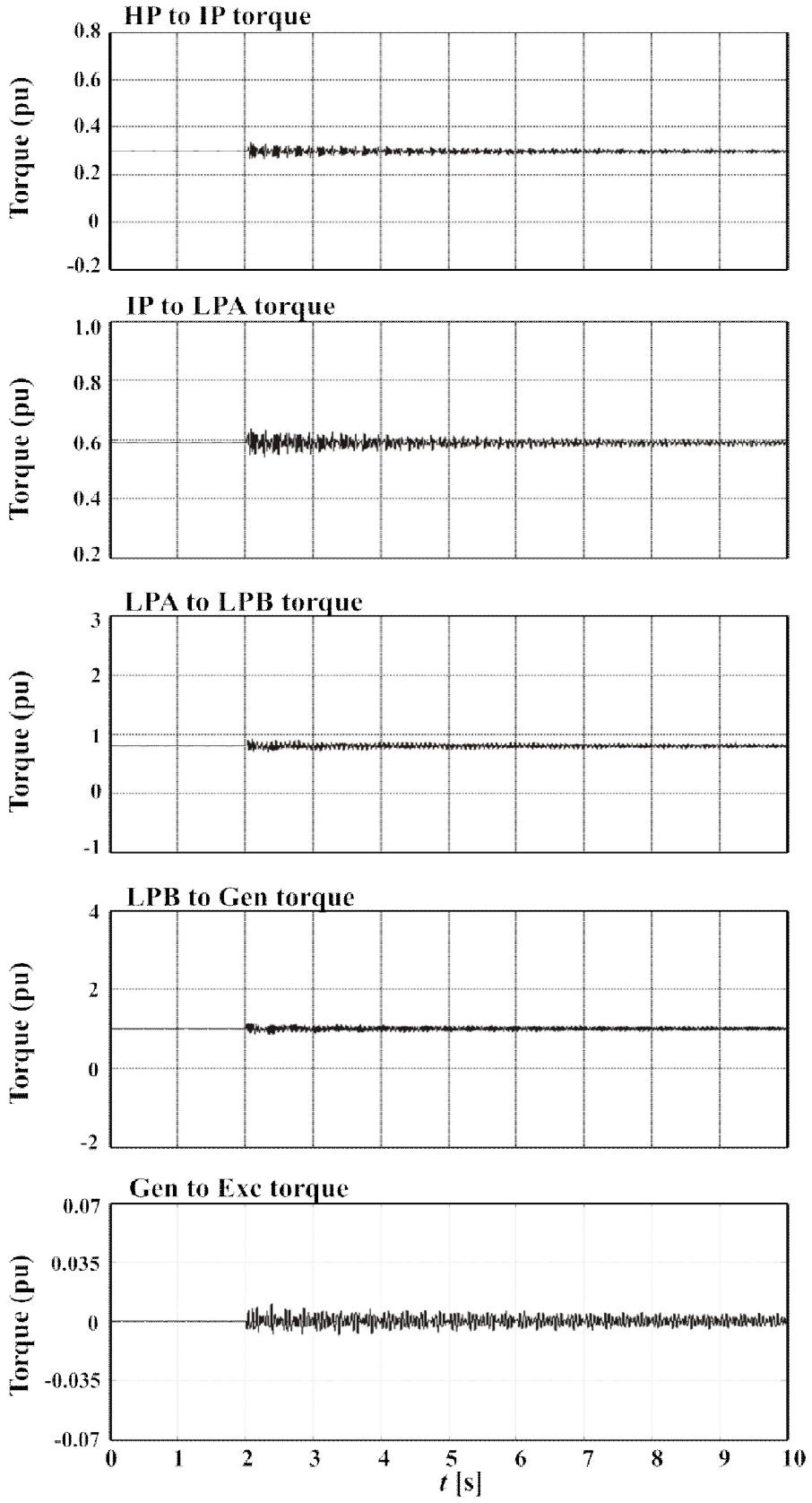

Figure 3.13: Hybrid controller for the VSC-HVDC link. Torque interactions in the multi-mass shaft of the Northern Scotland generator.

Figure 3.14 shows the active and reactive power modulation at Terminal A of the VSC-HVDC link. During the disturbance active power is modulated by ~2% and reactive power is modulated by ~15% for 2 seconds. However, it is noted that this is a small disturbance and a larger disturbance (such as a fault) would require a larger proportion of the active and reactive power to be modulated.

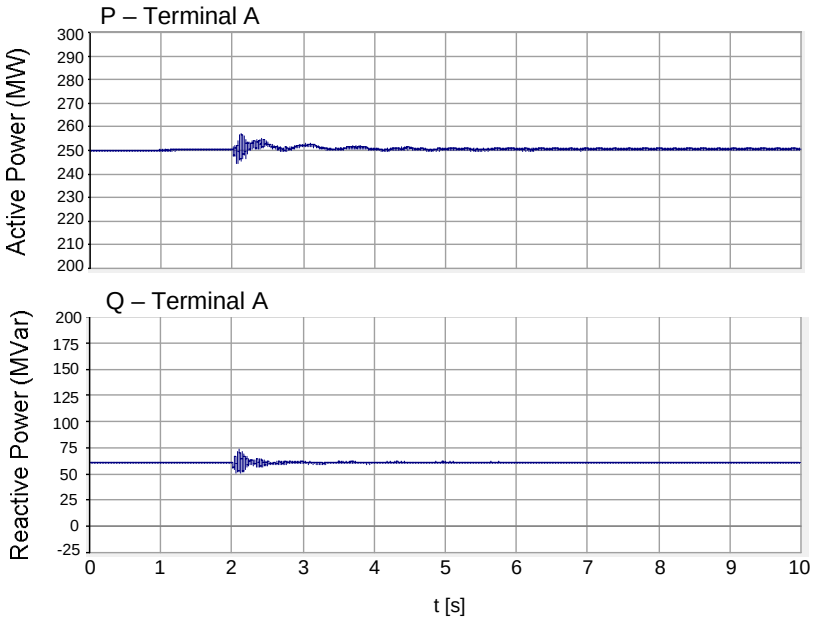

Figure 3.14: Hybrid controller for the VSC-HVDC link (Terminal A). Active and reactive power modulation in the VSC-HVDC link

Figure 3.15 shows the I_d and I_q currents at Terminal A of the VSC-HVDC link. Usually these currents are approximately 500A. However, following the disturbance, the I_d and I_q currents are modulated to damp the SSR oscillation. The traces show that ~200A of current is used for this purpose. It should be ensured that the current modulation does not cause the converter to exceed the current limits of each converter.

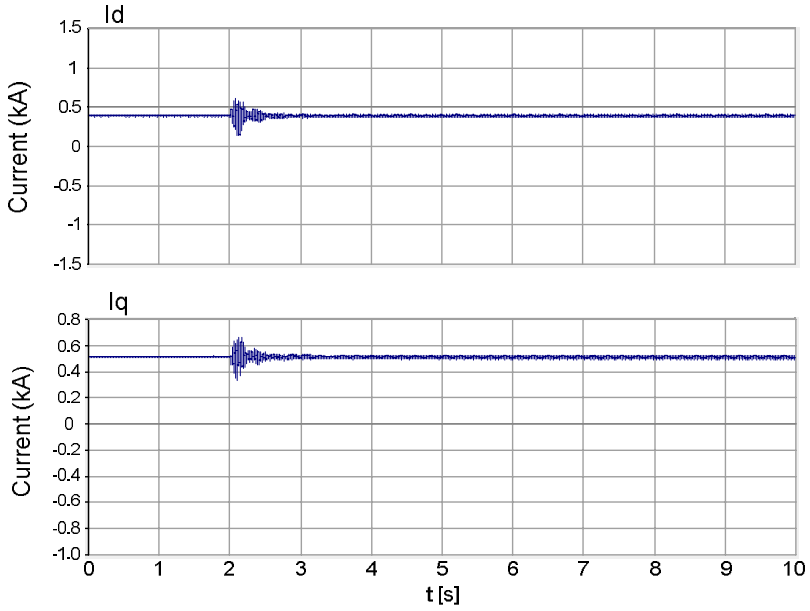

Figure 3.15: Hybrid controller for the VSC-HVDC link (Terminal A). Id and Iq modulation in the VSC-HVDC link

The simulated model of the 2020 GB transmission network with series compensation shows that SSR may arise when high levels of series compensation are used in the onshore AC network. When the VSC-HVDC links are included, the results in this chapter show that the converter can be used to damp SSR in addition to controlling active and reactive power. This is achieved by incorporating an auxiliary SSR damping loop into the active and reactive power controller.

Using this controller means that series compensation levels for the AC transmission system can be increased into normally unstable regions. The use of FACTS devices such as TCSC's to mitigate for SSR can be avoided.

Chapter 4 -

An Experiment for Damping Subsynchronous Resonance using a VSC-HVDC Link

4.1 INTRODUCTION

The SSR damping controller designed in Chapter 3 was tested using a real-time experiment. SSR was generated on an AC system simulated on a Real Time Digital Simulator (RTDS). The VSC controller was implemented on an experimental VSC-HVDC test rig. Analogue signals are exchanged between the RTDS and VSC-HVDC test rig. The results from the experimental test rig are shown with and without a SSR damper, mirroring Chapter 3.

A comparison was drawn between the experimental results from this chapter and the simulation results from Chapter 3.

4.2 DEVELOPMENT OF THE REAL TIME DIGITAL SIMULATOR FOR SSR STUDIES

The Real Time Digital Simulator, shown in Figure 4.1, is a real-time and fully digital power system simulator [101]. The simulator is designed to solve the electromagnetic transient simulation 'Dommel' algorithm [102] in real time. Models are created on simulator through a graphical design tool, RSCAD©. The experiment used a single rack

system containing four Giga Processor Cards (GPC), where each GPC card runs two 1GHz processors.

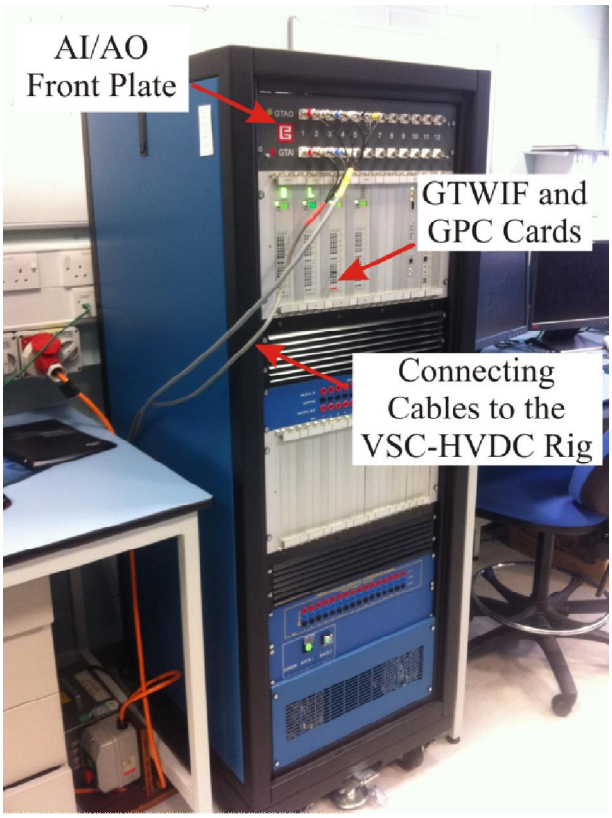

Figure 4.1: Real Time Digital Simulator

The GPC cards are controlled by the Giga Transceiver Workstation Interface Card (GTWIF) card, where models designed in RSCAD are uploaded.

For hardware-in-the-loop testing, the GPC cards are connected to Analogue Input (AI) and Analogue Output (AO) cards through a 2GHz fibre optic link. Here signals from external equipment were interfaced into the real time simulation.

Originally, the AI and AO cards were located internally within the RTDS cabinet. To ensure a reliable connection, the AI and AO terminals were brought to the front of the cabinet to allow interface to the VSC-HVDC rig through BNC (Bayonet Neill-Concelman) connectors. The fabricated AI/AO front plate is shown in Figure 4.2.

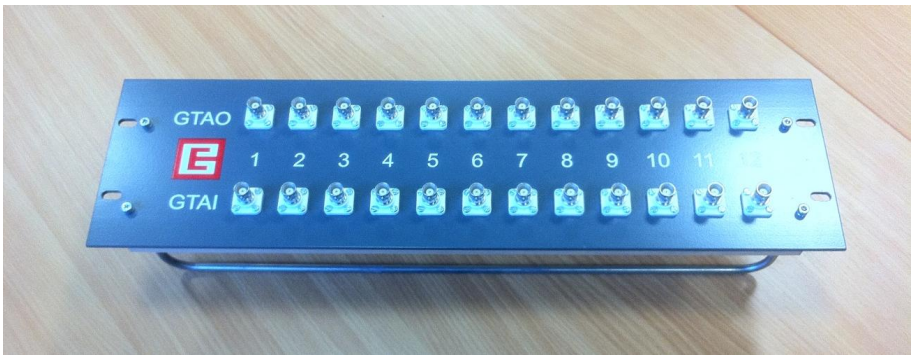

Figure 4.2: Fabricated AI/AO front plate for the RTDS

Hardware parameters for the RTDS can be found in Appendix C. Control parameters for the RTDS can be found in Appendix B.

4.3 CONFIGURATION OF THE VSC-HVDC RIG FOR SSR STUDIES

The VSC-HVDC test rig consists of three VSCs controlled through a dSPACE unit and is shown in Figure 4.3.

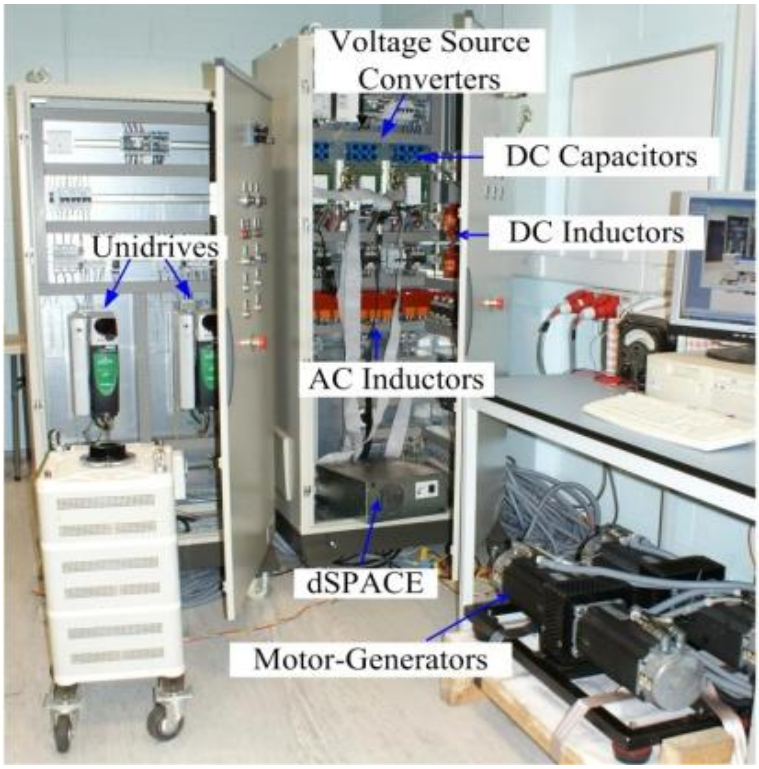

Figure 4.3: VSC-HVDC test rig

On the DC side of the VSC converters, the DC capacitors represent capacitor banks within the converter station. DC inductors represent the reactance of DC transmission cables. Digital gate drive signals are sent from the dSPACE unit to the individual VSC converters. The AC and DC voltage and current signals were generated as analogue signals and transmitted between the dSPACE unit and the VSC converters.

For the purposes of the experiment it was necessary to use specific analogue signals to interface between the RTDS and the VSC-HVDC rig. An interface board, shown in Figure 4.4, was designed and fabricated to facilitate the exchange of signals between the RTDS and VSC-HVDC rig. The interface board was positioned between the VSC's and the dSPACE unit. This allows analogue signals sent from the RTDS to be used as inputs to the dSPACE.

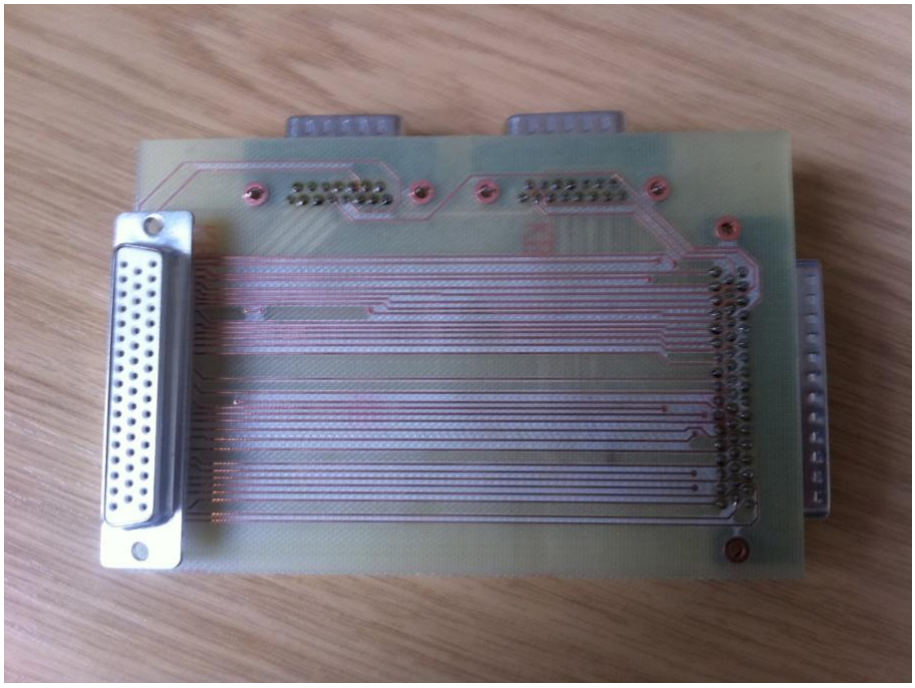

Figure 4.4: Interface board fabricated to allow the exchange of analogue signals between the RTDS and VSC-HVDC Rig

For the return path, analogue signals from the current transformers (CT), located on the VSC's AC terminals were measured and transmitted to the RTDS.

4.4 IMPLEMENTATION OF THE SSR DAMPER

The network used in the experiment, is shown in Figure 4.5, and was slightly different from the PSCAD simulated network designed in Chapter 3. The RTDS models the AC network in the same way as the PSCAD simulated network, albeit without the HVDC link. Instead a controlled current source was connected to Bus 5 to allow for the injection of the damping current. The AC equivalent system uses lumped inductances, as per the IEEE first benchmark model. The three terminals of the VSC-HVDC test rig operate independently. Unlike the simulation, there is no ordered active and reactive power flow. Active and reactive powers are used by the damping converter during damping. The roles of the VSC converters are: DC voltage source, amplifying converter and damping converter.

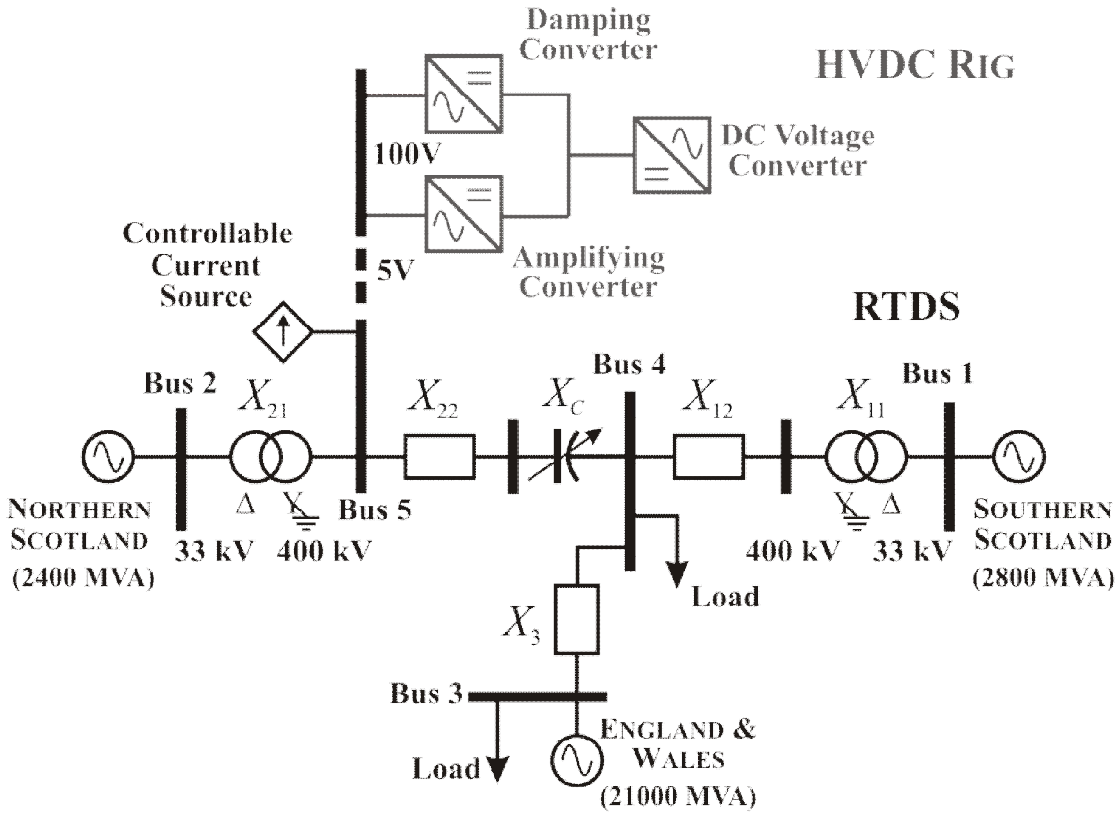

Figure 4.5: Schematic of the experiment design

4.4.1 DC VOLTAGE SOURCE

To work effectively the amplifying and damping converters were operated from a stiff DC voltage. This is provided by a VSC converter specifically designed to control DC voltage.

4.4.2 AMPLIFYING CONVERTER

The role of the amplifying converter was to establish an AC voltage. This is shown in Figure 4.6. At the RTDS, the simulated Bus 5 voltages are measured (400kV) and scaled at the AO card for transmission of the signal to the VSC/HVDC rig (5V). The amplifying converter is designed to control the AC voltage at its terminals at the nominal voltage for the rig (100V) using the voltage signal from the RTDS.

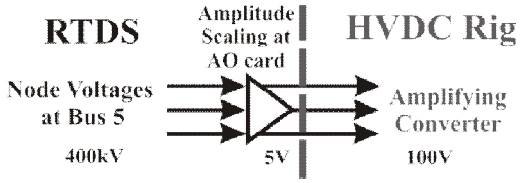

Figure 4.6: Signal exchange between the RTDS and the VSC-HVDC test rig for the amplifying converter

4.4.3 DAMPING CONVERTER

The role of the damping converter was to provide the anti-phase current used to damp SSR on the AC system developed on the RTDS. Figure 4.7 shows how the converter generated the damping signals.

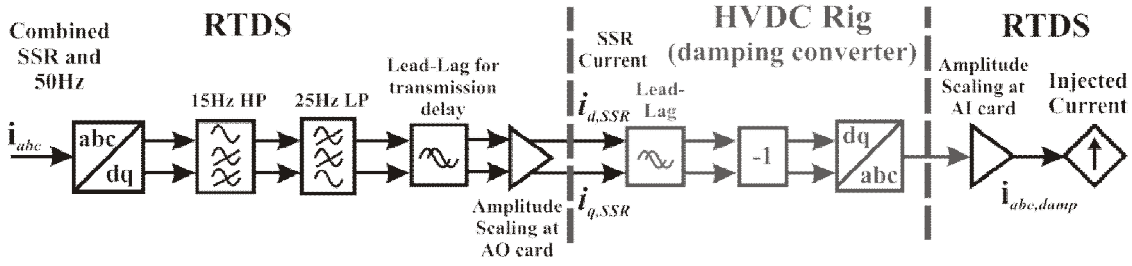

Figure 4.7: Signal exchange between the RTDS and the VSC-HVDC test rig for the damping converter

The currents (with SSR) were measured at Bus 5 on the RTDS system. The signals were then filtered through high pass (15Hz) and low pass (25Hz) filters to isolate the SSR frequency, removing the system synchronous frequency at 50Hz. By filtering on the RTDS, the amplitude of the SSR component of the signal was scaled to the nominal

transmission voltage of 5V at the AO card of the RTDS. This had the effect of minimizing noise. A lead-lag compensator is utilized to correct for the phase shift from the transmission delay. The *dq* current is then transmitted to the VSC-HVDC rig.

The damping converter receives the SSR currents and generates an anti-phase signal. The lead-lag compensator corrected for the phase shift from the filtering, whereas the –1 gain ensures the generated current was anti-phase in relation to the reference signal. The damping converter then generates this signal at its AC terminals. The currents were measured through current sensors on the AC side and sent back to the RTDS (again at 5V) and used as the reference currents to program controllable current sources.

These current sources injected the anti-phase current back into Bus 5 on the RTDS. The parameters of the control blocks and scaling factors at the AO and AI card are shown in Table 4.1.

Table 4.1: Relevant control parameters for the experiment

	Control Parameters	
Control Block	**Gain**	**Time Constant**
LEAD-LAG 1 (RTDS)	5	0.0038 (LEAD) 0.106 (LAG)
LEAD-LAG 2 (VSC-HVDC)	3	0.0042 (LEAD) 0.0096 (LAG)
AO SCALE (VOLTAGE SIGNALS)	400	N/A
AO SCALE (CURRENT SIGNALS)	4	N/A
AI SCALE	16	N/A

4.5 EXPERIMENTAL RESULTS

A time domain experiment was carried out on the multi-platform network shown in Figures 4.1- 4.5. In the experiment, a change in series compensation, from 30% to 40%, occurs at 2 seconds.

In the first experiment the damping converter in the VSC-HVDC test rig was not activated. In same way as the undamped system in Chapter 3, the system develops SSR. This is shown by an unstable AC system frequency and generator shaft torques in Figures 4.8 and 4.9. These show agreement with Figures 3.4 and 3.5, the undamped case that was simulated within PSCAD.

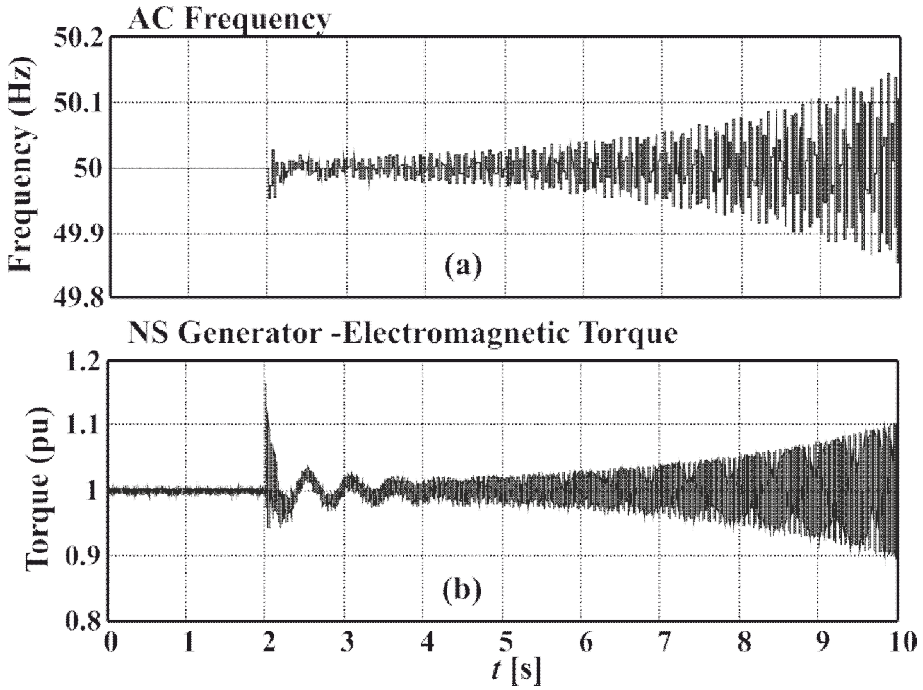

Figure 4.8: Experimental results (RTDS signals) of the undamped case.
(a) Frequency of phase a current of the Northern Scotland generator;
(b) Northern Scotland electromagnetic torque.

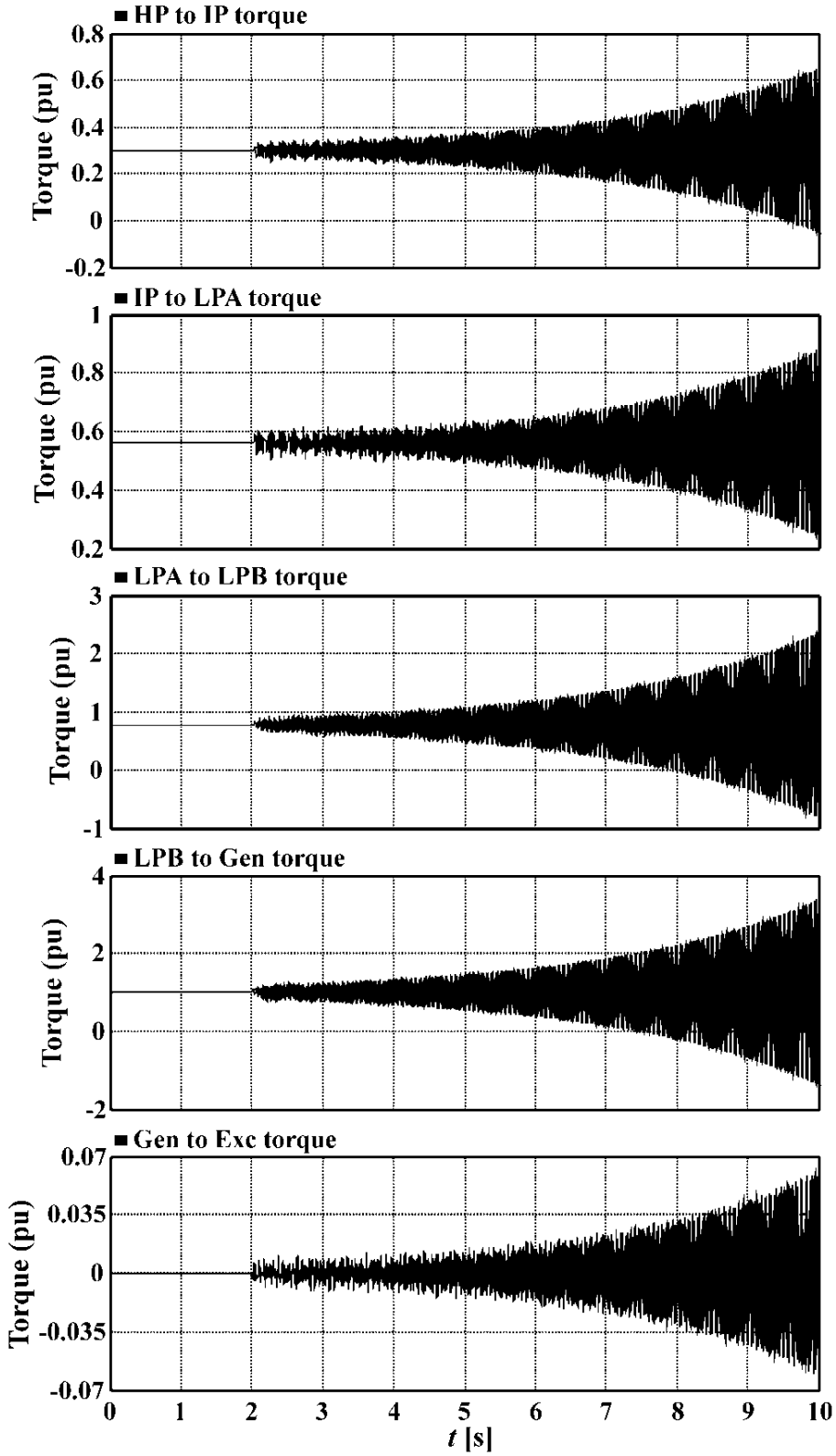

Figure 4.9: Experimental results (RTDS signals).
Torque interactions in the multi-mass shaft of the Northern Scotland generator

The results shown in Figure 4.10-12 are from the VSC-HVDC test rig. Figure 4.10 shows the *dq* SSR current signals sent from the RTDS to the HVDC rig. As SSR develops, these currents increase, with the controller limiting their magnitude to ±25A. Figure 4.11 shows the damping current produced by the damping converter (phases *a* and *b*). In this experiment the damping control was not activated. When the compensation level is increased at 2s no damping current is produced, only noise. Figure 4.12 shows the AC voltage produced by the amplifying converter; this imitates the RTDS bus 5 voltages albeit at a lower voltage magnitude. This is a product of the Bus 5 voltage on the RTDS and is amplified to the VSC-HVDC rig nominal working voltage.

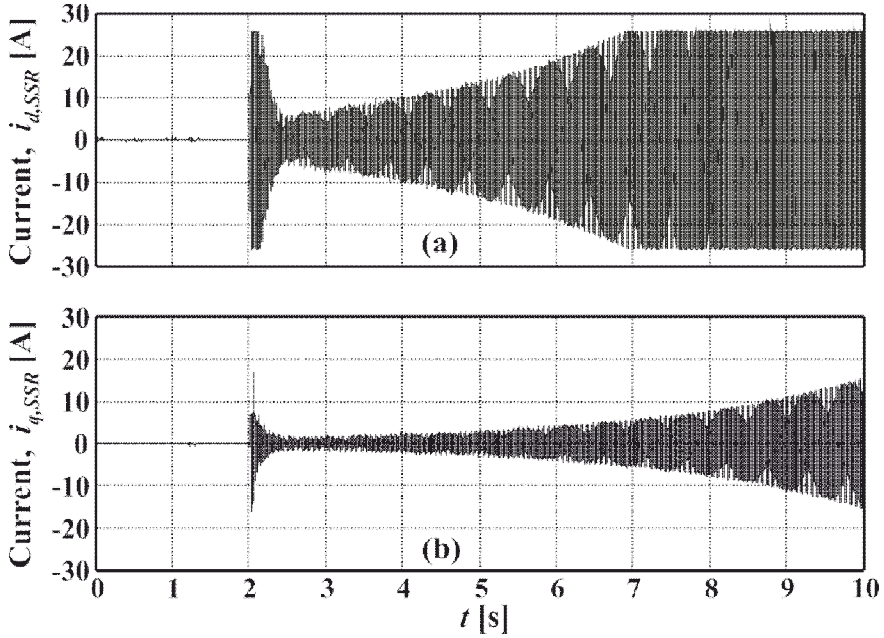

Figure 4.10: Experimental results (VSC-HVDC signals) of the undamped case.
(a) id currents of the subsynchronous component coming from the RTDS.
(b) iq currents of the subsynchronous component coming from the RTDS.

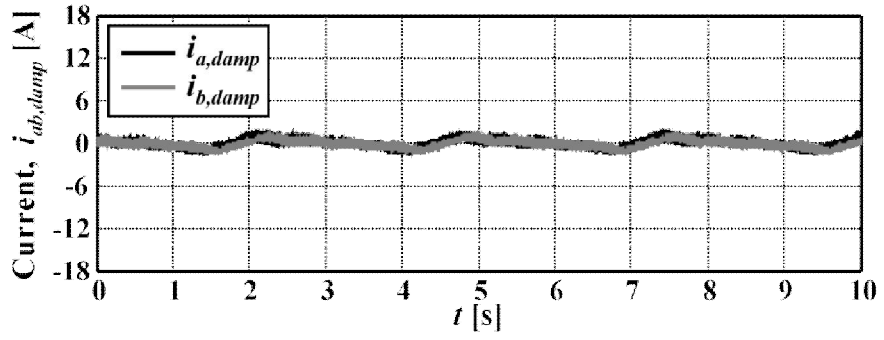

Figure 4.11: Experimental results (VSC-HVDC signals) of the undamped case. Three phase damping current from the HVDC (a & b phase).

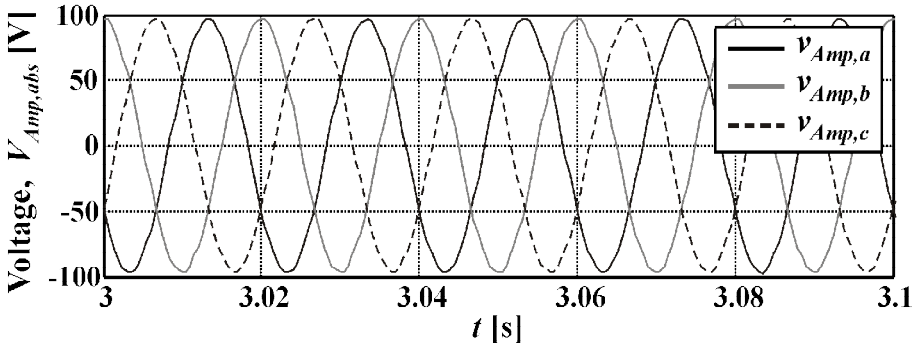

Figure 4.12: Experimental results (VSC-HVDC signals) of the undamped case.
Three-phase voltage from the amplifying converter

The experiment was repeated with the damping converter on the HVDC-VSC test rig activated. The plots in Figure 4.13 and 4.14 illustrate the effect the damping current had on the AC system. Following the change of series compensation from 30% to 40% at 2s, the damping current injected into the AC system prevents SSR from developing. This was shown by the stability in the AC system frequency and torques between turbine sections. Such results are consistent with the simulation results shown in Figures 3.12 and 3.13.

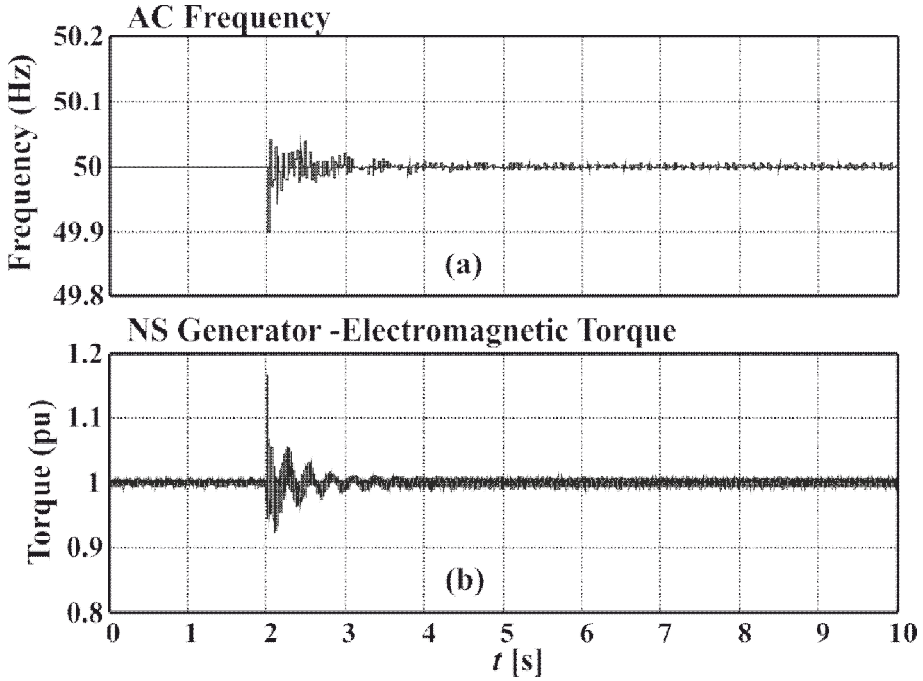

Figure 4.13: Experimental results (RTDS signals) of the damped case.
(a) Frequency of phase a current of the Northern Scotland generator.
(b) Northern Scotland electromagnetic torque.

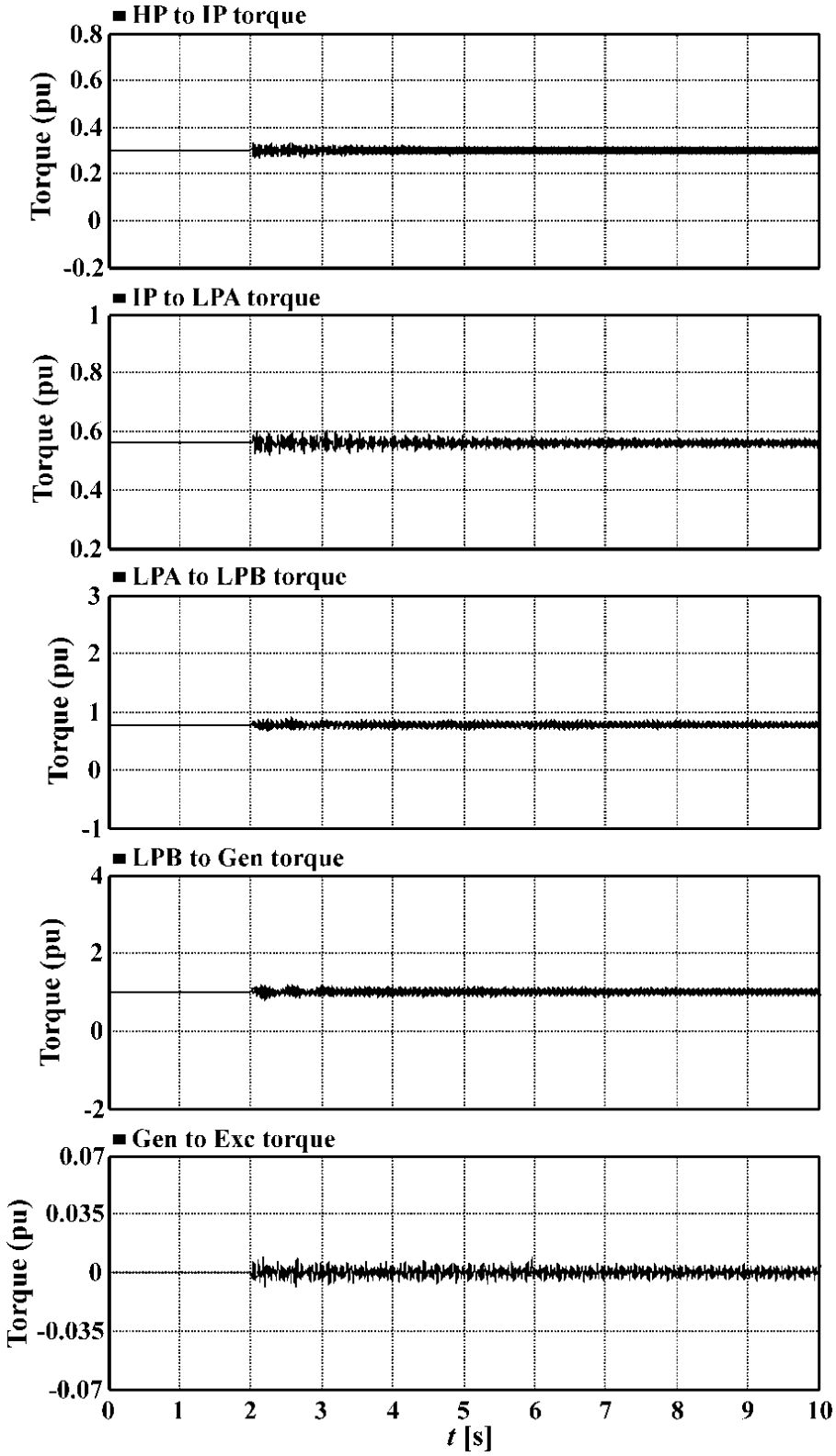

Figure 4.14: Experimental results (RTDS) of the damped case.
Torque interactions in the multi-mass shaft of the Northern Scotland generator.

The plots from Figure 4.15-17 demonstrated the behaviour of the VSC-HVDC. The SSR current component from the RTDS was shown in Figure 4.15. Initially the amplitude of the SSR current component was large, but decreased as the SSR is damped. The three-phase damping current that was generated by the damping converter is shown in Figure 4.16. Under normal conditions the amplitude of the current is very small and makes no contribution to the AC system. However after the series compensation level is changed, a damping current is produced. The AC voltage provided by the amplifying converter was stable throughout the change in series compensation as shown in Figure 4.17.

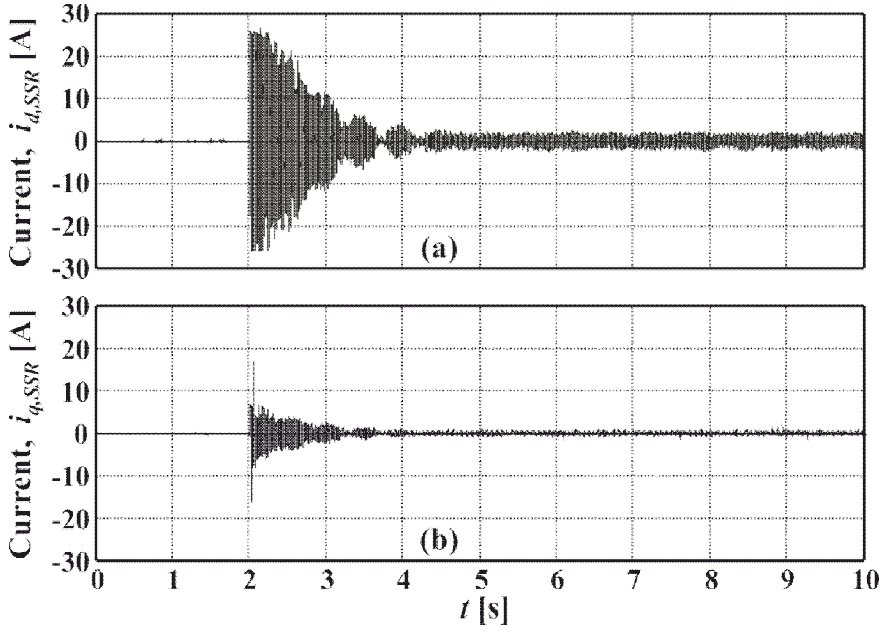

Figure 4.15: Experimental results (VSC-HVDC signals) of the damped case.
(a) id currents of the subsynchronous component coming from the RTDS.
(b) iq currents of the subsynchronous component coming from the RTDS.

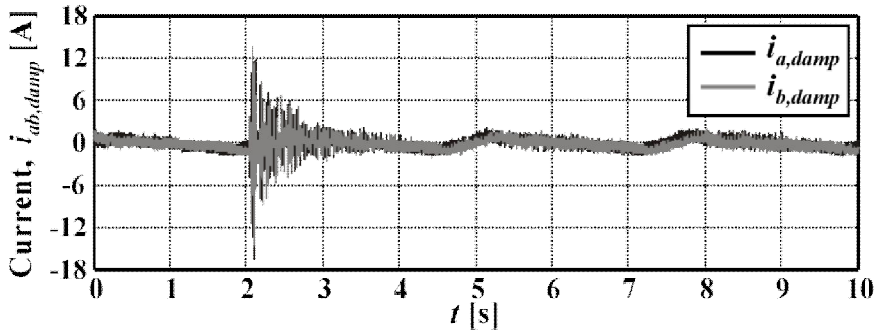

Figure 4.16: Experimental results (VSC-HVDC signals) of the damped case. Three phase damping current from the HVDC (a & b phase).

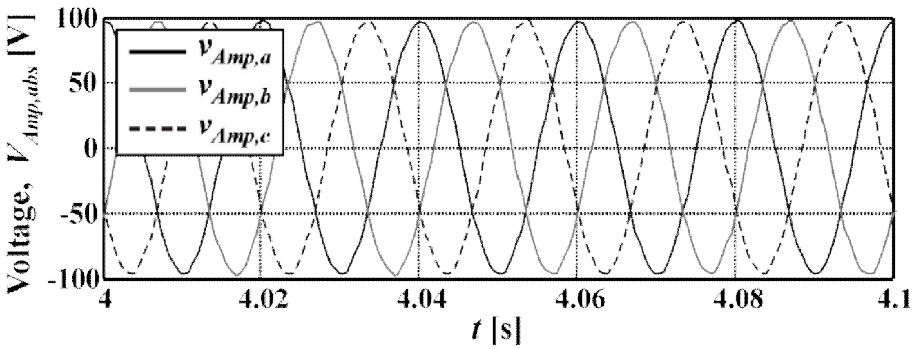

Figure 4.17: Experimental results (VSC-HVDC rig signals). Damping controller active. Three-phase voltage from amplifying converter

4.6 COMPARSION OF SIMULATION AND EXPERIMENT

Figure 4.18 shows a comparison between results obtained from the PSCAD simulation and from the RTDS/VSC-HVDC test rig. The signal chosen for comparison is the electromagnetic torque. In Figure 4.18(*a*) the undamped cases are compared, with the simulation and real-time experiment showing good agreement.

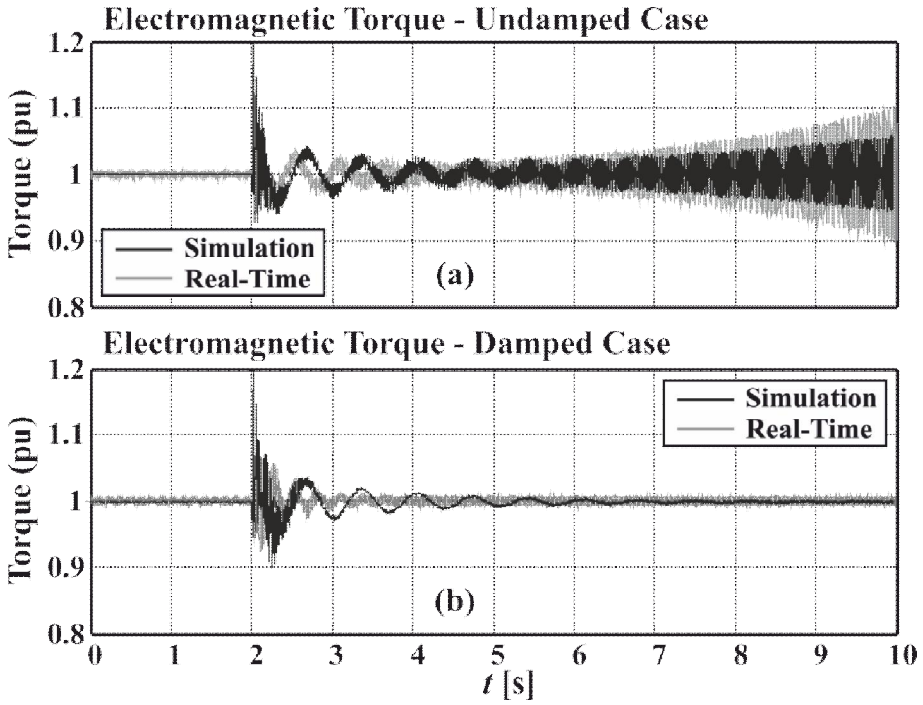

Figure 4.18: Comparison of simulation and real-time results. Northern Scotland electromagnetic torque with damping control (a) not active; (b) active

Similarly, Figure 4.18(*b*) addresses the damped cases and also shows good agreement. The improvement in response time from the experiment is due to the damper having full control over the active and reactive powers needed to perform damping. In the simulation case the converter responsible for damping is also maintaining active and reactive power set points.

In this chapter, an experiment was undertaken through a hardware-in-the-loop RTDS-HVDC test rig to assess the effectiveness of the damping controller described in chapter three. The results from the PSCAD simulation and the results from the experiment show a strong correlation.

Chapter 5 -

Fault Ride Through in Multi-Terminal DC Networks

5.1 INTRODUCTION

When faults occur within AC onshore networks, offshore multi-terminal HVDC (MTDC) networks are subjected to DC overvoltages, potentially damaging DC plant and cables and so wind farm power reduction controllers that limit the overvoltage were designed and tested. Power reduction at the wind turbines was achieved through control signals designed to decrease the voltage, or increase the frequency of the offshore AC wind farm network. These methods do not require dedicated fast communication systems. A similar control algorithm using the reduction of wind farm AC voltage method was simulated in [72].

The power reduction control systems were compared with a power dissipation method using a controlled DC chopper. A method which combines power reduction and power dissipation was also demonstrated. This would minimize the cost and footprint of the power electronic devices.

The four Fault Ride Through (FRT) methods designed and tested were:

- Reduction in the wind farm AC voltage
- Increase in the wind farm AC frequency

- Power dissipation through a DC chopper
- Reduction in the wind farm AC voltage and DC chopper in combination

The control systems were tested in a simulation model and on an experimental test rig. A fault occurs on the onshore AC network, requiring the control systems to take action to minimise a DC over voltage. The results from the simulation model and experimental test rig are shown for the four control systems. A comparison was drawn between the simulation results and the experiment results.

5.2 DESIGN OF THE FAULT RIDE THROUGH CONTROL SCHEMES

In all the control methods, the DC voltage was used to indicate whether there was an imbalance of energy imported into the network and energy exported from the network. As the DC voltage rises above a threshold value, the control systems takes remedial action to either reduce power from the wind farms or dissipate power in the DC network. Control parameters can be found in Appendix B.

The wind farms consist of wind turbines with Fully Rated Converters (FRC). A schematic of the wind farm connection to the VSC-MTDC network and the FRC is shown in Figure 5.1.

The mechanisms for power reduction were characterised by using the wind farm voltage or frequency, to reduce the power exported from the wind turbine generators. The fault on the onshore AC network caused the onshore AC voltage to reduce, this in turn caused the DC voltage to rise in the MTDC network.

The “reduction in wind farm AC voltage” control system used this DC voltage rise to reduce the AC wind farm voltage. The control system created an artificial AC fault on the offshore wind farm AC system. As the voltage dropped on the inverter side of the FRC, the converter current rose until it hits its current limit. At this point the wind turbine reduced its power, ultimately energy is shed from the mechanical system of the wind turbine.

The “increase in wind farm AC frequency” control system used the DC voltage rise to increase the wind farm AC frequency. The rise in AC frequency was sensed by the wind turbine which used this signal to reduce power output through a frequency control loop.

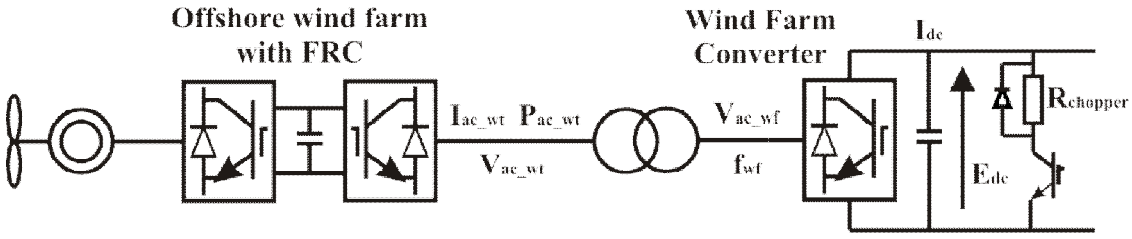

Figure 5.1: Schematic for the wind farm side and control parameters

5.2.1 REDUCTION IN THE WIND FARM AC VOLTAGE

Under normal conditions, the amplitude of the wind farm voltage, V_{ac_wf}, was maintained at its rated value, $V_{ac\_wf\_rated}$, through the wind farm side converter, such that

$$V_{ac\_wf} = V_{ac\_wf\_rated} \tag{4}$$

When a fault occurs within the AC onshore network, the DC voltage rose above its nominal value. As the DC voltage exceeds a defined control value, V_{dc_start}, the wind farm side converter reduced its AC voltage amplitude to

$$V_{ac\_wf} = \alpha V_{ac\_wf\_rated} \tag{5}$$

where α is a metric for the AC voltage reduction given by,

$$\alpha = \begin{cases} 1 & for\ V_{dc} < V_{dc\_start} \\ 1 - \frac{V_{dc} - V_{dc\_start}}{V_{dc\_max} - V_{dc\_start}} & for\ V_{dc\_start} < V_{dc} < V_{dc\_max} \\ 0.1 & for\ V_{dc} \geq V_{dc\_max} \end{cases} \tag{6}$$

where V_{dc} is the measured DC voltage, V_{dc_max} is the allowed maximum DC voltage and ,V_{dc_start} is a defined DC voltage which activates the controller. V_{dc_start} was set at 1.05pu of the nominal voltage to avoid activating under normal voltage variation.

The AC voltage reduction ratio α is a function of the DC voltage, reducing the AC voltage at the terminals of all the wind turbines in the wind farm. This voltage drop is consistent with the voltage drop on the onshore AC network. This is similar to a voltage reduction controller in [72]

As the current cannot increase further to compensate for the voltage drop, the overall power transfer of the converter will reduce. When the wind farms have all reached their current limits, their power outputs reduce at a rate determined by the control signal α.

Co-ordinated power reduction from multiple wind farms can be achieved using this method. The wind farm with the larger initial power output or smaller current rating reduced its power output first, because the converter's current limit will be reached first.

5.2.2 INCREASE IN THE WIND FARM AC FREQUENCY

A power reduction approach using an AC frequency increase, as an alternative to AC voltage reduction, was also used to reduce power from the wind turbines.

Under normal conditions, the frequency of the wind farm voltage, f_{wf}, was maintained at its rated value, f_{wf_rated}, through the wind farm side converter, such that:

$$f_{wf} = f_{wf\_rated} \tag{7}$$

When a fault occurs within the AC onshore network, the DC voltage will rise above its nominal value. As the DC voltage exceeds a defined control value, V_{dc_start}, the wind farm side increased the AC voltage frequency to

$$f_{wf} = (1 + \beta) f_{wf\_rated} \tag{8}$$

where β is given by,

$$\beta = \begin{cases} 0 & for\ V_{dc} < V_{dc\_start} \\ k_f \frac{V_{dc} - V_{dc\_start}}{V_{dc\_max} - V_{dc\_start}} & for\ V_{dc\_start} < V_{dc} < V_{dc\_max} \\ k_f & for\ V_{dc} \geq V_{dc\_max} \end{cases} \quad (9)$$

where V_{dc} is the measured DC voltage, V_{dc_max} is the allowed maximum DC voltage and ,V_{dc_start} is a defined DC voltage which activates the controller. V_{dc_start} is set at 1.05pu of the nominal voltage to avoid activating under normal voltage variation. k_f is a defined coefficient representing the maximum frequency deviation, it's value was chosen to ensure that the deviation in frequency is not too dramatic.

At the wind turbine converter, an auxiliary frequency controlled was implemented by the wind turbine. This would be responsible for using the frequency change in the wind farm to reducing power output of each turbine.

The control signal for the wind turbine, γ, was obtained through the wind farm frequency:

$$\gamma = \frac{f_{wf}}{f_{wf_{rated}}} - 1 \quad (10)$$

When a variation of the wind farm frequency is sensed by a wind turbine converter through a frequency sensor, the wind turbine converter will reduce its power output to:

$$P_{wf} = (1 - \frac{\gamma}{k_f}) P_{wf0} \quad (11)$$

where P_{wf0} is the initial power output from the wind turbine converter.

In a multiterminal HVDC grid with several wind farms, all the wind farms will start to reduce their power outputs at the same rate, given the same measured DC voltage.

5.2.3 POWER DISSIPATION THROUGH A DC CHOPPER

When a chopper resistor is installed in the HVDC grid, the duty ratio *d* is determined to control the chopper circuit and dissipate the extra power of the DC network so as to avoid the DC overvoltage.

Under normal conditions, *δ=0* so the chopper circuit is off.

Under fault conditions, the DC voltage rose above its nominal value. As the DC voltage exceeds a defined control value, V_{dc_start}, the duty cycle of the chopper is calculated by:

$$\delta = \begin{cases} 0 & for\ V_{dc} < V_{dc\_start} \\ \frac{V_{dc}-V_{dc\ start}}{V_{dc\_max}-V_{dc\_start}} & for\ V_{dc\_start} < V_{dc} < V_{dc\_max} \\ 1 & for\ V_{dc} \geq V_{dc\_max} \end{cases} \quad (12)$$

where V_{dc} is the measured DC voltage, V_{dc_max} is the allowed maximum DC voltage and V_{dc_start} is a defined DC voltage which activates the controller.

The power dissipated in the resistor is

$$P_{chopper} = \frac{(\delta V_{dc})^2}{R_{chopper}} \quad (13)$$

When using the DC chopper control system, there is no requirement for the wind turbines to reduce their power outputs.

5.2.4 REDUCTION IN WIND FARM AC VOLTAGE AND DC CHOPPER IN COMBINATION

The power reduction and power dissipation methods used alone all have disadvantages. Fast power reduction at the wind turbine can cause mechanical stresses. Power dissipation within the DC bus requires additional power electronics with the additional cost and footprint this entails.

A logical approach to reducing DC chopper cost and size and the mechanical stresses in the wind turbines would be to combine the methods. This has approach has been suggested in literature [67], but not tested.

In the event of a DC overvoltage both the DC chopper and AC voltage reduction control loops are initiated. The rate of reduction of AC voltage is limited, thus protecting the wind farm turbines from fast voltage change. As the power from the wind farm is reduced the DC chopper is required to dissipate less energy and therefore can be smaller in size, cost and footprint. The responsibility for avoiding a DC overvoltage is a combination of power reduction and power dissipation.

Long lasting AC faults were not tested in this chapter. However, in such a fault, the combined method would allow the DC chopper to be switched off at a defined temperature or time limit, thus avoiding overheating issues.

5.3 THE SIMULATION PLATFORM

For the simulation study, the MTDC network was modelled as a three terminal network consisting of two wind farm terminals and one grid side terminal. Wind farm 1 was rated at 400 Watts and wind farm 2 was rated at 300 Watts, these set points are chosen to allow comparison with the experimental test rig. In the simulation the FRC wind turbines are modelled as DC current sources behind the FRC's inverter, this is shown in Figure 5.2. The grid side terminal controls DC voltage and the wind farm terminals control the offshore wind farm frequency and AC voltage. Alternatively, a droop control system could be used.

A three-phase AC fault was triggered at 0.5 seconds and lasts for 140 milliseconds, after which the system recovers to its nominal voltage. For the power dissipation control methods, a DC chopper is installed on the DC side of wind farm 2. The chopper circuitry is placed on the wind farm side because in meshed DC networks it is expected that energy would need to be dissipated at the point at which it is generated.

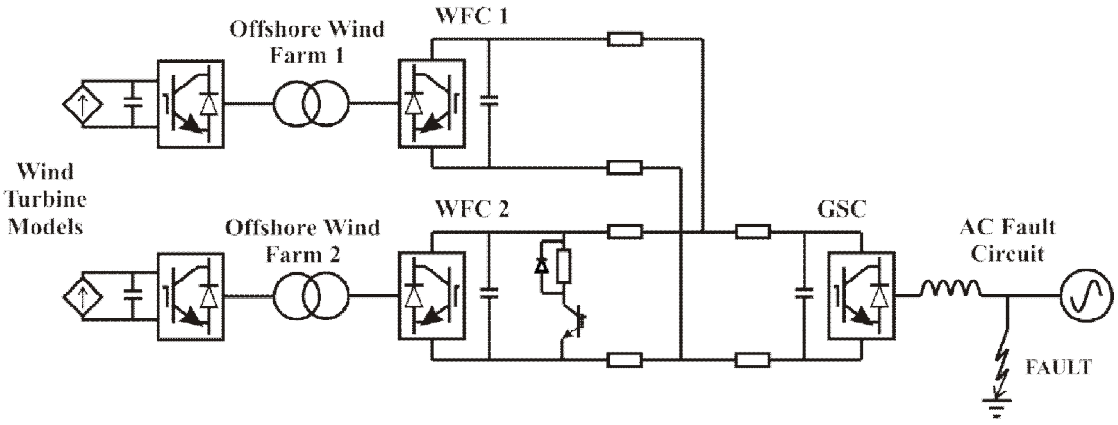

Figure 5.2: Network schematic showing two wind farms connected to one AC grid connection. An AC fault circuit is connected to the onshore terminal.

5.4 THE EXPERIMENTAL PLATFORM

The platform used for experimental implementation, shown in Figure 5.3, was based on two components: a three-terminal VSC-HVDC test rig and a PSS. The test rig consisted of three VSCs, two motor-generating units, a dSPACE controller and two Unidrive inverters (these control the motor, which operates the generating units). The VSC-HVDC test rig was used to model the multi-terminal HVDC transmission system and the wind turbines. The PSS is a general use power systems simulator and was simply used to model the AC fault circuit. Hardware parameters for the VSC-HVDC rig and the PSS can be found in Appendix C.

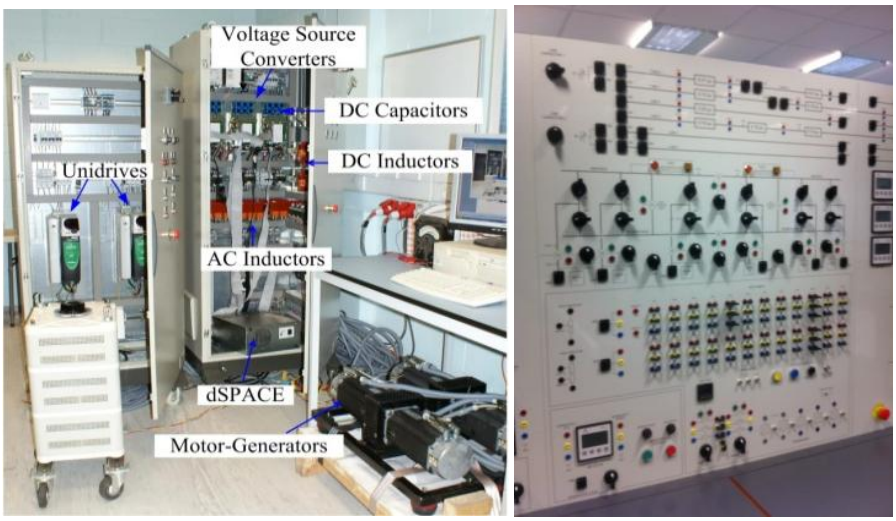

Figure 5.3: Experimental platform. HVDC test rig (left) and PSS (right)

The experimental schematic is shown in Figure 5.4. The onshore AC system and the DC system was the same as the simulation case, however in the experiment the wind turbine generators were connected directly to the wind farm converters. The wind turbine control is modelled within dSpace software. Upon a reduction in wind farm voltage or an increase in wind farm frequency, a new torque set-point is derived within software and a corresponding reduction was ordered to the Unidrive controlled motor. This caused a reduction in the power tranferred from the generators.

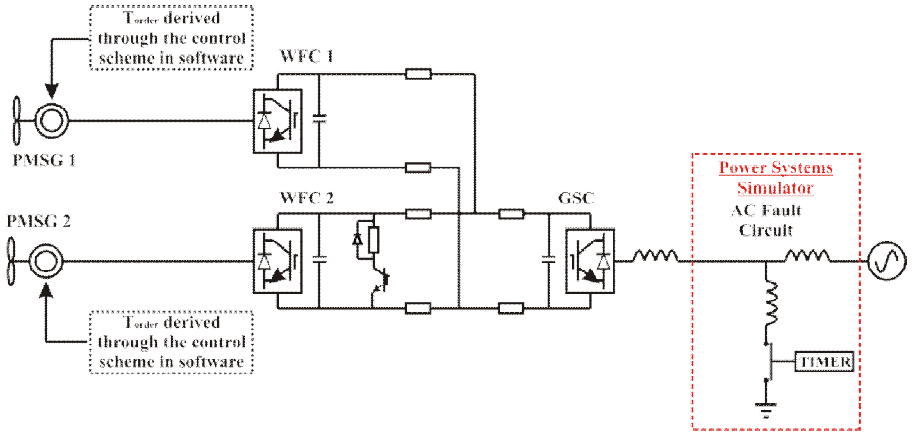

Figure 5.4: Experimental schematic showing two wind farms connected to one AC grid connection. The wind turbine rigs are connected directly to the wind farm converters. The AC fault circuit is located on the PSS.

5.4.1 AC ONSHORE FAULT

For the experiment, the fault circuit was designed to mimic a three-phase to ground fault near the AC grid connection terminal, similar to the fault circuit designed in [103]. The testing of the control schemes was performed by programming a timer on the PSS to a specified fault time. During the time when the fault circuit is closed, a voltage dip appears on the AC side of the grid converter and limits the power exported to the AC onshore grid.

A trace of the AC voltage and current at the onshore grid terminal is shown in Figure 5.5. As the contactor to ground is closed, the voltage drops to approximately 0.3pu. The fault current rises to 3pu instantaneously and settles at 2pu. Following the clearing of the fault after 140ms the AC voltage and current returns to normal.

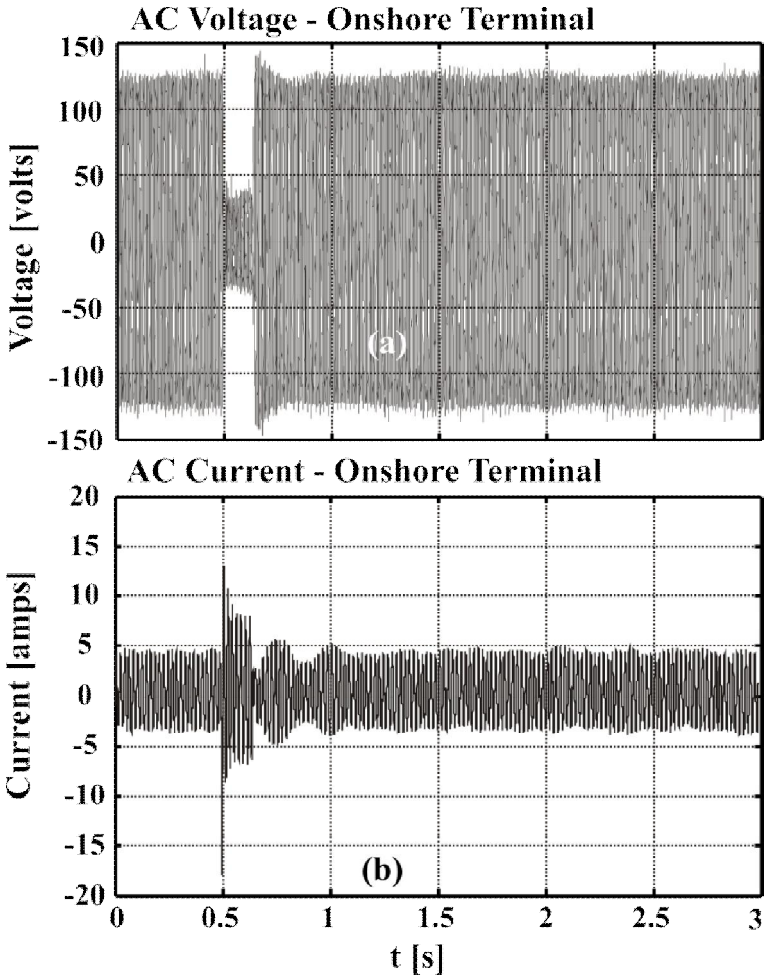

Figure 5.5: AC voltage and currents at the onshore terminal during the fault

Whilst the onshore AC voltage reduced, the transfer capacity of the onshore converter is similarly reduced. This rejected load means that there is an excess of energy on the DC bus, increasing the DC voltage across the MTDC network.

5.5 RESULTS

The results were gathered from time domain simulations and experiments. The simulations were performed on PSCAD/EMTDC and plotted on MATLAB. The experimental results were also plotted in MATLAB. The simulation results are shown side-by-side with the experimental results to allow for easy comparison.

5.5.1 REDUCTION IN THE WIND FARM AC VOLTAGE

As the AC onshore grid voltage reduces this causes a rise in the DC voltage as shown in Figure 5.6(a). A threshold value (V_{dc_start}) of 260 volts was chosen with a maximum (V_{dc_max}) value of 270 volts.

As the DC voltage threshold value is crossed the controller was designed to decrease the AC wind farm voltage. To achieve this, a control signal α was generated to reduce wind farm AC voltage as shown in Figure 5.6(b). The AC voltage reduces until, in the simulation, the minimum voltage level of 0.1pu was reached. This limit is imposed to avoid the machine stalling in the experiment. For consistency the limit is also applied to the simulation model. The experiment shows a drastic reduction in AC voltage although the minimum voltage was not reached. This due to the faster response of the simulation compared to the experiment.

The individual wind turbines used this reduction in wind farm AC voltage to reduce their output. The co-ordinated response by the two wind farms can be seen in Figure 5.6(c) which shows the power transfer at each terminal. As wind farm converter 1 is exporting more power it runs into its current limit first. It then reduces to the power capacity of wind farm 2, at this point both wind farms reduce power.

After the fault has cleared the DC voltage returns to its nominal value of 245 volts. The undershoot of the DC voltage to 230 volts can be explained by the large onshore AC system inductance which is included to limit fault current in the experiment.

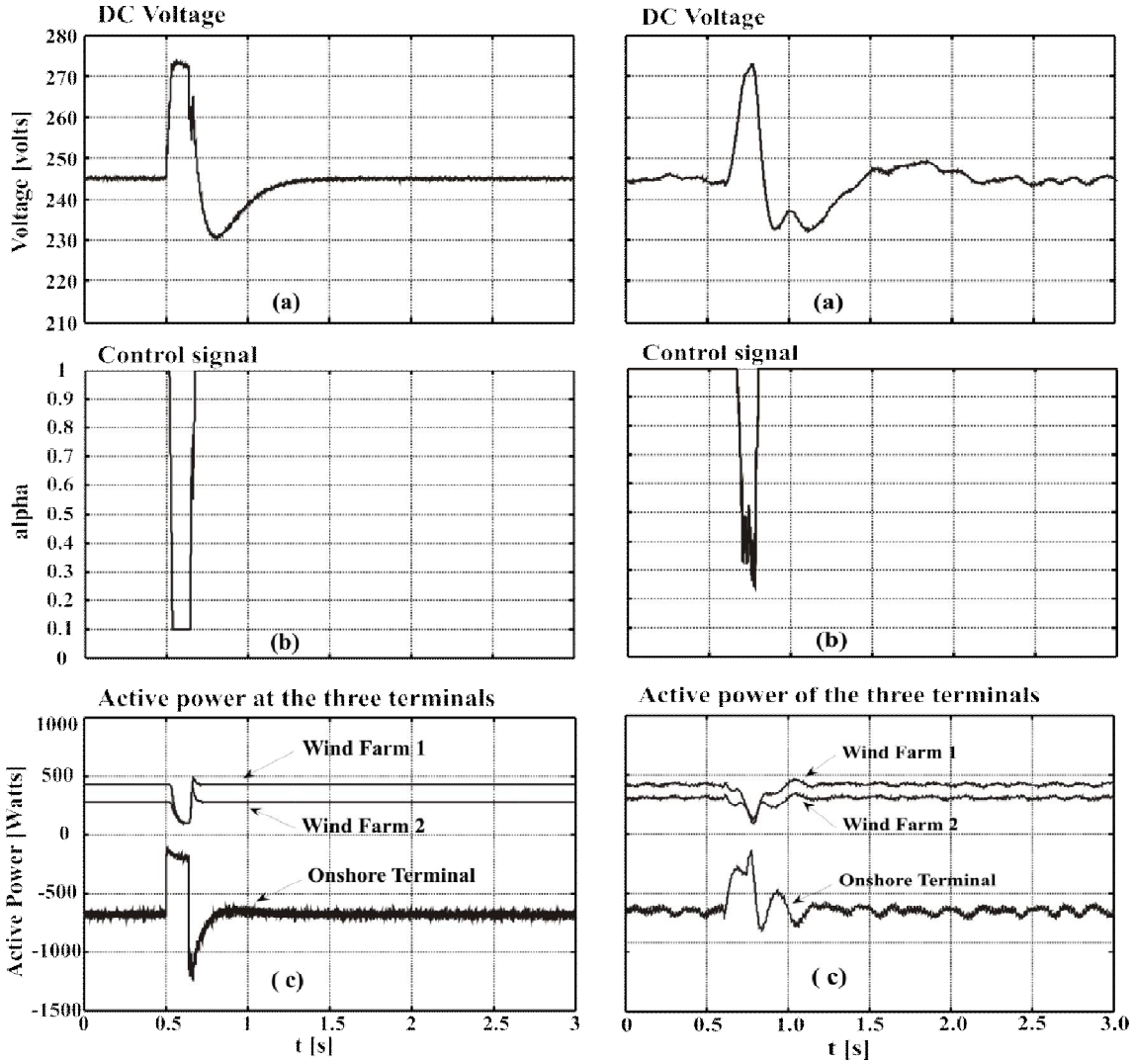

Figure 5.6: FRT by reducing wind farm AC voltage.
PSCAD simulation (left) and experimental results (right)
(a) DC voltage
(b) Control signal **α** to set the AC voltage
(c) Power flows at the three terminals

5.5.2 INCREASE IN THE WIND FARM AC FREQUENCY

As the AC onshore grid voltage reduces this causes a rise in the DC voltage as shown in Figure 5.7(a). Again, a threshold value (V_{dc_start}) of 260 volts was chosen with a maximum (V_{dc_max}) value of 270 volts.

As the DC voltage threshold value is crossed the controller was designed to increase the AC wind farm frequency, as shown in Figure 5.7(b). The frequency increases until, in the simulation, the maximum frequency limit of 60Hz is reached. The experiment shows an increase in frequency up to value of 57Hz. This due to the faster response of the simulation compared to the experiment.

The individual wind turbines use the reduction in wind farm AC voltage to reduce their output. The power at each terminal is shown in Figure 5.7(c). Under this control system, both wind farms reduce their power at the same rate, due the frequency in both wind farms increasing at the same rate.

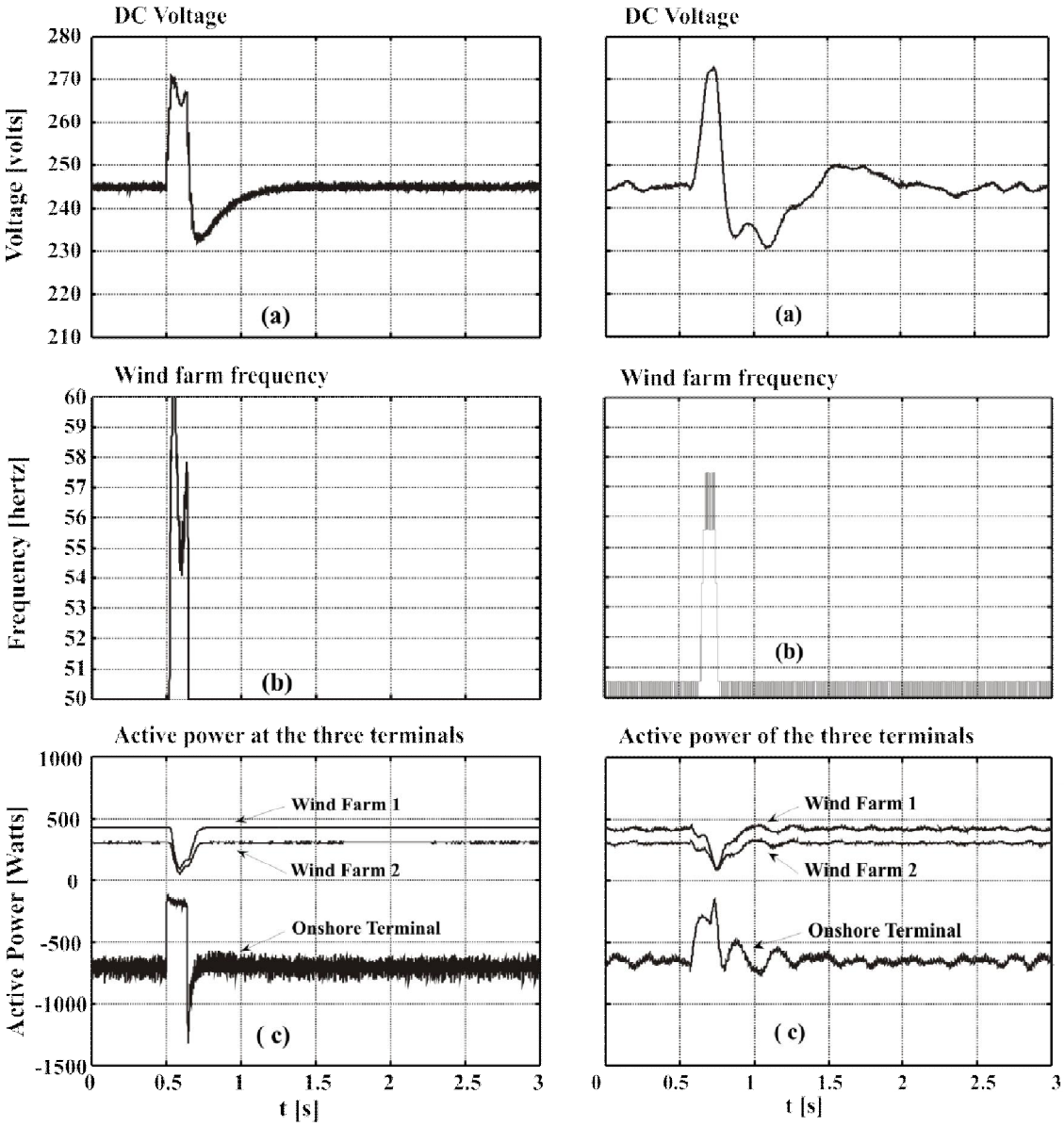

Figure 5.7: FRT by frequency increase of the wind farm.
PSCAD simulation (left) and experimental results (right)
(a) DC voltage
(b) Wind farm frequency
(c) Power flows at the three terminals

5.5.3 POWER DISSIPATION THROUGH A DC CHOPPER

As the AC onshore grid voltage reduces this causes a rise in the DC voltage as shown in Figure 5.8(a). Again, a threshold value (V_{dc_start}) of 260 volts was chosen with a maximum (V_{dc_max}) value of 270 volts.

As the DC voltage threshold value is crossed the controller was designed to initiate the DC chopper circuit to dissipate excess energy in the DC network. The duty cycle, δ, of the chopper circuit increases as shown in Figure 5.8(b). This controls how much power is dissipated by the resistor in the DC bus. The resistor was sized at 45Ω, which could dissipate 1.33kW of power at this DC voltage.

The power transfer across each terminal is shown in Figure 5.8(c). There is no corresponding reduction in power imported from wind farms as the energy is dissipated in the DC network. Compared to the power reduction approach the maximum DC overvoltage is reduced, and the response to the fault is faster. However, a direct comparison cannot be drawn as the exact nature of the response is dependent on the size of the resistor.

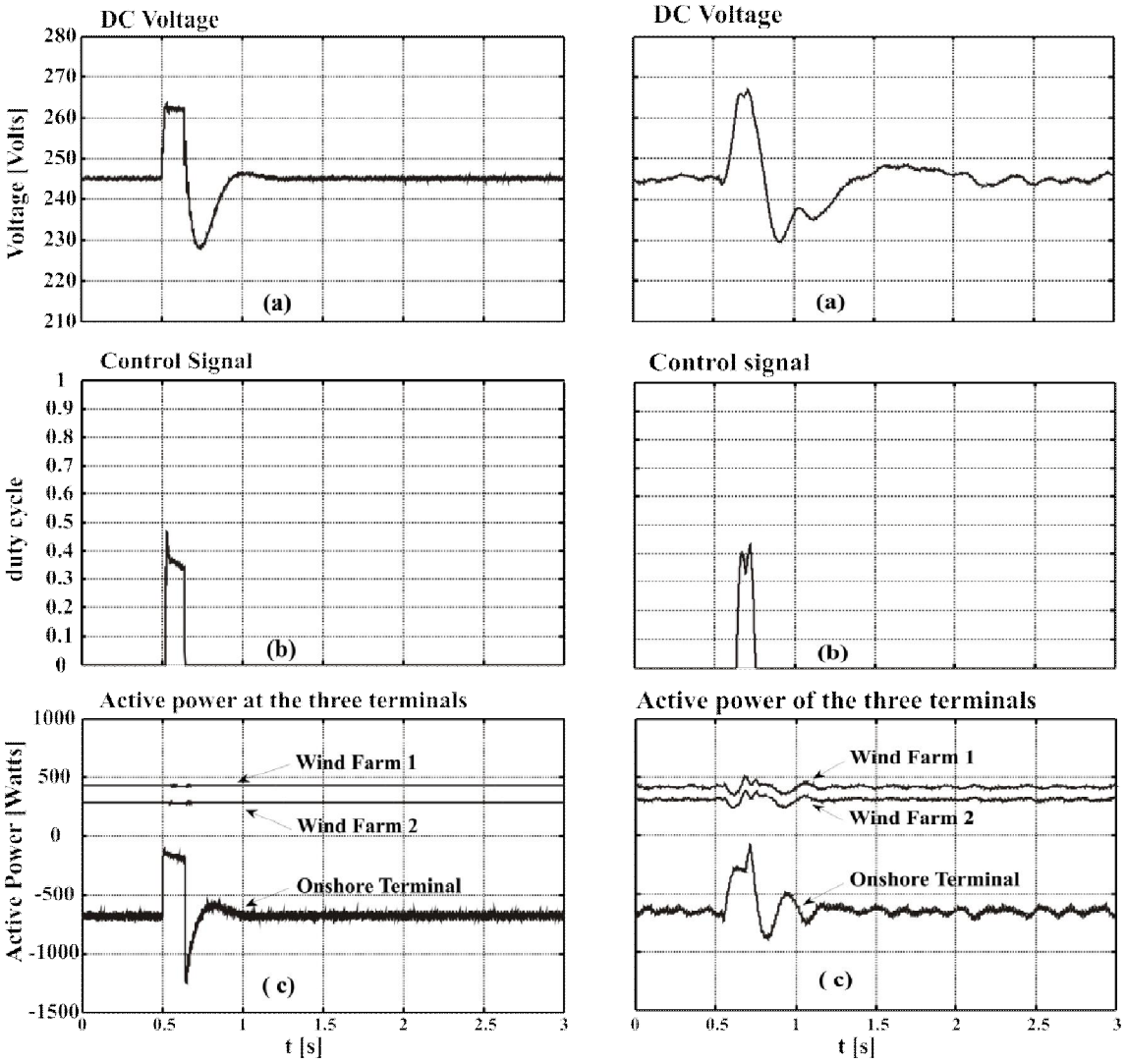

Figure 5.8: FRT by power dissipation in the DC chopper.
PSCAD simulation (left) and experimental results (right)
(a) DC voltage
(b) Duty cycle d to control the DC chopper circuit
(c) Power flows at the three terminals

5.5.4 REDUCTION IN WIND FARM AC VOLTAGE AND DC CHOPPER IN COMBINATION

As the AC onshore grid voltage reduces this causes a rise in the DC voltage as shown in Figure 5.9(a). Again, a threshold value (V_{dc_start}) of 260 volts was chosen with a maximum (V_{dc_max}) value of 270 volts.

As the DC voltage threshold value is crossed the controller was designed to initiate both the AC wind farm voltage reduction and the DC chopper circuit.

The duty cycle, δ, of the chopper circuit increases and the control signal, α, reduces as shown in Figure 5.9(b). Compared to operating each control scheme alone, improvements were made.

As the magnitude of AC voltage reduction was lower, this will ease mechanical stress on the wind turbines. Taking the experimental results, a minimum voltage of 0.5pu was reached against 0.25pu for AC voltage reduction in alone.

As the maximum duty cycle of the chopper reaches a lower value, a small chopper could be used. Again taking the experimental results, a maximum duty cycle of 0.39 was reached against 0.43 for the DC chopper operating alone. As the power dissipated by the chopper is proportional to the square of the duty cycle, this equates to large reduction in power dissipation.

The power transfer across each terminal is shown in Figure 5.9(c). For this fault type and duration, only one wind farm needs to reduce its power output. For larger reductions in AC voltage or longer faults, both wind farms maybe required to reduce power.

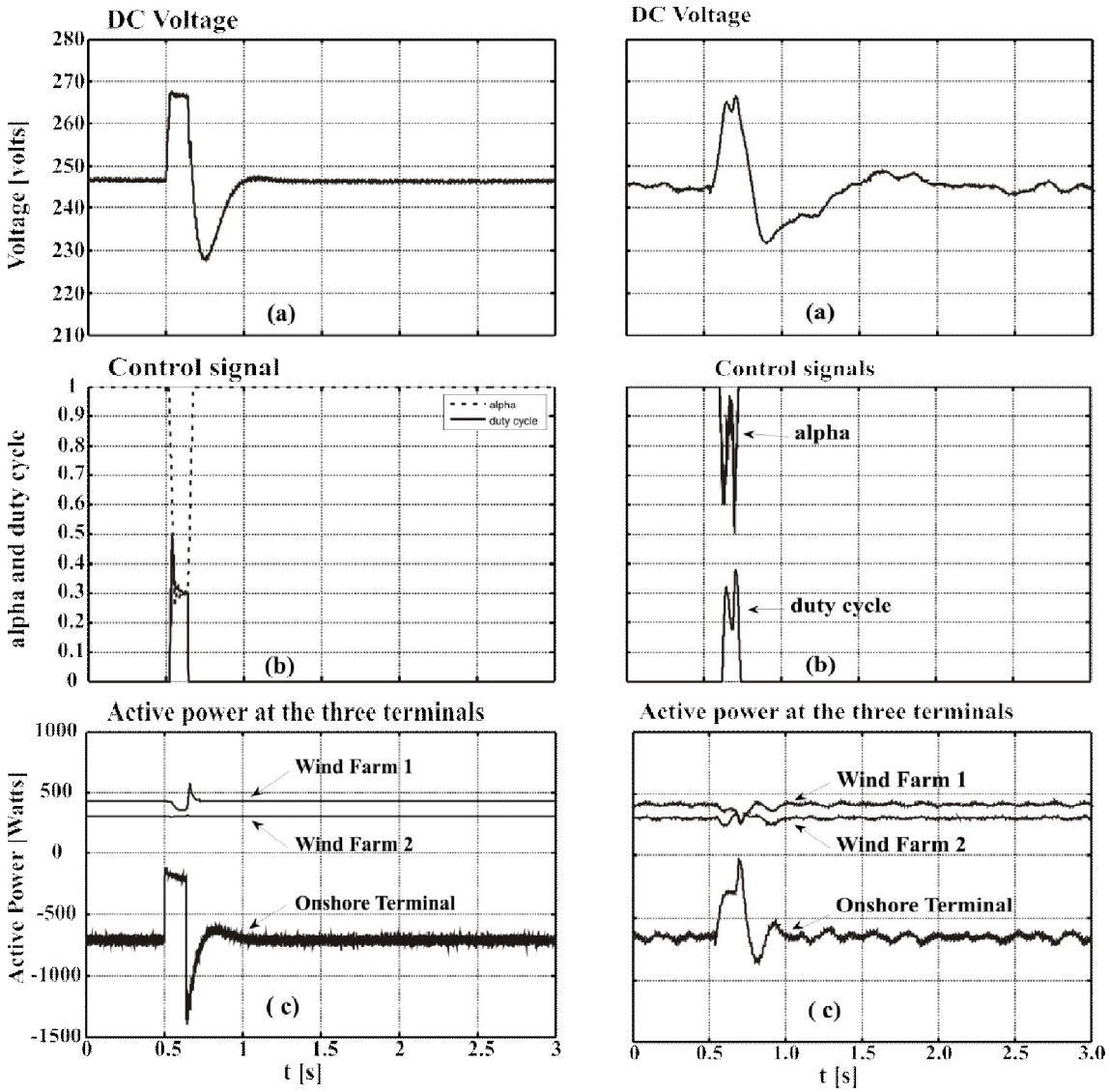

Figure 5.9: FRT by DC chopper and reduction in the wind farm AC voltage
PSCAD simulation (left) and experimental results (right)
(a) DC voltage
(b) Duty cycle d to control the DC chopper circuit and control signal a to set the AC voltage
(c) Power flows at the three terminals

5.6 COMPARISON OF SIMULATION AND EXPERIMENT

Figure 5.10 shows a direct comparison between results obtained from the PSCAD simulation the experiment, these are the traces from Figure 5.8(a) overlaid. The signal used for comparison is the DC voltage trace from the DC chopper control schemes.

The results from the simulation and the experiment show good agreement. The control response from the simulation is slightly faster, this was expected as physical signals need to be measured and transmitted within the experiment.

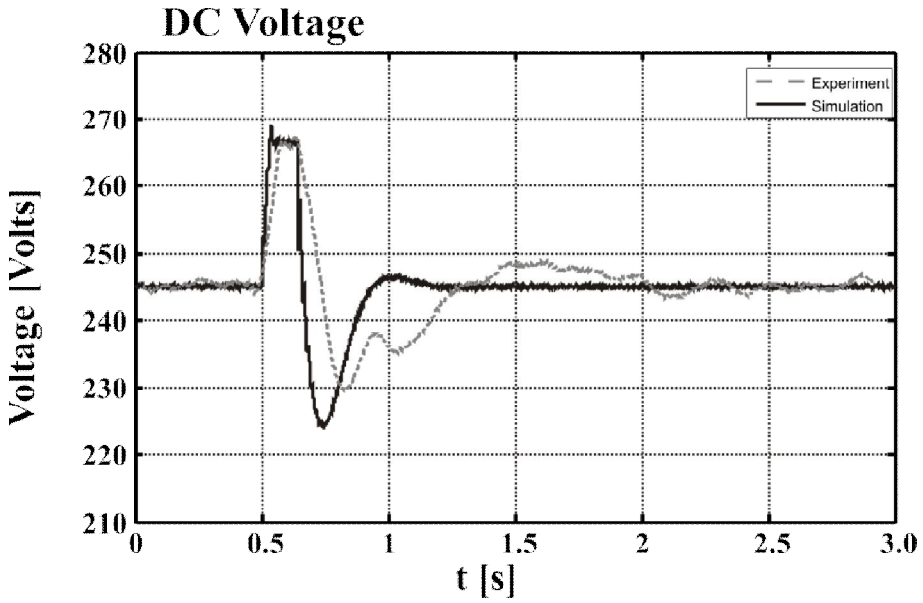

Figure 5.10: Comparison of simulation and experimental results. The DC voltage from the "power dissipation through a DC chopper" control scheme

5.7 DISCUSSION

The FRT capability of multi-terminal HVDC networks will be a key test to ensure the feasibility of offshore DC networks. This capability can be achieved through power reduction and power dissipation techniques, or a combination of the two. The FRT control schemes were simulated in PSCAD and verified on an experimental VSC-HVDC rig.

The simulation results show that both the power reduction and power dissipation control schemes alone can demonstrate the required FRT capability. Of the three methods, the power dissipation provides the best response. However a comparison is

difficult as different sized chopper resistors would affect the DC voltage. Comparing the simulations and experiment results for each case shows good agreement.

A more commercial solution was to combine power reduction and power dissipation to minimize the size and cost of power electronics. Also, the AC voltage reduction can be managed to limit mechanical stress to the wind turbines. It would be possible to implement all three control systems simultaneously, although this was not tested in this research.

For longer faults the DC chopper could be switched off, either after a defined time period or at a defined temperature. Power reduction at the wind turbines would then account for the FRT capability. This was not undertaken due to time and equipment limitations.

Chapter 6 -

Conclusions and Further Work

6.1 CONCLUSIONS

6.1.1 DAMPING SUBSYNCHRONOUS RESONANCE

Proposed reinforcements for the GB transmission network towards 2020 include onshore series compensation and offshore HVDC links. Possible adverse effects of the series compensation reinforcement, in the form of SSR were shown by simulating a series compensated three-machine network in PSCAD, which resembles the operation of the mainland GB system in the 2020.

For the offshore VSC-HVDC link, a primary control scheme was designed in order to control the active and reactive power. SSR mitigation was achieved through an auxiliary control loop within the VSC. The primary controller and auxiliary damper were combined. Simulation results show that the combined controller was able to control active and reactive power and damp subsynchronous resonance.

A hardware VSC-HVDC test rig was designed and built to ensure the damper could be implemented and to validate the simulation model. For the experiment a RTDS was used to model the AC system. Although simplified network representations were employed, the models have the flexibility to incorporate generation plant and

transmission networks of more complex systems. This would allow generator plant owners and transmission system operators to assess the impacts of series compensation, the SSR phenomenon and its mitigation in detailed system studies.

A comparison between the simulation model results and the experimental results was made, showing good agreement between them.

As VSC-HVDC is utilized more in future, the flexibility of the converters can be used to damp SSR in adjacent AC transmission systems. This may be cost effective by eliminating the requirement for additional power electronics equipment (such as TCSCs).

6.1.2 FAULT RIDE THROUGH OF MTDC NETWORKS

The fault ride through capability of MTDC networks will be a key attribute to ensure the feasibility of offshore DC networks. TSO's have FRT requirements in their Grid Codes.

A simulation model of a MTDC system was built in PSCAD software. The topology used was two wind farms and one grid connection, with a three phase fault included on the AC grid.

The FRT capability was achieved through power reduction and power dissipation techniques, with four control systems investigated in this research. Each control system was simulated, power reduction and power dissipation controller alone demonstrated FRT capability.

A commercially attractive solution was to combine power reduction and power dissipation to minimize the size and cost of power electronics. Power reduction can be managed to limit mechanical stress in the wind turbines. Redundancy is provided by using two control systems independently; each can operate alone if required.

A hardware VSC-HVDC test rig was built to assess the control systems and validate the simulation model. A comparison between the simulation model results and the experimental results was drawn, showing good agreement between them.

6.1.3 CONTRIBUTIONS OF THE THESIS

The following objectives were set and achieved:

(1) To design a control scheme for the damping of SSR in the onshore AC network, of the 2020 GB transmission system.

(2) To design and build a laboratory based experiment to demonstrate SSR damping. A flexible AC equivalent system was created on an RTDS and a hardware test rig was developed for the VSC-HVDC link.

(3) To design and compare several FRT control schemes for MTDC networks, using a combination of power reduction and power dissipation techniques.

(4) To design and build a laboratory based experiment to demonstrate FRT control schemes. A hardware test rig was developed for a multi-terminal VSC-HVDC link; in addition a Power Systems Simulator was used to test onshore AC fault circuits.

6.1.4 ACHIEVEMENTS OF RESEARCH

The outcomes of this research were written up in a journal paper and two conference papers.

(1) Livermore L, Liang J, Ekanayake J, "MTDC VSC Technology and its applications for Wind Power", Universities Power Engineering Conference (UPEC), Cardiff, 2010.

(2) Livermore L, Ugalde-Loo C, Liang J, Ekanayake J, Jenkins N, "Damping of Subsynchronous Resonance using a VSC-HVDC Link", 17th Power Systems Computation Conference (PSCC), Stockholm, 2011.

(3) Livermore L, Ugalde-Loo C, Mu Q, Liang J, Ekanayake J, Jenkins N. "Damping of SSR using a VSC-HVDC Link in a Series-compensated GB Transmission Network", IEEE Transactions on Power Systems, Submitted.

In addition, simulations and experiments have been demonstrated to industrial partners including National Grid, and a manufacturer of HVDC equipment, Alstom Grid. Through the FlexNet collaboration of universities and industry, the research was disseminated to research peers.

Additionally, expertise from this research has contributed to the CIGRE B4.58 technical report 'Devices and methodologies for load flow control in MTDC networks' due for publication in 2013.

6.2 FURTHER WORK

Following the analysis of simulation and experimental results, further avenues of research are available. A brief summary of potential research question is given in this section.

6.2.1 AN ADAPTIVE SSR DAMPING CONTROLLER

An adaptive SSR damper would be able to damp SSR at a range of frequencies, caused by a range of reactances in the electrical network and/or change of mechanical parameters of the turbine set. A potential solution could be achieved by a wide band pass filter or by filtering out the 50Hz component and damping out the remainder frequencies.

6.2.2 FAULT RIDE THROUGH OF MTDC NETWORK WITH MULTIPLE ONSHORE GRID TERMINALS

Load rejection into an onshore grid occurs during an AC fault near to the onshore terminal. In a multi-terminal HVDC network, it is possible to re-route the flow of power through additional onshore terminals (assuming they are not similarly affected). This would reduce the need for power dissipation and power reduction from the wind farms. An extreme case would be the entire loss of an onshore terminal due to maintenance or a fault.

Unbalanced faults in the onshore AC network will lead to load rejection on the offshore DC network. The effect of the unbalanced AC fault on the DC network would be different to the three-phase to ground fault tested in this thesis. Simulation and experimental tests could be performed using the model and test rig.

During AC faults multiterminal networks should not only ride through the fault but also inject reactive power into the AC onshore grid to support the AC voltage. This control algorithm could be included into the onshore grid controller as an auxiliary or emergency function.

APPENDIX A – THREE MACHINE SYSTEM PARAMETERS (IN P.U.)

Machine rating: Southern Scotland: 2800 MVA, 33 kV. Northern Scotland: 2400 MVA, 33 kV. England and Wales: 21000 MVA, 400 kV. Base frequency: $f_b = 50$ Hz, $\omega_b = 2\pi f_b$.

Synchronous generators (on base of machine rating): $R_a = 0.002$, $X_l = 0.17$, $X_q = 2.07$, $X_q' = 0.906$, $X_q'' = 0.234$, $X_d = 2.13$, $X_d' = 0.308$, $X_d'' = 0.234$, $X_{mq} = 1.9$, $X_{md} = 1.96$, $\tau'_{d0} = 6.0857$s, $\tau'_{q0} = 1.653$s, $\tau''_{d0} = 0.0526$s, $\tau''_{q0} = 0.3538$s.

Single mass shaft (Southern Scotland and England/Wales generators): Inertias (MWs/MVA): $H_{SScot} = 3.84$, $H_{EW} = 5$. Damping coefficients (p.u. T/p.u. speed dev.): $D_{SScot} = D_{EW} = 0.1$.

Multi-mass shaft (Northern Scotland generator): Inertias (in MWs/MVA): $H_H = 0.092897$, $H_I = 0.155589$, $H_{LA} = 0.858670$, $H_{LB} = 0.884215$, $H_G = 0.868495$, $H_X = 0.0342165$. Self and mutual damping coefficients (in p.u. T/p.u. speed dev.): $D_H = D_I = D_{LA} = D_{LB} = 0.1$, $D_G = D_X = 0$, $D_{HI} = D_{IA} = D_{AB} = D_{BG} = 0.2$, $D_{GX} = 0.005$. Torsional stiffness (in p.u. T/rad): $K_{HI} = 19.303$, $K_{IA} = 34.929$, $K_{AB} = 52.038$, $K_{BG} = 70.858$, $K_{GX} = 2.822$.

Transformers, transmission lines and loads (on a 1000 MVA base): $X_{11} = 0.14$, $X_{21} = 0.07$, $X_{12} = 0.01$, $X_{22} = 0.1$, $X_3 = 0.05$. X/R = 10. Shunt capacitors in representations of the lines, $X_{CSh} = 20$ p.u. Loads: $P_{L3} = 17.73$, $Q_{L3} = 2.4847$. $P_{L4} = 2.0$, $Q_{L4} = 0$.

APPENDIX B – CONTROL PARAMETERS

PSCAD SSR DAMPING SIMULATION

VSC-HVDC Link Rating: 250MW

Primary controller: *Active power*: K_{PI} = 0.0001, τ_{PI} = 0.05. *Reactive power*: K_{PI} = 0.01, τ_{PI} = 0.5. I_d *current*: K_{PI} = -0.5, τ_{PI} = 0.003. I_q *current*: K_{PI} = 2.5, τ_{PI} = 0.01. *DC voltage*: K_{PI} = 0.02, τ_{PI} = 0.8. *Reactive power 2*: K_{PI} = -0.1, τ_{PI} = 0.001. I_d *current*: K_{PI} = 0.5, τ_{PI} = 0.005. I_q *current*: K_{PI} = -0.1, τ_{PI} = 0.001.

Auxiliary controller: *BPF* center freq. 20Hz, *Lead-lag compensator*: gain $K_{L\text{-}L}$ = 10, time constants τ_{Lead} = 0.0040, τ_{Lag} = 0.0090.

RSCAD SSR DAMPING SIMULATION

Damping controller: *HPF*: cut-off freq. 15Hz, 4 pole-pairs. *LPF*: cut-off freq. 25Hz, 4 pole-pairs. *Lead-lag comp. (trans.)*, $K_{L\text{-}L}$ = 5, τ_{Lead} = 0.0428, τ_{Lag} = 0.015. *Scaling (trans.)*: *RTDS* → *HVDC* current factor 4, voltage factor 400. *HVDC* → *RTDS* current factor 16. *Lead-lag comp. (damp.)*: $K_{L\text{-}L}$ = 5, τ_{Lead} = 0.0042, τ_{Lag} = 0.0096.

PSCAD FRT SIMULATION

Converter 1: *DC voltage*: K_{PI} = 2, τ_{PI} = 0.01. *Reactive Power*: K_{PI} = 0.3, τ_{PI} = 0.03. I_q current: K_{PI} = 25, τ_{PI} = 0.003.

Switching frequency 4 kHz.

Wind farm operating points: Wind farm 1 - 400 watts, Wind farm 2 – 300 watts

Nominal DC voltage: V_{dc_rated}= 245v. Threshold voltage V_{start} = 260v. Maximum DC voltage: V_{max} = 270V. AC fault duration: t = 140ms.

AC voltage reduction control: AC voltage, V_{wf_rated} = 120v, minimum voltage limitation = 0.1p.u.

Frequency increase: Frequency, frated = 50Hz, maximum frequency limitation = 60Hz. k_f = 0.2

dSPACE FRT CONTROLLER

Converter 1: *DC voltage*: K_{PI} = 0.1, τ_{PI} = 0.05. *Reactive Power*: K_{PI} = 0.01, τ_{PI} = 0.1. I_q current: K_{PI} = 2, τ_{PI} = 0.1. I_d current: K_{PI} = 2, τ_{PI} = 0.1.

Switching frequency 4 kHz.

Wind farm operating points: Wind farm 1 - 400 watts, Wind farm 2 – 300 watts

Nominal DC voltage: V_{dc_rated}= 245v. Threshold voltage V_{start} = 260v. Maximum DC voltage: V_{max} = 270V. PSS timed fault: t = 140ms.

AC voltage reduction control method: AC voltage, V_{wf_rated} = 120v, minimum voltage limitation = 0.1p.u.

Frequency increase: Frequency, frated = 50Hz, maximum frequency limitation = 60Hz. k_f = 0.2

APPENDIX C – HARDWARE PARAMETERS

VSC-TEST RIG

VSCs: Nominal = 1kVA, Max = 10kVA, *Topology*: Two level, 3-*Φ* without neutral wire. *IGBT Model*: SKiiP 23NAB12T4V1

DC Voltage: Nominal = 245V, Max = 900V. *Switching Frequency:* Nominal 4kHz, Max = 20kHz. *Thermal Trip*: Max = 80 ^{o}C

AC Inductors: L_{AC} = 2.2mH. *DC Inductors*: L_{DC} 2.4mH, R_{eq} = 0.15Ω. *DC Capacitor*: *C* = 1020uF. *DC chopper:* chopper resistance, $R_{chopper}$ = 45Ω

Current Sensor: *Accuracy* ±0.3%. *Current*: Nominal = 25A_{RMS}, Max 55A_{RMS}. Voltage Sensor: *Accuracy* ±0.05%. *Voltage*: Nominal ±12.5V, Max ±100V

dSPACE model: DS1005.

Generators: *Model* = Emerson 142U2E300BACAA165240. *Rated Torque* = 18N. *Max Speed* = 4800rpm. *Rated Power* = 5.65kW. *Drive VPWM* = 380/430AC.

REAL TIME DIGITAL SIMULATOR

Racks: 1.

Cards: 1 GTWIF, 4 GPC (2 IBM PPC750GX, 1 GHz), 1 GTIRC, 1 GTDI, 1 GTDO, 1 GTAI, 1 GTAO, 1 GTNET.

POWER SYSTEMS SIMULATOR

AC Inductors: $L_{CIRCUIT}$ = 19.2mH, L_{FAULT} = 7.7mH. *Timer*: Omron H5CX

REFERENCES

[1] U.S. Energy Information Administration, “International Energy Outlook 2011,” 2011.

[2] International Energy Agency, “World Energy Outlook: Executive Summary,” OECD Publishing, Sep. 2011.

[3] The European Parliament and the Council of the European Union, *Directive 2009/28/EC on the promotion of the use of energy from renewable sources*. Official Journal of the European Union, 2009, p. 31.

[4] Committee on Climate Change, “The Renewable Energy Review Executive Summary,” 2010.

[5] HM Government, “The UK Low Carbon Transition Plan: National Strategy for Climate and Energy,” 2009.

[6] HM Government, *Meeting the Energy Challenge: A White Paper on Energy*. 2007.

[7] Department of Energy and Climate Change, *Electricity Market Reform (EMR): White Paper 2011*. 2011.

[8] National Statistics, “Energy Trends,” 2012.

[9] J. Li, P. Shi, and H. Gao, “China Wind Power Outlook,” 2010.

[10] US Department of Energy, “A National Offshore Wind Strategy: Creating an Offshore Wind Energy Industry in the United States,” 2011.

[11] Global Wind Energy Council, “Global Wind Report,” 2011.

[12] Global Wind Energy Council, “Indian Wind Energy Outlook 2011,” 2011.

[13] The Crown Estate, “UK Offshore Wind Report 2011,” 2011.

[14] National Grid Ltd, “Offshore Development Information Statement,” 2010.

[15] Alstom Grid, *HVDC: Connecting to the Future*, 1st ed. 2010.

[16] M. P. Bahrman, “HVDC transmission overview,” in *2008 IEEE/PES Transmission and Distribution Conference and Exposition*, 2008, pp. 1–7.

[17] Forewind, “Dogger Bank Facts and Figures,” 2012. [Online]. Available: http://www.forewind.co.uk/dogger-bank/overview.html. [Accessed: 10-Aug-1BC].

[18] Electricity Networks Strategy Group, “Our Electricity Transmission Network: A Vision for 2020,” 2012.

[19] C. Hor, J. Finn, G. Thumm, and S. Mortimer, “Introducing Series Compensation in the UK Transmission Network,” in *ACDC 2010*, 2010.

[20] Aberdeen Renewable Energy Group, “Offshore Wind Capabilities in Aberdeen City and Shire,” 2011.

[21] SSE, “Our Innovation Strategy,” 2011.

[22] ABB, “Tesla vs Edison: the war of the currents,” 2011. [Online]. Available: http://www.abb.com/cawp/seitp202/c646c16ae1512f8ec1257934004fa545.aspx.

[23] W. Long and S. Nilsson, “HVDC transmission: yesterday and today,” *IEEE Power and Energy Magazine*, vol. 5, no. 2, pp. 22–31, Mar. 2007.

[24] W. Litzenberger, “A Short History of the Pacific HVDC Intertie,” in *IEEE Power Systems Conference and Exhibition*, 2006, pp. 24–27.

[25] S. Cole and R. Belmans, “Transmission of bulk power,” *IEEE Industrial Electronics Magazine*, vol. 3, no. 3, pp. 19–24, Sep. 2009.

[26] O. Peake, “The History of High Voltage Direct Current Transmission,” in *3rd Australasian Engineering Heritage Conference 2009*, 2009, pp. 1–8.

[27] W. Litzenberger, “Advances in HVDC Technology as applied to the Pacific HVDC Intertie,” in *2008 IEEE/PES Transmission and Distribution Conference and Exposition*, 2008, pp. 1–4.

[28] H. Stomberg, B. Abrahamsson, and O. Saksvik, “Modern HVDC Thyristor Valves,” in *ICEE 96, Beijing China*, 1996.

[29] J. Arrillaga, Y. H. Liu, and N. R. Watson, *Flexible Power Transmission: The HVDC Options*. 2007.

[30] B. R. Andersen, “HVDC transmission-opportunities and challenges,” *AC and DC Power Transmission, 2006. ACDC 2006. The 8th IEE International Conference on*, pp. 24–29, 2006.

[31] Siemens, “High Voltage Direct Current Transmission - Proven Technology for Power Exchange,” 2010.

[32] Siemens, “Ultra HVDC Transmission System.” [Online]. Available: http://www.energy.siemens.com/hq/en/power-transmission/hvdc/hvdc-ultra/#content=Description.

[33] CIGRE WG B4.37, “VSC Transmission,” *Design*, no. April. p. 82, 2005.

[34] N. Flourentzou, V. G. Agelidis, and G. D. Demetriades, “VSC-Based HVDC Power Transmission Systems: An Overview,” *IEEE Transactions on Power Electronics*, vol. 24, no. 3, pp. 592–602, Mar. 2009.

[35] N. Hörle, K. Eriksson, and T. Nestli, “Electrical supply for offshore installations made possible by use of VSC technology,” in *Cigre 2002 conference, Paris, France*, 2002.

[36] L. Stendius and P. Jones, “The Challenges of Offshore Power System Construction - Bringing Power Successfully to Troll A, One of the Worlds Largest Oil and Gas Platforms,” in *8th IEE International Conference on AC and DC Power Transmission*, 2006.

[37] B. R. Andersen, “Topologies for VSC transmission,” *Power Engineering Journal*, vol. 16, no. 3, p. 142, 2002.

[38] M. Davies, M. Dommaschk, J. Dorn, J. Lang, D. Retzmann, and D. Soerangr, “HVDC PLUS – Basics and Principle of Operation,” 2008.

[39] S. P. Teeuwsen, “Modeling the Trans Bay Cable Project as Voltage-Sourced Converter with Modular Multilevel Converter design,” in *2011 IEEE Power and Energy Society General Meeting*, 2011, pp. 1–8.

[40] Alstom Grid, “HVDC-VSC : transmission technology of the future,” *Think Grid*, pp. 13–17, 2011.

[41] M. M. C. Merlin, T. C. Green, P. D. Mitcheson, D. R. Trainer, D. R. Critchley, and R. W. Crookes, “A New Hybrid Multi-Level Voltage-Source Converter with DC Fault Blocking Capability,” in *ACDC 2010*, 2010.

[42] J. Lai, S. Member, and F. Z. Peng, “Multilevel Converters-A New Breed of Power Converters,” *IEEE Transactions on Industry Applications*, vol. 32, no. 3, pp. 509–517, 1996.

[43] A. Lesnicar and R. Marquardt, “An innovative modular multilevel converter topology suitable for a wide power range,” in *2003 IEEE Bologna Power Tech Conference Proceedings,*, 2003, vol. 3, pp. 272–277.

[44] F. Schettler, H. Huang, and N. Christl, “HVDC transmission systems using voltage sourced converters design and applications,” in *2000 Power Engineering Society Summer Meeting (Cat. No.00CH37134)*, vol. 2, pp. 715–720.

[45] M. P. Bahrman, J. G. Johansson, and B. A. Nilsson, “Voltage Source Converter Transmission Technologies: The Right Fit for the Application,” in *Power Engineering Society General Meeting 2003*, 2003.

[46] T. M. Haileselassie, M. Molinas, and T. Undeland, “Multi-Terminal VSC-HVDC System for Integration of Offshore Wind Farms and Green Electrification of Platforms in the North Sea,” in *Nordic Workshop on Power and Industrial Electronics*, 2008, pp. 1–8.

[47] L. Xu, L. Yao, and C. Sasse, “Grid Integration of Large DFIG-Based Wind Farms Using VSC Transmission,” *IEEE Transactions on Power Systems*, vol. 22, no. 3, pp. 976–984, Aug. 2007.

[48] M. Hyttinen, J.-O. Lamell, and T. . Nestli, “New application of voltage source converter (VSC) HVDC to be installed on the gas platform Troll A,” in *CIGRE Session 2004*, 2004, p. 8.

[49] J. Häfner and B. Jacobson, “Proactive Hybrid HVDC Breakers - A key innovation for reliable HVDC grids,” in *Cigre 2011 Bologna Symposium - The Electric Power System of the Future*, 2011.

[50] ENTSOE, “Offshore Grid Development in the North Seas,” 2011.

[51] D. Van Hertem, M. Ghandhari, and M. Delimar, “Technical limitations towards a SuperGrid — A European prospective,” in *2010 IEEE International Energy Conference*, 2010, pp. 302–309.

[52] J. Blau, “Europe Plans a North Sea Grid,” *Spectrum*, pp. 12–13, 2010.

[53] European Commision, *NSCOGI report 2011*, no. 027. 2011.

[54] Energy and Climate Change Commitee, *A European Supergrid: Seventh Report of Session 2010-12*, vol. I. 2011.

[55] ABB, “The HVDC Transmission Québec - New England.” [Online]. Available: http://www.abb.co.uk/industries/ap/db0003db004333/87f88a41a0be97afc125774b003e6109.aspx.

[56] CIGRE WG B4.52, “HVDC Grid Feasibility Study,” 2012.

[57] T. Nakajima and S. Irokawa, “A control system for HVDC transmission by voltage sourced converters,” in *199 IEEE Power Engineering Society Summer Meeting. Conference Proceedings (Cat. No.99CH36364)*, 1999, vol. 2, pp. 1113–1119.

[58] J. Liang, O. Gomis-Bellmunt, J. Ekanayake, N. Jenkins, and L. Jun, “Control of multi-terminal VSC-HVDC transmission for offshore wind power,” in *Power Electronics and Applications, 2009. EPE ’09. 13th European Conference on*, 2009, pp. 1–10.

[59] T. M. Haileselassie, K. Uhlen, and T. Undeland, “Control of Multiterminal HVDC Transmission for Offshore Wind Energy,” in *Nordic Wind Power Conference*, 2009, pp. 1–7.

[60] C. D. Barker and R. Whitehouse, “Autonomous Converter Control in a Multi-Terminal HVDC System,” in *ACDC 2010*, 2010.

[61] T. K. Vrana and O. B. Fosso, “Active Power Control with Undead-Band Voltage & Frequency Droop for HVDC Converters in Large Meshed DC Grids,” in *EWEA Conference, Copenhagen, April 2012*, 2012, pp. 2–5.

[62] L. Tang and B.-T. Ooi, “Locating and Isolating DC Faults in Multi-Terminal DC Systems,” *IEEE Transactions on Power Delivery*, vol. 22, no. 3, pp. 1877–1884, Jul. 2007.

[63] O. Gomis-Bellmunt, J. Liang, J. Ekanayake, R. King, and N. Jenkins, “Topologies of multiterminal HVDC-VSC transmission for large offshore wind farms,” *Electric Power Systems Research*, vol. 81, no. 2, pp. 271–281, Feb. 2011.

[64] National Grid Ltd, “Connection Conditions, Issue 4 Revision 12,” 2012.

[65] I. Moore, “Review of Transmission System Connection Requirements,” 2011.

[66] A. A. Van Der Meer, R. L. Hendriks, and W. L. Kling, “A Survey of Fast Power Reduction Methods for VSC Connected Wind Power Plants Consisting of Different Turbine Types,” in *Wind Power to the Grid -EPE Wind Energynergy*, 2009.

[67] L. Harnefors, Y. Jiang-Hafner, M. Hyttinen, and T. Jonsson, “Ride-Through Methods for Wind Farms Connected to the Grid via a VSC-HVDC Transmission,” in *Nordic Wind Power Conference*, 2007, pp. 145–150.

[68] G. Ramtharan, A. Arulampalam, J. B. Ekanayake, F. M. Hughes, and N. Jenkins, “Fault ride through of fully rated converter wind turbines with AC and DC transmission systems,” *IET renewable power generation*, vol. 3, no. 4, pp. 426–438, 2009.

[69] L. Xu and L. Yao, “DC voltage control and power dispatch of a multi-terminal HVDC system for integrating large offshore wind farms,” *IET Renewable Power Generation*, vol. 5, no. 3, p. 223, 2011.

[70] D. H. Nguyen and M. Negnevitsky, “A review of fault ride through strategies for different wind turbine systems,” in *20th Australasian Universities Power Engineering Conference (AUPEC)*, 2010, pp. 1–5.

[71] A. Mullane, G. Lightbody, and R. Yacamini, “Wind-Turbine Fault Ride-Through Enhancement,” *IEEE Transactions on Power Systems*, vol. 20, no. 4, pp. 1929–1937, Nov. 2005.

[72] A. Egea-Alvarez, A. Junyent-Ferre, O. Gomis-Bellmunt, L. Jun, J. Ekanayake, N. Jenkins, and J. Liang, “Operation and control of VSC-HVDC multiterminal grids for offshore wind,” in *Power Electronics and Applications, EPE ’11*, 2011, pp. 1–9.

[73] IEEE Subsynchronous Resonance Working Group, “Terms, Definitions and Symbols for Subsynchronous Oscillations,” *IEEE Transactions on Power Apparatus and Systems*, vol. PAS-104, no. 6, pp. 1326–1334, 1985.

[74] K. R. Padiyar, *Analysis of subsynchronous resonance in power systems*. Kluwer, 1999.

[75] D. N. Walker, C. E. J. Bowler, R. L. Jackson, and D. A. Hodges, “Results of subsynchronous resonance test at Mohave,” *IEEE Transactions on Power Apparatus and Systems*, vol. 94, no. 5, pp. 1878–1889, Sep. 1975.

[76] North American Electric Reliability Corporation, “Sub-Synchronous Interaction between Series Compensated Transmission Lines and Generation,” 2011.

[77] R. Grünbaum, P. Halvarsson, P. Jones, A. B. B. Ab, and S.- Vasteras, “Series Compensation for Extended Utilization of Power Transmission Systems,” in *ACDC 2010*, 2010.

[78] Siemens, “Discover the World of FACTS Technology,” 2011.

[79] R. Grünbaum, P. Halvarsson, and P. Jones, “Series Compensation for Increased Power Transmission Capacity,” in *Power Electronics, Machines and Drives (PEMD 2010)*, p. 2010.

[80] Siemens, “FACTS – Flexible AC Transmission Systems Series Compensation,” 2010.

[81] ABB, “Series Compensation Boosting Transmission Capacity,” 2010.

[82] S. G. Helbing and G. G. Kiuady, “Investigations of an Advanced Form of Series Compensation,” *IEEE Transactions on Power Delivery*, vol. 9, no. 2, 1994.

[83] S. Pan, D. Rai, and S. O. Faried, “Damping Power System Oscillations Using a Hybrid Series Capacitive Compensation Scheme,” in *2011 IEEE Trondheim PowerTech*, 2011, pp. 1–6.

[84] N. Kakimoto, A. Iida, M. Seki, K. Minoyama, and T. Takuma, “Clarification of the SSR Mitigation Mechanism of a TCSC,” *Electrical Engineering in Japan*, vol. 120, no. 4, pp. 168–175, 1997.

[85] R. J. Piwko and E. Larsen, “HVDC System Control for Damping of Subsynchronous Oscillations,” *IEEE Transactions on Power Apparatus and Systems*, no. 7, pp. 2203–2211, 1982.

[86] T. Smed and G. Andersson, “Utilising HVDC to damp power oscillations,” *IEEE Transactions on Power Delivery*, vol. 8, no. 2, pp. 620–627, 1993.

[87] Y. Pipelzadeh, B. Chaudhuri, and T. C. Green, “Wide-area power oscillation damping control through HVDC: A case study on Australian equivalent system,” in *IEEE PES General Meeting*, 2010, pp. 1–7.

[88] N. Prabhu and K. R. Padiyar, “Investigation of Subsynchronous Resonance With VSC-Based HVDC Transmission Systems,” *IEEE Transactions on Power Delivery*, vol. 24, no. 1, pp. 433–440, Jan. 2009.

[89] P. Kundur, *Power System Stability and Control*. McGraw-Hill, 1994.

[90] P. M. Anderson, B. L. Agrawal, and J. E. Van Ness, *Subsynchronous resonance in power systems*. IEEE Press, 1989.

[91] IEEE Subsynchronous Resonance Task Force, “First benchmark model for computer simulation of subsynchronous resonance,” *IEEE Transactions on Power Apparatus and Systems*, vol. 96, no. 5, pp. 1565–1572, Sep. 1977.

[92] R. G. Farmer, A. L. Schwalb, and E. Katz, “Navajo project report on subsynchronous resonance analysis and solutions,” *IEEE Transactions on Power Apparatus and Systems*, vol. 96, no. 4, pp. 1226–1232, Jul. 1977.

[93] IEEE Subsynchronous Resonance Task Force, “Second Benchmark Model for Computer Simulation of Subsynchronous Resonance,” *IEEE Transactions on Power Apparatus and Systems*, vol. PAS-104, no. 5, pp. 1057–1066, 1985.

[94] C. E. Ugalde-Loo, J. B. Ekanayake, and N. Jenkins, “Subsynchronous resonance on series compensated transmission lines with quadrature boosters,” in *2011 IEEE Trondheim PowerTech*, 2011, pp. 1–7.

[95] O. M. Neto and D. C. Macdonald, “Analysis of subsynchronous resonance in a multi-machine power system using series compensation,” *International Journal of Electrical Power & Energy Systems*, vol. 28, no. 8, pp. 565–569, Oct. 2006.

[96] F. M. Hughes, O. Anaya-lara, N. Jenkins, and G. Strbac, “Control of DFIG-Based Wind Generation for Power Network Support,” *IEEE Transactions on Power Systems*, vol. 20, no. 4, pp. 1958–1966, 2005.

[97] F. M. Hughes, N. Jenkins, and G. Strbac, “Contribution of DFIG-based wind farms to power system short-term frequency regulation,” *IEE Proceedings: Generation, Transmission and Distribution*, vol. 153, no. 2, 2006.

[98] M. Hughes, O. Anaya-Lara, and N. Jenkins, “Generic Network Model for Wind Farm Control Scheme Design and Performance Assessment,” in *European Wind Energy Conference & Exhibition, London, UK*, 2004, pp. 1–7.

[99] F. M. Hughes, O. Anaya-Lara, N. Jenkins, and G. Strbac, “A Power System Stabilizer for DFIG-Based Wind Generation,” *IEEE Transactions on Power Systems*, vol. 21, no. 2, pp. 763–772, May 2006.

[100] C. E. Ugalde-Loo, J. B. Ekanayake, and N. Jenkins, “Subsynchronous Resonance in a Series Compensated GB Transmission Network,” *IET Generation, Transmission and Distribution*, 2012.

[101] P. Forsyth and R. Kuffel, “Utility applications of a RTDS Simulator,” in *Power Engineering Conference, 2007. IPEC 2007. International*, 2007, pp. 112–117.

[102] W. Dommel, “Digital Computer Solution of Electromagnetic Transients in Single- and Multiphase Networks,” *IEEE Transactions on Power Apparatus and Systems*, no. 4, pp. 388–399, 1969.

[103] M. Molinas, B. Naess, W. Gullvik, and T. Undeland, “Control of Wind Turbines with Induction Generators Interfaced to the Grid with Power Electronics Converters,” in *International Power Electronics Conference, IPEC 2005*, 2005.